DEVELOPMENT OF A NOVEL *IN VITRO* BLOOD BRAIN BARRIER MODEL FOR THE EVALUATION OF NANOMEDICINES

A Dissertation
Presented to
The Academic Faculty

by

Candice Megan Hovell

In Partial Fulfillment
of the Requirements for the Degree
Doctor of Philosophy in Biomedical Engineering the
Wallace H. Coulter Department of Biomedical Engineering

Georgia Institute of Technology and Emory University
December 2017

DEVELOPMENT OF A NOVEL *IN VITRO* BLOOD BRAIN BARRIER MODEL FOR THE EVALUATION OF NANOMEDICINES

Approved by:

Dr. YongTae (Tony) Kim, Co-Advisor
School of Mechanical Engineering
Georgia Institute of Technology

Dr. Hang Lu
School of Chemical and Biological Engineering
Georgia Institute of Technology

Dr. Lakeshia Taite, Co-Advisor
College of Veterinary Medicine and Biomedical Sciences
Texas A&M University

Dr. Brandon Dixon
School of Mechanical Engineering
Georgia Institute of Technology

Dr. Gilda Barabino, Co-Advisor
Dean of Engineering
The City College of New York

Dr. Edward Botchwey
School of Biomedical Engineering
Georgia Institute of Technology

Dr. Maribel Vazquez
School of Biomedical Engineering
The City College of New York

Date Approved: June 29, 2017

For my family, old and new.

ACKNOWLEDGEMENTS

First and foremost, I would like to broadly acknowledge all of the teachers, mentors, and advisers that have contributed to my intellectual development and scientific training over the last 22 years. In the last five years, I have had the privilege of training under three advisors: Dr. Lakeshia Taite, Dr. Gilda Barabino, and Dr. YongTae (Tony) Kim. In particular, I would like to thank Dr. Tony Kim for taking me on as a co-advised student and investing as much time and thought into my advisement as he does for his own students. I am incredibly thankful for the many opportunities I have had in the Kim Lab to contribute to a wide range of projects, to learn new skills and techniques, and to travel and present my work at professional conferences. I would like to thank Dr. Lakeshia Taite for her constant and thoughtful advisement throughout the course of my graduate studies. I would also like to thank Dr. Taite for always taking the time talk (even if it was just for a laugh), for her help with my NSF GRF applications, and for identifying and dispelling my imposter syndrome. I would like to thank Dr. Gilda Barabino for introducing me to Dr. Kim, for her continued advisement throughout the course of my research, and for educating me on the broader impacts of scientific achievement. I would also like to acknowledge and thank my committee members: Dr. Brandon Dixon, Dr. Ed Botchwey, Dr. Hang Lu, and Dr. Maribel Vazquez for contributing their time, expertise, and insight to my work. In addition, I would like to harken back to my undergraduate days and thank Dr. Ryan Earley for taking me into his lab when I was a freshman at the University of Alabama. It was in the Earley Lab that I gained my first exposure to the scientific process in action and

solidified my resolve to pursue studies at the graduate level. Finally, I want to thank Stan Gillispie for teaching me the incredible power of a positive attitude.

I am very honored to have had the opportunity to complete my graduate studies at Georgia Tech, and I am especially thankful to have had the support and encouragement of seemingly an entire department along the way. I want to acknowledge Dr. Mike Davis, Shannon Sullivan, and Dr. Kyla Ross for their commitment to the students of the BME program. I would also like to thank Shannon for personally taking the time to help me to navigate the non-academic challenges that arise over the course of graduate education. I would also like to broadly thank the many friends and lab mates that I have come to know and admire these last five years. In particular, I would like to thank Betsy Campbell, Cheryl San Emeterio, Claire Olingy, Giuli Salazar Noratto, Efrain Cermeño Blondet, Micheal Tanes, Weipeng Zhou, Yoshi Sei, Song Ih Ahn, and Jiwon Yom.

I would also like to take the time to acknowledge my family for their contributions to my success. First of all, I would like to thank Lee and Diana Hovell for being great parents. In addition to prioritizing education, constantly encouraging me to try new things, and teaching me that the only real form of failure is quitting, I would like to specifically thank my parents for all the books. Thank you, Mom, for introducing me to story time at “our friend the library” when I was just a baby and for checking out “Hooked on Phonics” week after week to teach me how to read in pre-school. Thank you, Dad, for driving me all the way into town every Thursday night and then patiently waiting hours for me to pick out my next round of books at Barnes and Noble. Thank you both for spoiling me with an unlimited book budget. Those books changed my life. Reading taught me to think for

myself, to seek out new knowledge independently, to communicate clearly, and (eventually) to have confidence in my own ideas and abilities.

In addition to having amazing parents, I have the great good fortune to be a sister to two exceptional women. Thank you to my older sister Brittany for setting the bar high. You never backed down from a challenge, and you never gave up. Your success made my own goals feel achievable, and I count myself lucky to have had such a strong trailblazer one year ahead of me in life. Thank you, Carley, for teaching me to be humble, helping me learn to laugh at myself, teaching me what it means to be truly kind, and for setting an example of fierce independence. You are my younger sister, but I have always looked up to you (literally and metaphorically).

I would be remiss if I did not also acknowledge my partner Logan Hester for going above and beyond to support me. Whether it meant cat sitting, being a human alarm clock, buying my groceries, performing the physical labor of menial tasks, or donating intellectual labor, you never hesitated to do anything and everything you could to support me, and I will always be grateful for your contributions to my success. Thank you for all the chess games, the 70mph seadoo rides, the planet earth marathons, the morning dances, the all-day debates, and for going on adventures all over the world with me at the drop of a hat. Most of all, thank you for being my perspective this last year and reminding me that I already have so very much to be proud of and thankful for.

Finally, I would like to acknowledge and thank Cicero Lynx Hovell for being the best kitty in the entire world and for always being there to remind me that work (even science) is not everything.

TABLE OF CONTENTS

LIST OF TABLES

LIST OF FIGURES

LIST OF SYMBOLS AND ABBREVIATIONS

AD	Alzheimer's Disease
ADMET	Absorption, distribution, metabolism, excretion, toxicity
ApoA1	Apolipoprotein A1
ApoE3	Apolipoprotein E3
BBB	Blood brain barrier
BTB	Blood tumor barrier
CnI	Collagen one
CNS	Central nervous system
CSF	Cerebrospinal fluid
ECM	Extracellular matrix
FDA	Food and Drug Administration
GDP	Gross domestic product
HA	Human astrocyte
Hy	Hyaluronic Acid
HBMEC	Human brain microvascular endothelial cell
HBVP	Human brain vascular pericyte
HDL	High density lipoprotein
HT-qPCR	High throughput quantitative polymerase chain reaction
HY	Hyaluronic acid
IAM	Immobilized artificial membranes
L-	Denotes culture in MLS-BBB system
LOA	Likelihood of approval

LogBB	Log (brain concentration/blood concentration)
LPNP	Lipid polymer nanoparticle
Mat	Matrigel (growth factor reduced)
MB	Medulloblastoma
MLS-BBB	Microfluidic lumen system of the blood brain barrier
NP	Nanoparticle
NVU	Neurovascular unit
OOAC	Organ-on-a-chip
PAMPA	parallel artificial membrane permeability assay
PBS	Phosphate buffered saline
PD	Parkinson’s disease
PDL	Poly-D-Lysine
PDMS	Polydimethylsiloxane
PEG	Polyethylene glycol
PF127	Pluronic F-127
Pgp	p-glycoprotein
PS	Permeability by surface area
QSAR	Quantitative structure–activity relationship
QSPR	Quantitative structure–property relationship
RMT	Receptor mediated transcytosis
ROI	Region of interest
SP-	Denotes spheroid culture
SSH	Sonic hedgehog
TC	Tenascin C
TEER	Trans endothelial electrical resistance

TNFα	Tumor necrosis factor alpha
TW-	Denotes transwell culture

SUMMARY

The blood brain barrier (BBB) is the term given to the specialized microvasculature of the central nervous system (CNS) responsible for the regulation of molecular transport into the brain from systemic circulation. While the BBB is critical for proper neuronal function, it also presents a significant barrier to efficient drug delivery due to its restriction of paracellular and transcellular molecular transport and the presence of major drug resistant proteins like p-glyocoprotein (Pgp). Currently available *in vitro* models for the preliminary evaluation of novel drug candidates are primarily simple, static culture models, which have been demonstrated to have poor predictive abilities, resulting in significant wastes of time and resources during subsequent preclinical and clinical studies. In recent years, organ-on-a-chip (OOAC) platforms have emerged as a potential means of improving the predictive power of *in vitro* assays. By allowing researchers to combine human cell lines with relevant chemical and mechanical cues *in vitro*, OOAC models provide a means to better balance simplicity and physiological relevance when conducting mechanistic studies.

Despite a large number of increasingly complex *in vitro* BBB models being presented in the literature, no model has been adapted for widespread use in preliminary drug studies in place of traditional, static culture transwell systems. This can be attributed to a number of factors including a lack of sufficient evidence that demonstrates their increased predictive power over simpler models, increased cost of fabrication and operation, lack of ability to perform high throughput screening, and increased technical expertise required to establish these models. Furthermore, several key components must be

integrated in the model as they contribute to the expression of BBB relevant endothelial cell specializations including exposure to shear stress, direct cell-cell interactions between relevant cell types, and a functional lumen structure. Additionally, recent research indicates that proper extracellular matrix (ECM) composition is necessary for the non-reactive culture of astrocytes, a critical cellular component for *in vitro* BBB modeling.

In this work, we present a novel microfluidic lumen system of the BBB (MLS-BBB) for the evaluation of multifunctional nanomedicines engineered for the treatment of medulloblastoma (MB). Our MLS-BBB is designed to co-culture human astrocytes (HA) and human brain vascular pericytes (HBVP) with a cylindrical lumen of immortalized human brain microvascular endothelial cells (iHBMEC). Our MLS-BBB facilitates the administration of tunable shear rates to a lumen of endothelial cells in direct contact with supporting astrocyte and pericyte cells within a hydrogel system optimized to facilitate the appropriate culture of astrocytes, and is to our knowledge, the first model to do so. We employed high throughput qPCR techniques to simultaneously analyze the expression of 81 BBB relevant endothelial specializations such as junctional proteins (ZO-1, Claudins, JAMs, etc.), specialized transporters (GLUT-1, CAT1, TfR, etc.) and drug resistant proteins (Pgp, ABCC1, ABCC4, etc.). Our results indicate that our system provides a marked increase in physiological relevance relative to transwell culture systems. Our model was further validated through comparison to BBB spheroids, by examination of model response to perturbations of the optimized ECM composition, and by examination of model response to the administration of TNFα, an inflammatory cytokine. Our model is currently being employed in parallel with traditional transwell systems and *ex vivo* brain slice cultures in the preliminary evaluation of a novel nanomedicine designed for the

treatment of sonic hedgehog driven (SSH) MB to evaluate the functional utility of the MLS-BBB in such studies. One of the ultimate goals of OOAC model development is eventual adaptation by the community for preclinical assessment of novel drug compounds. By combining comprehensive characterization with assessments of our model's functional utility relative to standard *in vitro* controls, we believe our work constitutes a significant step towards the realization of this goal.

CHAPTER 1. INTRODUCTION AND SPECIFIC AIMS

1.1 Objective

The blood brain barrier (BBB) poses a significant challenge to the development of drugs for central nervous system (CNS) diseases due to the decrease in vascular permeability that results from the specialization of the endothelial cells of the BBB. The BBB is particularly challenging to study *in vivo* due to the imaging limitations posed by the skull and the sensitive nature and limited regenerative potential of neuronal tissue. As a result, a wide diversity of *in vitro* models of the BBB exist for the study of drug interaction with, and transport through, the BBB. Among these models, only simple, static culture assays are widely used for the preclinical assessment of novel drug compounds, despite increasing literature evidence indicating their poor predictive power. Thus, *the* ***objective*** *of this thesis is to design, characterize, and demonstrate the utility of a novel in vitro BBB model for the evaluation of new drug compounds.*

1.2 Motivation

This work is primarily ***motivated*** *by the high cost and low success rate of drugs developed for CNS targets.* The Tufts Center for the Study Drug Development estimates that the average drug requires an investment of approximately 2.6 billion dollars and 15 years to develop, with over half of this investment being spent in the preclinical stages. Despite continuous advancements in drug screening technology and increased investment in drug development, the likelihood of approval (LOA) for new drug candidates (Phase 1 to approval) is only 9.6% has remained stagnated in recent decades. When paired with

increasingly dire projections for the incidence of neurodegenerative diseases like Alzheimer's disease (AD), the need for improved *in vitro* tools for the rapid and efficient evaluation of novel drug candidates becomes readily apparent.

1.3 Aim 1: Development of MLS-BBB

In recent years, OOAC devices have emerged as a potential means to increase the predictivity of *in vitro* screening tools. While many microfluidic models of the BBB are available in the literature, none so far have been adapted for use as preclinical screening tools. This can be attributed to several factors including a lack of demonstration of increased predictive power over simpler methodologies and the inability to facilitate high throughput evaluation of novel drug candidates. Furthermore, existing OOAC models of the BBB still lack the inclusion of one or more parameters that have been demonstrated as critical for the proper recapitulation of relevant BBB function such as the presence and appropriate culture of support cells types (astrocyte and pericyte) and the ability to facilitate the exposure of endothelial cells to physiologically relevant shear stress. We hypothesized that integration of a 3D perfusable lumen of endothelial cells in direct co-culture with relevant support cell types within a hydrogel system tuned mimic the ECM of brain tissue would result in the development of a microfluidic BBB model with increased physiological relevance. Hydrogel composition was tuned via the culture and subsequent analysis of hydrogel encapsulated human astrocytes (HA) for markers of reactive gliosis. Perfusable channels were created in our tuned hydrogel system using a previously described sacrificial element methodology, and wall shear stress was generated and maintained via pump facilitated gravity driven flow (PF-GDF). BBB lumen formation was assessed via staining for a relevant tight junction protein (ZO-1), and multicellular architecture was visualized

via staining for distinct cell markers (HBMEC, CD13; HBVP, αSMA; HA, GFAP) and morphological observation.

1.4 Aim 2: High Throughput Characterization of MLS-BBB

A literature review for distinct functions of brain endothelial cells will quickly yield hundreds of potential targets that have been demonstrated to be either characteristically or differentially expressed at the BBB. However, the bulk of OOAC models of the BBB currently available in the literature are only characterized with a handful (~5-10) of metrics. Predictive ability of BBB models is largely dependent on the degree to which the endothelial cells can recapitulate the specializations found in BBB *in vivo*. Thus, we chose to characterize our MLS-BBB model via high throughput quantitative PCR (HT-qPCR) analysis of the expression of 81 BBB relevant endothelial cell specializations. In order to determine the relative strengths and weakness of our MLS-BBB, we also analyzed endothelial cells from transwell (TW) and spheroid (SP) BBB cultures. To determine whether our model would respond dynamically to stimulation, we also assessed the response of our MLS-BBB model to inflammation via administration of TNFα. Lastly, we examined the effect of perturbations to the ECM composition on the expression of BBB relevant specializations in our MLS-BBB system.

1.5 Significance

This work constitutes a significant contribution to the fields of tissue engineering and OOAC research by producing the first (to our knowledge) *in vitro* model of the BBB capable of simultaneously incorporating a perfusable lumen of endothelial cells in direct contact with both astrocyte and pericyte cells within a hydrogel system tuned to facilitate

the appropriate culture of astrocytes. Furthermore, through the comprehensive characterization of our model, we have produced a body of evidence that facilitates direct comparison of the performance of our MLS-BBB to other commonly used *in vitro* BBB models for a wide range of BBB relevant endothelial cell specializations. It is our hope that such validation will contribute to the growing body of evidence demonstrating the inferiority of currently used models and encourage more widespread experimentation with and adaptation of OOAC models in the preclinical assessment of novel drug candidates.

CHAPTER 2. BACKGROUND

2.1 Motivation

As stated, the objective of this thesis is to design, characterize, and demonstrate the utility of a novel *in vitro* BBB model for the evaluation of nanomedicines engineered for the treatment of MB. This work is primarily motivated by the high cost and low success rate of drugs developed for CNS targets. The Tufts Center for the Study Drug Development estimates that the average drug requires an investment of approximately $2.6 billion and 15 years to develop, with over half of this investment being spent in the preclinical stages. Despite continuous advancements in drug screening technology and increased investment in drug development, the LOA for new drug candidates is only 9.6% and has remained stagnated in recent decades [1].

There are many challenges in the drug development pipeline that contribute to this high probability of failure in clinical trials, ultimately culminating in a drastic increase in healthcare spending. Healthcare spending now accounts for 17% of GDP in the United States [2], and in cases of diseases like cancer, this cost burden often gets shifted to the patient. In 2012, twelve out of the thirteen novel cancer drugs approved by the FDA were priced at over $100,000 annually, creating a significant financial burden for patients [3]. This pricing is particularly disturbing considering that cancer treatment often involves a combination of multiple chemotherapeutics, radiation treatment, and surgery [4]. Improvements in the drug development pipeline are critical to the mitigation of such costs to society and individuals.

The high cost associated with such drugs and their development is multifactorial in origin. Many critics cite redundancies in clinical trials between competing pharmaceutical companies, lack of information and data sharing between competing pharmaceutical companies, and inflated price valuation by pharmaceutical companies as major factors [3], but the high cost of development is also thought to be largely due to the lack of predictive screening tools available for the preclinical assessment of novel drug candidates leading to failures in human clinical trials [5].

Clinical trial failures most typically result from the inability to demonstrate efficacy (56%) or the presentation of adverse drug events (28%) [6], indicating that current preclinical assessment is not sufficiently robust to remove poor drug candidates prior to investment in human clinical trials. Several techniques exist for the preclinical evaluation of new drug candidates including computer modelling techniques (*in silico*), testing with cultured cells (*in vitro*), and evaluation in animal models (*in vivo*). Currently, new drug candidates are identified from a library of potential compounds and evaluated in static cell culture before being evaluated *in vivo* in an animal model. While static culture assays are a necessary first step in evaluation of new compound toxicity, such simple assays are unable to accurately capture the complexity of *in vivo* response and often yield results that are not predictive of animal model or human patient response. Furthermore, *in vivo* validation can often be convoluted by organism complexity and the physiological variation between the study animal and a human patient.

In response to these challenges, the field of tissue engineering has produced a number of OOAC model systems that are particularly promising candidates for incorporation into preclinical drug assessment workflows [7]. These devices aim to improve the predictivity

of preclinical assessment by allowing for the culture of human cells in more physiologically relevant microenvironments. Such OOAC devices have demonstrated the potential to serve as more predictive early stage screening tools that can efficiently evaluate new drug compounds, and it has been widely speculated that the modification of preclinical assessment to include OOAC validation will lower developmental costs, accelerate developmental timelines, and increase affordability of new drug products.

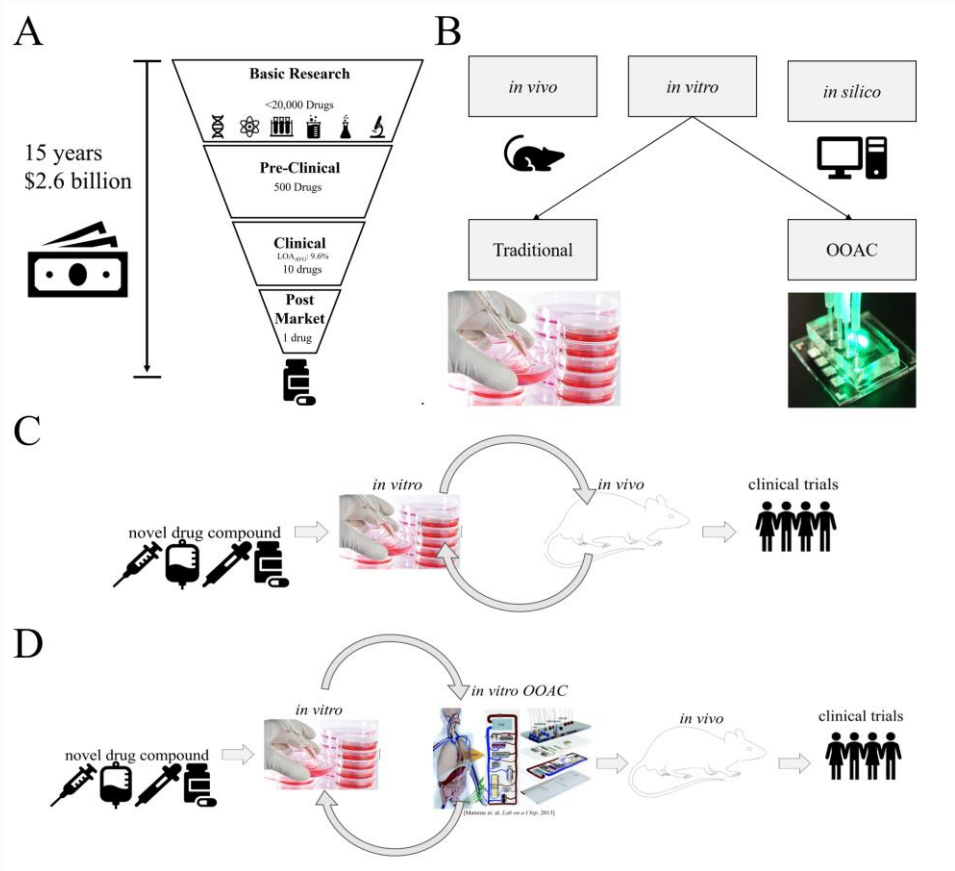

Figure 1. Preclinical assessment of novel drug compounds. (A) The drug develpoment pipeline can be broken down into four stages: basic research, pre-clinical research, clinical evaluation and post market study (B) A number of *in vivo*, *in vitro* and *in silico* techniques are available for use in preclincal evaluation and in recent years *in vitro* validation has expanded to include validation via OOAC models (C) Current preclinical assessment worflow (D) Proposed integration of OOAC models into preclinical assessment.

2.2 Organ-on-a-Chip Models (OOAC)

OOAC platforms have arisen from the fields of microchip manufacturing and tissue engineering research as a potential improvement to existing preclinical screening tools [8, 9]. OOAC models are *in vitro* cell culture platforms that are created by microchip manufacturing methods to house living cells in relevant multicellular architectures within a perfusable culture chamber. OOAC models aim to bridge the gap between static cell culture systems and animal models by leveraging advances in microfluidic technology and 3D tissue engineering to create simple, but predictive, screening platforms that better recapitulate innate *in vivo* physiology while readily facilitating detailed mechanistic observation. By allowing researchers to combine human cell lines with relevant chemical and mechanical cues *in vitro*, OOAC models provide a means to better balance simplicity and physiological relevance when conducting mechanistic studies [10].

2.2.1 Comparison to In Vitro and In Vivo Models

While OOAC models are still far from displacing animal studies or simple cell culture assays in the drug development process, OOAC models could carve out their own niche in the drug development pipeline as they provide several distinct advantages over both *in vitro* and *in vivo* systems for preliminary drug studies (**Table 1**). For example, OOAC models readily facilitate the incorporation of relevant chemical and mechanical cues that simpler *in vitro* models lack. By recapitulating proper multicellular architecture, incorporating perfusable vasculature, and tuning to proper physiochemical microenvironments, OOAC devices have been used to replicate aspects of tissue and organ level functionality that are not achievable in conventional 2D or 3D *in vitro* cell culture

systems [11]. Furthermore, in addition to being much more cost effective than animal studies for early stage evaluation, OOAC models enable the use of human cell lines and proteins, which helps to minimize the gap in translation that can arise from species to species variation during *in vivo* validation. OOAC models also allow for real time monitoring of target systems and enable detailed mechanistic study of organ systems and transport phenomena that cannot always be easily imaged *in vivo* (brain), allowing researchers to gain insight into time dependent processes that would be obscured in an animal model in which sometimes only end point data can be collected [10-14].

Table 1. Comparison of *in vitro, in vivo* and OOAC model capabilities.

Desired Capability	In Vivo	In Vitro	OOAC	In Silico
Human Cells and ECM	No	Yes	Yes	No
Application to Personalized Medicine	No	Yes	Yes	Yes
Appropriate Microenvironment	Yes	No	Yes	No
Control over Microenvironment	No	Yes	Yes	No
Ability for Organ Level Function	Yes	Limited	Potential	No
Real Time Observation	No	Limited	Yes	Yes
High Throughput	No	Yes	Potential	Yes
Ability for Pharmacodynamic Studies	Yes	No	Potential	Yes

2.2.2 Economic Justification for Development of OOAC BBB Models

As noted, the development of new drugs is an expensive and time-consuming process. Neurological and oncology drugs are even less likely to succeed in clinical development, with LOAs of 8.4% (n=1304) and 5.2% (n=3163), respectively. These probabilities of success are significantly lower than other disease areas such as haematology (26.1%, n=283), infectious disease (19.1%, n=916), respiratory (12.8%, n=428), and gastroenterology (15.1%, n=156), indicating a particularly dire need for improvements to early stage screening tools for the evaluation of CNS drug candidates [1].

When combined with projection figures for increasing incidence of neurogenerative diseases such as AD, which is estimated to affect as many as 13.2 million people by 2050, the urgent need for better preclinical screening tools for CNS pathologies becomes evident. The cost for caring for AD patients in America is projected to total $259 billion in 2017. Medicare ($131 billion) and Medicaid ($44 billion) programs, programs largely funded by taxpayers and their employers, bear the majority of this expense [15]. While the primary focus of this work is the development of a BBB model for the evaluation of brain cancer therapeutics, the BBB poses an additional challenge to the development of any neurological therapeutic. The production of better screening tools for CNS compounds will help to accelerate the drug development pipeline, decrease the cost of treatments, and could also play a significant role in mitigating the cost to society posed by high incidence, debilitative neurological pathologies like AD.

2.2.3 Current Status and Challenges

Promising OOAC models have been developed for a number of organ systems [16] including lung [11, 17], liver [18, 19], heart [20, 21], intestine [22-24], kidney [25-29], bone marrow [30], skin [31-33], and brain [34, 35]. While many of these devices have demonstrated significant improvements over traditional *in vitro* culture systems, with the exception of liver-on-a-chip, lung-on-a-chip, and kidney-on-a-chip, many have yet to be adapted widely in the scientific community due to several key challenges [7, 8, 12, 36]. OOAC models can be costly to fabricate and operate, often requiring cleanroom facilities and technically trained personnel. Additionally, OOAC models are rarely conducive to high throughput studies, a capability that is necessary for adaptation by the pharmaceutical development industry. Researchers cite many other technical challenges including:

standardization of models, difficulty maintaining mechanical and chemical cues (pressure and solute balance within chips), difficulty integrating non-destructive monitoring capabilities such as trans endothelial electrical resistance (TEER) electrodes, and difficulty recovering cells from chips for downstream experimentation or analysis [12].

In addition to these unresolved challenges, the establishment of a functional, perfusable, vasculature component is technically challenging to repeatedly achieve *in vitro*. However, due to the ubiquitous need to vascularise tissue constructs for long term experimentation, several techniques have emerged in the literature that enable the reliable formation and perfusion of vascular constructs within microchip platforms. These methods are discussed in the immediately ensuring sections. OOAC models of the BBB have their own distinct requirements and challenges that are discussed in more detail in the ensuing sections and are summarized in **Table 3**. Despite these challenges and current limitations, OOAC models have already demonstrated the potential to improve the drug discovery and drug development process and have garnered renewed and increased investment by research institutions (NIH/NCATS, NSF, CASIS, DARPA, FDA) and the pharmaceutical industry in recent years [36, 37].

2.2.4 Incorporation and Perfusion of Vasculature in OOAC Devices

The establishment of functional and perfusable vasculature for nutrient delivery to OOAC devices is essential to the successful development of any OOAC device and is especially critical for the fabrication of a BBB-on-a-chip device. While no gold standard practice currently exists for the fabrication of vasculature within OOAC devices, the ubiquitous need to vascularize tissue constructs for long term study has resulted in the

establishment of several methods for the formation and perfusion of vasculature within OOAC systems. These methods can be broadly categorized into prevascularization based techniques and vasculogenesis and angiogenesis based techniques [38-41].

Prevascularization based techniques include subtractive methods such as the incorporation and dissolution of a sacrificial element [42, 43], viscous fingering [44], and needle based molding, as well as additive methods such as soft lithography and PDMS stamping techniques [45, 46], layer by layer stacking [47], hybrid methods involving micro milling and lithography techniques [48], bioprinting [49-51], and image based laser guided techniques [52-54].

Angiogenesis and vasculogenesis based techniques leverage the natural capabilities of cells to form microvessel constructs. Angiogenesis refers to the formation of new blood vessels from existing blood vessels and vasculogenesis refers to the differentiation of precursor cells into endothelial cells and ensuring formation of a primitive vascular network [55]. Photolithography techniques can be used to create PDMS housings whose geometry facilitates the endogenous formation of microvessels either by vasculogenesis or angiogenesis. Additionally, angiogenesis and vasculogenesis can be accomplished via the administration of growth factor gradients to cells [56], through the use of functionalized biomaterials, via the co-culture of multiple cell types [57] or via a combination of these methods [40].

While many of these methods have been under active investigation discussion in the community for many years, the technical difficulties surrounding the more sophisticated methods, such as the bioprinting and image guided laser techniques, were

still substantial at the inception of this work. Thus, we chose to adopt a sacrificial element method for use in our work due to the simplicity and customizability of the workflow [42].

Once a vascular construct is established, media perfusion can be initiated and controlled in a variety of ways. Pressure gradients can be driven by gravity, surface tension, osmosis, or by direct infusion or withdrawal via syringe pumps. Peristaltic pumping, centrifugal pumping, electrokinetic pumping and electroosmotic pumping have also been used to drive flow through microfluidic devices [58]. Each of these methodologies has its own distinct capabilities, advantages, and disadvantages that are briefly summarized in **Table 2.** For our study, we originally planned to use syringe pumps to generate flow through our MLS-BBB; however, this proved impossible due to the low mechanical strength of the hydrogel used, the tendency of bubbles to form on the surface of the housing, and the propagation of mechanical disturbances from the syringe pump to the MLS-BBB device. As a result, we used a modified version of gravity driven flow to facilitate the long term, stable, perfusion of our devices. Specific details of flow generation using this method can be found in **Section 3.2.5**.

Table 2. Comparison of pumping methodologies used to drive flow through microfluidic chips.

Property	Gravity	Surface Tension	Osmosis	Syringe	Vacuum	Peristaltic	Electric	Centrifugal
Potential for surface fouling	Low	Moderate	Low	Low	Low	Low	High	Low
Potential for mechancial disturbances	Low	Low	Low	Moderate	Moderate	Moderate	Low	Moderate
Potential for chemical disturbances	Low	Low	Moderate	Low	Low	Low	Moderate	Low
Potential for electrical distrubances	Low	Low	Low	Low	Low	Low	High	Low
Ability to facilitate microscopy	Yes	Yes	Yes	Yes	Yes	Yes	Yes	Yes
Ability to facilitate media recirculation	Moderate	No	No	No	No	Yes	Moderate	No
Ability to generate pulsatile flow	No	No	No	Yes	No	Yes	Yes	Moderate
Ability to generate steady flow	Moderate	No	Yes	Yes	Moderate	Moderate	Moderate	Moderate

2.3 The Blood Brain Barrier (BBB)

To successfully recapitulate the BBB on a chip, is it necessary to first examine the relevant anatomy (structure) and physiology (function) of innate human BBB. The BBB is challenging to study *in vivo*, and many aspects of BBB physiology remain convoluted and under investigation by the scientific community. The following sections present a condensed overview of the current literature available on the biology of the BBB, with emphasis placed on the impact of cellular architecture and ECM composition on the function of the system, followed by a summary of existing *in vitro*, *in vivo*, and *in silico* models of the BBB with a discussion of their relative strengths and weaknesses.

2.3.1 Distinct Biology of BBB Endothelial Cells

The BBB is the term given to the anatomically specialized endothelial cells that make up the microvessels of the CNS. The BBB protects sensitive neuronal tissue from circulating toxic compounds and contributes to the maintenance of neuronal homeostasis

by restricting the influx of systemically circulating ions and neurotransmitters, while allowing for immune surveillance with minimal inflammation [59]. In contrast to the unlined microvessels that exist elsewhere in the body, the microvessels of the brain are composed of endothelial cells that are lined abluminally by pericytes and wrapped by astrocytic end feet [60]. The endothelial cells of the BBB are highly specialized [61-65] and are characterized by the differential expression of a number of proteins [63, 66]. For example, BBB endothelial cells have an increased expression of tight junctions between neighboring cells that greatly limits the paracellular diffusion of polar molecules [67-69]. Additionally, the endothelial cells of the BBB have a decreased number of fenestra and pinocytic vesicles, resulting in limited transcellular trafficking. Thus, essential molecules are largely transported via a variety of specialized transcellular pathways (**Figure 2**). Large or nonpolar molecules that cannot exploit one of these transcellular pathways cannot enter the brain [70, 71]. It has been estimated that these specializations limit the transport of up to 98% of molecules, constituting a significant hurdle for drug delivery [72].

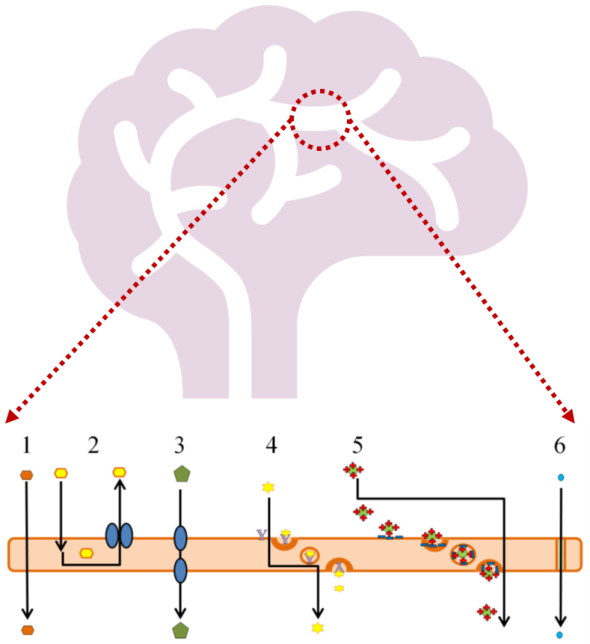

Figure 2. Available routes of transport across the BBB. Small, non-polar, lipid soluble compounds can passively diffuse through endothelial cell membranes into the cytoplasm (1) Carrier molecules chaperone necessary compounds (3) and remove unwanted compounds from the cytoplasm (2). Large, polar, molecules that cannot passively cross the lipid bilayer of the cell membrane are transported by either receptor mediate transcytosis (RMT) (4) or adsorptive mediated transcytosis (5). Very small polar molecules can passively diffuse through the tight junctions connecting neighbouring endothelial cells (6).

2.3.2 The Neurovascular Unit (NVU)

In order to understand how the BBB will respond to stimuli, it is critical to understand the underlying structure that contributes to proper endothelial barrier function. The neurovascular unit (NVU, **Figure 3**) is the functional unit of the BBB and is composed of five cell types that work together to regulate transport and maintain the homeostatic environment necessary for optimal neuronal function. It is the proper function of the multicellular NVU, as opposed to endothelial cells alone, that is critical for the maintenance of BBB barrier integrity [73-75]. One feature to note is that the cellular architecture of the

NVU changes at different levels of circulation (arteries ➔ arterioles ➔ capillaries) where the vasculature performs different functions. At the arteriole level, the NVU is most relevant to metabolism, rather than molecular transport, and is critical for regulating dilation and contraction of vessels in response to increased brain activity [59, 71]. It should be noted that the scope of this work is limited to the study of the BBB and NVU at the capillary level of circulation, the primary site of drug delivery, nutrient transport, and waste removal in tissue. Thus, all references to BBB or NVU are in reference to capillary BBB.

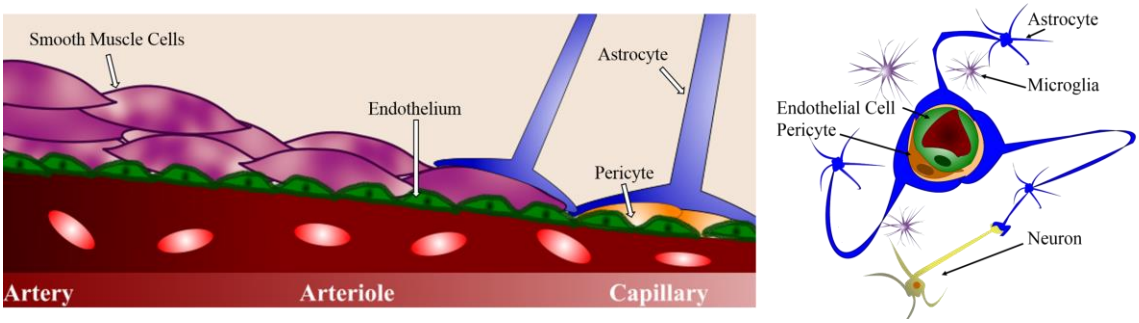

Figure 3. Cellular composition of the neurovascular unit. Distinct cellular architecture characterizes the BBB at different levels of circulation, enabling specialization to facilitate specific tasks (bulk transport of blood vs. molecular transport). At the capillary level, the endothelial cells of the BBB are connected via tight junctions and are partially surrounded by pericyte cells that provide structural support and are largely responsible for the secretion of the ECM proteins that comprise the shared pericyte and endothelial basal lamina. Astrocytic end feet encircle the microvessel wall and provide a link to neuronal activity. Microglia, specialized brain immune cells, serve as the first line of defense against toxic compounds or bacteria that are able to cross the BBB.

When harvested and cultured in 2D cell culture, brain endothelial cells rapidly de-differentiate and lose their "BBB-like" properties [76]. It has been well documented that exposure to astrocyte cells can facilitate the partial recovery of certain BBB relevant endothelial cell specializations by stimulating the increased expression of junctional proteins between neighboring endothelial cells [60] and, until recently, many researchers considered the presence of astrocyte cells or astrocyte conditioned media as sufficient for

the maintenance of the specialized endothelial microvessels of the BBB. However, in recent years it has become evident that correct endothelial cell differentiation and function relies on the proper multicellular local environment and its surrounding ECM [76-80].

This work has chosen to narrow the scope of study to focus on endothelial, astrocyte, and pericyte cells for the first iteration of our MLS-BBB device as literature evidence indicates that these three cell types are most directly related to barrier function. Contact of astrocyte endfoot projections with endothelial cells provides the trophic cues necessary for the expression of tight junction proteins between endothelial cells that restrict paracellular diffusion. Additionally, astrocytes secrete chemical factors that can modulate the permeability of the endothelial cell layer (and to a lesser degree, dilation of microvessels) in response to neuronal stimulation [60]. Pericyte exposure provides the necessary stimuli for BBB appropriate surface receptor expression levels that allow brain endothelial cells to selectively uptake compounds via transcellular pathways. Pericytes also play a central role in structural organization of endothelial cells by synthesizing and secreting most elements of the basement membrane (an approximately 40nm thick layer of collagen IV, laminin, and fibronectin), thereby aiding in barrier stabilization and polarization. Pericytes have also been implicated as necessary for BBB embryogenesis, regulation of blood flow in capillaries, and successful angiogenesis [78, 80, 81]. All three cell types (endothelial, astrocyte, and pericyte) are intrinsically programmed to respond to stimuli from one another, enabling them to form and maintain the NVU *in vitro* [82].

2.3.3 Extracellular Matrix Composition of the Brain and BBB

Brain ECM is different from ECM of other tissues in several ways. In general, the ECM of the brain contains relatively small amounts of fibrous proteins (collagens, fibronectin) that constitute the bulk of other ECMs and comparatively high amounts of glycosaminoglycans, both bound to proteins (proteoglycans) and unbound (hyaluronan). ECM composition varies spatially in the brain and can be broken down into three general compartments for a simplified introduction: the basement membrane or basal lamina, the perineuronal nets, and the neural interstitial matrix. The basement membrane is a thin boundary layer separating the endothelial cells of the BBB from parenchymal tissue and is composed largely of collagen IV, entactin (laminin-nidogen complexes), dystroglycan, perlecan, and fibronectin. The perineural nets surround neuronal cell bodies and proximal dendrites and are composed largely of proteoglycans, tenascin R, and link proteins. The neural interstitial matrix is a dense network of hyaluronan, proteoglycans, tenascins, and link proteins. Select fibrous proteins and adhesive proteoglycans are also present in small amounts in the neural interstitial matrix [83].

The ECM of basement membrane is most relevant to this work, but attention should also be paid to the ECM composition that is most relevant and appropriate for astrocyte culture (neural interstitial matrix), as astrocytes influence the endothelial cells of the BBB via endfoot contact. Additionally, it has been demonstrated that suboptimal culture of astrocytes results in astrocyte activation to a reactive gliosis state [84]. While activated astrocytes do a play a role in responding to and repairing damaged brain tissue, activation has also been shown to cause neuronal damage and has been implicated in the progression of a number of disease states [85-88]. Thus, when considering ECM composition for the

creation of a physiological BBB model, it is essential to balance the needs of astrocyte cells with those of the endothelial cells or the result is likely to be a pathophysiological rather than physiological model.

2.3.4 Challenges to Drug Delivery and Potential Solutions

While the BBB is critical for proper neuronal function, it also presents a significant barrier to efficient drug delivery to brain tissues due to its restriction of paracellular and transcellular molecular transport and the presence of major drug resistant proteins like Pgp [89]. The BBB is virtually impossible to study in human patients due to the sensitivity and limited regenerative potential of neuronal tissue and the imaging and monitoring limitations posed by the skull. As a result, a plethora of model systems (*in vitro*, *in vivo*, *in silico*) exist for preliminary examination of BBB drug penetrance and are discussed in more detail below. Experimentation with these models has yielded insight into BBB structure and function and has led to the development of a few techniques to increase drug permeance into the brain such as disruption with ultrasonic microbubbles [90] and osmotic infusion [91]. Osmotic infusion based techniques are invasive, requiring direct intracerebral or intraventricular injection, and both methods necessitate the temporary disruption of the BBB, creating an opportunity for injury, infection, toxicity, and spatially variable drug delivery.

In contrast to the brute force efforts of osmotic infusion and ultrasonic cavitation, olfactory transport has been proposed as a potential means to bypass the BBB entirely by direct administration to the nasal endothelium and ensuing transport into the brain via the olfactory nerves [92-94]. Intranasal delivery is currently used in approximately 2% of

dosing protocols for commercially available drug products. Among these products are hormone replacement therapies (estradiol), pain management drugs (butorphanol, sumatriptan, zolmitriptan) and allergy medications (fluticasone) [95, 96]. However, the practical application of this delivery route is limited to a restricted pool of drugs and target delivery sites due to the sensitivity of the nasal epithelium, the small volume of the nasal cavity, potential for mucociliary drug clearance, and the potential variance in dosing resulting from fluctuating pH of the mucosal membrane of the nasal epithelium. It has been demonstrated that some of the dosing restrictions that result from the sensitivity of the nasal epithelium and restricted volume of the nasal cavity can be mitigated by the encapsulation of drugs in nano-scale drug delivery systems. Such nanomedicines have been shown to enhance the delivery of intranasal drugs. However, delivery of therapeutically relevant doses to the brain via nasal administration has yet to be successfully demonstrated in humans [96].

To date, no existing techniques or therapies can either circumvent or reversibly alter the BBB at a specific site without compromising the integrity of the system. As a result, many researchers have devoted study to the development of biologically or chemically engineered compounds that can act as "Trojan horses" to escort payloads across the BBB. Endogenously transported compounds are limited to gases (oxygen, carbon dioxide, etc.), metabolic products (glucose, etc.), hormones (estrogen, etc.), and small neutral lipophilic compounds. Several studies indicate that passive transport of nanoparticles (NPs) can be achieved at sizes below 15nm [97], leading researchers to speculate on the potential of nanoscale drug delivery vectors as a means to shuttle compounds across the BBB [98]. Particles between 15nm and 100nm also have potential to penetrate to the brain, but uptake

efficiency decreases exponentially with increasing size. This decrease can be partially mitigated via modifications to the surface of the NP to increase lipophilic properties and reduce surface charge. It has been demonstrated that when systemically administered, these small, neutral lipophilic particles bind with endogenously circulating lipoproteins like apolipoprotein E (ApoE), which then help to chaperone the particles across the BBB. Additionally, particles can be engineered to contain monoclonal antibodies to exploit known routes of transport via receptor mediated transcytosis (RMT) [99]. A comprehensive review of the current state of the art of nanomedicine is outside the scope of this work, but more information on the interactions of NPs with the BBB and a discussion of NP platforms used in this and closely related studies is included in the ensuing sections for additional context.

2.3.5 In Vivo Methods for Studying the BBB

There are several methodologies and metrics available for the study of the BBB and the quantification of drug penetration *in vivo*. The two most widely used methods are the ratio of steady-state concentration of a compound in the brain to concentration in the blood (logBB) which is used to determine the extent of brain penetration by a drug, and the measurement of permeability by surface area (PS) that is used to determine the rate of brain penetrance. Other methods of study include knock out or gene deficient animals, and microdialysis for the determination of free drug concentration in the brain. For many targets, free drug concentration (unbound to brain lipids and off target sites) is the most critical metric for evaluating dosage parameters. Due to the technical difficulty of microdialysis methods, the ratio of cerebrospinal fluid (CSF) drug concentration to plasma drug concentration can be used in some cases as a metric to approximate the concentration

in interstitial brain fluid. While these models and methods do yield substantial information, the *in vivo* methods for studying drug interaction with the BBB are technically difficult to perform and low throughput do to the limitations imposed by the relatively small size of study animals (mice, rats) and limited access to target tissues. As a result, much of the early stage evaluation of new drug candidates for BBB crossing ability is carried out first in *in vitro* models or via *in silico* modelling [100].

2.3.6 In Silico Methods for Studying the BBB

In the last few decades, improvements in computing technology have revolutionized every branch of science, and there has been considerable interest and effort devoted to building computational models that will be able to predict drug interaction with and transport across the BBB. Computational prediction relies on large datasets to build robust, predictive models. Such modelling efforts for the BBB were originally limited by a lack of minable datasets. For example, the largest logBB dataset available for study in 2003 only consisted of about 150 compounds. Despite this limitation, early models built using these resources led to the generation of several general "rules of thumb" for designing drugs with BBB crossing abilities and were able to successfully predict penetrance for ~80% of tested compounds [101]. More recently, *in silico* modelling methods have been created for more specific examinations (e.g. nanoparticle specific interactions with the BBB) and have contributed support to the field through modelling of quantitative structure-activity (QSAR) or structure-property (QSPR) relationships, molecular metabolism, molecular docking, and molecular dynamic simulations to predict absorption, distribution, metabolism, excretion, and toxicity (ADMET) properties [102].

2.3.7 Cell Free Methods for Studying the BBB

Due to the many challenges of modeling the BBB both *in vivo* and *in vitro*, a number of creative solutions have been attempted in the field over the years. One such example is the development of high performance liquid chromatography columns composed of immobilized artificial membranes (IAMs) that were engineered to have properties similar to biological membranes. Despite the complete lack of biological components, some of these attempts were moderately successful at ranking compounds according to BBB permeability but were not adaptable to high throughput operations [100].

Another cell free technology that can be used to study the BBB is the parallel artificial membrane permeability assay (PAMPA). Originally developed as a surrogate to predict gastrointestinal absorption, the PAMPA system has been successfully used for predicting the permeability of drugs across other biological barriers. By altering the lipid content and composition of the artificial membranes, PAMPA has been demonstrated to be capable of predicting drug permeability across the BBB with a reasonable degree of accuracy [103].

2.4 In Vitro Models for the Study of the BBB

In addition to available *in vivo*, *in silico*, and cell free BBB models, a multitude of *in vitro* models of the BBB are available for the preliminary evaluation of novel drug candidates. These models range in complexity from simple, static, mono-culture systems to 3D multicellular constructs within microfluidic chips that integrate flow and on-board barrier monitoring capabilities. As discussed above, the function of the BBB is heavily dependent on properties of its structural composition, both cellular and extracellular. As

such, there are a number of specific requirements for a BBB model to be considered functional and accurate: cell to cell interactions leading to proper cellular architecture [82, 104], the expression of tight junctions between endothelial cells, relative exposure to promoting factors, exposure to physiologically relevant flow, and appropriate endothelial cell surface receptor expression [105, 106]. Additionally, to be useful in the context of drug discovery and the evaluation of new drug candidates, the model needs to be able to be replicated easily and reliably and would ideally facilitate adaptation to a high throughout platform [5, 107]. While many *in vitro* models exist in the literature [108-118] (recent examples summarized in **Table 3)**, none currently incorporate all the necessary stimuli for proper BBB formation and maintenance. Presented below is an overview of the most common sub types of *in vitro* BBB models: static 2D culture systems, "organoid" systems, and microfluidic systems. Due to the diversity of microfluidic designs, microfluidic models are further broken into microfluidic transwell systems (μF-TW), and microfluidic lumen systems (μF-L) for discussion.

2.4.1 Static 2D Culture Systems

Static culture systems are the most commonly used model for preliminary analysis of BBB drug interaction *in vitro* due to their affordability, simplicity, and high throughout capabilities. Brain endothelial cells (both primary and immortalized cells have been sourced from various origins including human, rat, mouse, etc.) are commonly used for early stage evaluation of toxicity. Transwell plates in which cells are cultured on a semi-permeable polycarbonate membrane suspended between two media reservoirs are also a common tool for preliminary drug screening due to their ability to co-culture up to three cells types simultaneously, ability to perform non-destructive barrier measurements via

TEER electrodes, and ability for high throughput scale up [119]. Transwell tri-cultures of endothelial, astrocyte and pericyte cells have recently become more common in the literature [82], and while they do provide advantages to mono-culture systems (more appropriate junctional and surface receptor expression is mediated by presence of astrocytes and pericytes, respectively), they are limited in their ability to recapitulate *in vivo* physiology due to the lack of direct cell contact between cells types limiting cell to cell signalling to that which can be accomplished via the diffusion of soluble factors and the absence of flow, a critical for proper endothelial cell differentiation [120].

2.4.2 Organoid Culture

It is well established in the literature that 3D culture is superior to 2D culture *in vitro*. *In vivo,* cells respond to a number of cues including mechanical and chemical stimulation from the surrounding cells and ECM [121]. Spheroid culture techniques emerged in the 1950s as one of the first 3D cell culture systems. While they were originally used for the study of tumor aggregates, spheroids have been applied to many other organ systems. Multicellular spheroidal BBB (SP) models are simple to make, requiring only the three cell types (and appropriate cell culture reagents), a multichannel pipette, and an agarose coated round bottom well plate (or hanging droplet culture plate). When co-cultured in suspension within an appropriate plate, astrocyte, pericyte, and endothelial cells will spontaneously arrange into spheroids with a physiologically relevant distribution of cells. Astrocytes localize in the core, pericytes localize in the middle, and endothelial cells line the outside of the spheroid. Flow cytometry analysis of endothelial cells from these cultures has further supported literature evidence that indicates the expression of key receptors relies on direct contract with both astrocyte and pericyte cells simultaneously.

Exclusion of either cell type, or sequential exposure of all cell types decreased the degree to which endothelial cells mimicked *in vivo* properties [82]. Spheroids provide several advantages over other *in vitro* models due to their ability to facilitate direct contact and appropriate arrangement of relevant cell types in 3D, ease of scale up, affordability, and simplicity. Spheroid cultures are not capable of facilitating TEER measurements, but they can be monitored via optical and fluorescent miscopy throughout experimentation. In addition, BBB spheroid cultures are not currently able to incorporate flow, but studies to accomplish such culture systems using microfluidics are underway in the scientific community for other organ systems and could be readily adapted to the culture of BBB spheroids [35, 82, 122].

Other "organ level" assays available for the study of the BBB include commercially available angiogenesis assays (Corning Matrigel). In these assays, brain endothelial cells can be cultured alone or in combination with relevant support cells and evaluated using standardized assay metrics. These models are of particular use to the study of the blood tumor barrier (BTB) and the evaluation of anti-angiogenic chemotherapeutics. Like spheroids, these simple and affordable assays are capable of scale up and readily facilitate microscopic monitoring in a format that allows for the direct cell contact of relevant cell types in a 3D microenvironment. However, the microtubule structures formed by such assays are not perfusable and cannot be used for permeability or drug transport studies, limiting their use in drug development [82, 123].

2.4.3 Microfluidic Culture of the BBB

As discussed above in the review of OOAC models for drug discovery and development, recent advancements in microfabrication technologies have enabled the emergence of microfluidic culture systems for the study of many organ systems, including the BBB. Microfluidics allow researchers the ability to precisely control the microenvironment in a spatial and temporal fashion that cannot be accomplished with other *in vitro* systems. Additionally, microfluidics enable the culture of cells in more relevant dimensions (i.e. micro- vs. milli-) [106]. Despite a large investment into the development of *in vitro* BBB devices, no physiologically relevant *in vitro* BBB models currently exist. Major challenges lie in the integration several key components that maintain the key functionality and physiological relevance: endothelial cell specialization in response to shear stress [120, 124], direct cell-cell interactions between cells types [82, 125], and appropriate lumen geometry [104]. Recent publications in the field have made progress in addressing these issues individually, but none so far have been successful in the simultaneous incorporation of these parameters. Additionally, none of the currently published *in vitro* BBB models take the composition of the ECM into consideration during design, despite significant evidence that ECM composition can impact the health and relevant culture of NVU cell types [84]. Due to the dire need for better *in vitro* BBB screening tools, a number of different techniques have been employed in an attempt to integrate these key components into a single system, resulting in a diversity of microfluidic models of the BBB in the literature [108, 110, 112, 116, 118, 126-128].

2.4.3.1 Microfluidic Transwell Models of the BBB (μF-TW)

As the name implies, microfluidic transwell systems are microscale adaptations of transwell culture systems. Although some single layer devices exist, these devices are typically multi-layered microfluidics, resulting in increased cost and technical expertise to fabricate and operate. Due to the complex nature and small culture area, microfluidic transwell systems have a limited ability to recover cells from culture for downstream analysis. Owing to the diversity of designs (single and double layered) microfluidic transwell systems vary in their ability for high resolution microscopy during experimentation, but many readily facilitate the incorporation of electrodes for TEER measurements, enabling them the distinct advantage of performing real time barrier monitoring during experimentation in the presence of flow.

Of the μF-TW BBB devices in the literature, the Wikswo group has produced the most comprehensive model to date. Their device can facilitate the co-culture of primary human endothelial, pericyte, astrocyte, and neuron cells in the presence of flow. Endothelial cells are seeded on a transwell membrane in one compartment, and support cells are suspended in a collagen I gel in a separate chamber. This model included more cell types in the presence of flow than any other model to date, but it is limited by the inclusion of the transwell membrane that prevents direct cell signaling from the support cells to the endothelial cells and the presence of a sub-optimal hydrogel system for neural cell culture. Additionally, they reported limitations in their ability to take reliable TEER measurements [118].

2.4.3.2 Microfluidic Lumen Models of the BBB (μF-L)

As discussed in previous sections, the development of engineered tissue systems with a functional and perfusable vasculature component has long been a challenge in the field of tissue engineering. In recent years, this problem has been addressed with the development of several protocols for the reliable construction of channels within hydrogels or microfluidic devices that can be seeded with endothelial cells to form perfusable vessels of consistent size and geometry (**Section 2.2.4**). Of these technologies, only the viscous fingering and direct seeding of endothelial cells into preformed PDMS channels have been employed in the context of an *in vitro* BBB lumen device design.

Using the viscous fingering technique, the Ingber Lab has produced a 3D μF-L model of the BBB that is able to incorporate *either* astrocytes or pericytes along with an endothelial lumen in a collagen I hydrogel. This model successfully facilitates the co-culture of support and endothelial cells in a lumen structure, but remains limited due to the inappropriate matrix composition, large lumen diameter (~1mm), and inability to simultaneously incorporate multiple support cell types. Additionally, as noted by the authors, the device is further limited due to the exuberant amount of media needed to maintain constant flow at a rate that will generate physiologically relevant shear stress in the lumen [110].

The Kamm group has also produced a μF-L model of the BBB. Their model utilizes micropillars to spatially compartmentalize different cell laden hydrogels around a square PDMS channel that is seeded with endothelial cells to form a lumen. Their device facilitates the co-culture of primary rat astrocytes, endothelial cells, and neurons in a collagen I

hydrogel, but cell contact is limited by the spatial compartmentalization of relevant cells types to their separate culture chambers [129].

Table 3. Summary of recently published in vitro BBB models.

First Author	Publication Year	Digital Object Identifier (DOI)	Model Name	Model Type	BBB Cell Types Used [origin, p/i]	3D ECM	Cell Contact	High Throughput	Relative Cost	Shear	Fabrication
Adriani	2017	10.1039/C6LC00638H	N/A	μF-L[a]	hCMEC/D3 [human,i]; cortical neurons [rat,p]; astrocytes [rat,p]	Collagen I	Limited[b]	No	Moderate	No	Simple
Herland	2016	10.1371/journal.pone.0150360	3D BBB Chip	μF-L	hBMVEC [human,p], HBP [human,p], HA [human,p]	Collagen I	Limited[c]	No	Moderate	Limited[d]	Moderate
Walter	2016	10.1016/j.snb.2015.07.110	N/A	μF-TW	hCMEC/D3 [human,i]; endothelial [rat,p]; astrocyte [rat,p]; and pericyte [rat,p]	None	No	No	Moderate	Yes[e]	Moderate
Wang	2016	10.1002/bit.26045	BBBOC	μF-TW	BMEC [human,hiPSC derived]; atrocytes [rat,p]	None	No	No	Moderate	Yes	Complex
Cho	2015	10.1038/srep15222	N/A	μF-L	RBE4 [rat,i]	Collagen I	No	No	Moderate	No	Moderate
Kim	2015	10.1063/1.4917508	N/A	μF-L	b.End3 [mouse,i]	Collagen I[f]	No	No	Moderate	Yes	Moderate
Brown	2015	10.1063/1.4934713	NVU	μF-TW	hBMVEC [human, p]; HP [human, p]; HA [human, p]; neurons [human, hiPSC derived]	Collagen I	No	No	Moderate	Yes	Complex
Sellgren	2015	10.1063/1.4935594	N/A	μF-TW[g]	bEnd.3 [mouse, i]; C8D1A [mouse, i]	Collagen I	No	No	Moderate	Yes	Moderate
Deosarkar	2015	10.1371/journal.pone.0142725	B^3C	μF-TW	RBEC [rat, p]; neonatal astrocytes [rat, p]	None	No	No	Moderate	Yes	Moderate
Prabhakarpandian	2014	10.1039/c2lc41208j	SyM-BBB	μF-TW	RBE4 [rat, i]	None	N/A	No	Moderate	Yes	Complex
Urich	2013	doi:10.1038/srep01500	MSC-BBB	SP	HBMEC [human, p]; HA [human, p]; HBVP [human, p]	None	Yes	Yes	Low	No	Simple
Griep	2013	10.1007/s10544-012-9699-7	BBB on a Chip	μF-TW	hCMEC/D3 [human, i]	None	No	No	Moderate	Yes	Moderate
Achyuta	2013	10.1039/C2LC41033H	N/A	μF-TW	RBE4 [rat, i]; "Nerual Cell Mix" [rat, p: ~4% neurons, 95% astrocytes, 1% microglia]	None	No	No	Moderate	Limited[i]	Moderate[j]
Booth	2012	10.1039/c2lc40094d	μBBB	μF-TW	b.End3 [mouse, i]; C8D1A [mouse, i]	None	No	No	Moderate	Yes	Complex
Yeon	2012	10.1007/s10544-012-9680-5	N/A	μF-TW	HUVEC [human, p]	None	No	No	Moderate	Yes	Moderate
Cucullo	2010	doi.org/10.1038/jcbfm.2010.162	DIV-BBB	μF-TW[k]	HBMEC [human, p]; HA [human, p]	None	No	No	Moderate	Yes	Moderate
Nakagawa	2008	10.1016/j.neuint.2008.12.002	N/A	TW	RBEC [rat, p]; cerebral astrocytes [rat, p]; cerebral pericytes [rat, p]	None	No	Yes	Low	No	Simple
Notes											

[a]Authors use an angiogensis chip that could potentially be classified seperately [b]Contact is limited by pillars compartmentalizing seperate support cell cultures [c]Only one support cell type at a time was co-cultured with the endothelial cells [d]Flow was not continuously maintained during experimentation due to exuberant media requirement [e]Authors use perstaltic pumping method to recirculate media [f]Authors used a bioprinting methodology [g]polyester membrane

2.5 Pathophysiology of the BBB

2.5.1 The Blood Tumor Barrier (BTB)

While the development of a healthy BBB model is the primary focus of this work, because the downstream application is use in the development of novel nanomedicines for the treatment of MB, a brief discussion of pathophysiological BBB is necessary. In cases of cancer, drug delivery to brain tumors is further limited by the presence of the BTB, a secondary barrier that develops from tumor microvessels. Interestingly, BTB physiology varies with tumor type and sometimes within tumor subtypes. While some tumor BTBs maintain the limited permeability of healthy BBB, typically tumor BTBs are more

permeable than healthy BBB. This increase in permeability, or “leakiness”, in the microvessels immediately surrounding tumor sites has been demonstrated to be the result of tumor cell mediated tight junction degradation. Existing *in vitro* BTB models are adaptations of established BBB models, and face the same challenges [89, 130].

2.5.2 The BBB and Medulloblastoma (MB)

A particularly relevant example of the implications of BBB/BTB physiology on tumor prognosis and treatment can be illustrated by examination of the different subtypes of MB. MB is the most common pediatric brain tumor, accounting for 10% of all childhood cancer fatalities. MB is classified into sub types based on the presence of certain genetic mutations and the site of origin of the tumor. Cases associated with mutations to the sonic hedgehog (SHH) pathway are more aggressive, carry a poorer prognosis, are more resistant to chemotherapy, and are more likely to recur. By comparison, cases that are associated with mutations to the WNT/β-catenin signaling pathways tend to be very curable. This difference in prognosis and treatability has recently been found to be due to differences in how the tumors affect the integrity of the BBB. In WNT subtype MB, the tumor cells secrete inhibitors to the WNT signaling pathway that result in disruptions to BBB integrity and an increase in barrier permeability. This increase in permeability around the tumor site enables more effective delivery of chemotherapeutics and contributes to the disparity in prognosis between the subtypes of MB [131].

2.6 Nanomedicine

Nanomedicine is a broad and diverse field with potential applications in imaging and diagnostics, cancer treatment, and the treatment of neurological diseases, and NP platforms have been developed for a wide range of diagnostic, therapeutic, and combinatorial ("theranostic") applications. A comprehensive review of the field of nanomedicine as whole is outside the scope of this work, but is readily available elsewhere [132-137]. A brief overview of synthesis techniques and an overview of the NP types proposed for use in our future studies is briefly presented for context. This work is interested in the interaction of our NPs with the BBB. Specifically, this and future work aims to determine whether functionalization of lipid polymer nanoparticles (LPNP) with apolipoprotein A1 (ApoA1) will translate to an increase in BBB penetrance, and if this penetrance could be visualized and quantified in our MLS-BBB. Furthermore, through such studies, we aim to determine if our MLS-BBB will provide more predictive results of ensuing *in vivo* studies (mice) relative to transwell culture. Thus, examples of NP based approaches for increasing BBB penetrance are briefly discussed, with focus paid to the influence of physical and chemical particle properties on BBB NP interactions.

2.6.1 Nanoparticle Strategies for Crossing the BBB

As discussed in **Section 2.3.2**, nanoparticle platforms have been under active investigation as a potential "Trojan Horse" strategy to increase drug delivery to the brain. NPs are particularly good candidates for such studies due to their size and tuneable physiochemical properties [97, 138, 139]. Effective delivery across biological barriers is essential for the successful development of effective nanomedicines, and targeted delivery

of drugs across endothelial barriers remains a significant challenge for brain targets, where transport is extremely limited by the BBB. A number of NPs have been studied for their potential BBB crossing abilities [140], of which only LPNP and high-density lipoprotein (HDL) particles are contextually relevant to this work.

2.6.1.1 High Density Lipoprotein (HDL)

HDL is an endogenous nanoparticle involved in a wide range of functions in the body that is a prime candidate for use in drug delivery studies due to its natural immunogenicity and ability to be transported by cellular receptors [137]. Apolipoproteins like ApoA1 and ApoE from natural HDL can be utilized to make engineered HDL-mimetic NPs that maintain bioactivity similar to native HDL [141]. HDL particles are particularly well suited as BBB crossing vectors due to their small size (10-25nm), and ability to be transported by endogenous transporters [137].

2.6.1.2 Lipid Polymer Nanoparticles (LPNP)

LPNPs are composed of a stable polymeric core surrounded by a lipid shell that can be functionalized with polyethylene-glycol (PEG) polymers to increase retention in circulation by reducing filtration from circulation by the liver and kidneys. LPNPs exhibits complementary characteristics of both polymeric NPs and liposomes, enabling their superior drug loading and delivery [134]. Many researchers have demonstrated interest in further optimizing the potential of LPNPs by hybridizing them with components of naturally occurring NPs such as the apolipoproteins associated with HDL [141].

2.6.2 Microfluidic Synthesis of BBB Crossing Nanoparticles

While nanoparticle composition is of most importance to BBB crossing ability, the synthesis methodology also warrants brief discussion as robust synthesis is critical for the reliable production of particles with homogenous physiochemical properties, a necessary factor in the successful implementation of any nanoparticle system. NP synthesis was traditionally conducted via bench top reactions in which nanoprecipitation occurred upon agitation of immiscible solvents with magnetic stirring or vortex mixing. While such reactions do produce nanoparticles, such production methods often result in particles that are inhomogeneous in their size and composition, rendering them poor candidates for translation to drug products that must meet industry standards for consistent quality and purity. Additionally, bench top synthesis is a batch process that is not conducive to scale up to industry relevant production levels that would be necessary for the completion of human clinical trials. Thus, benchtop synthesis, while sufficient for preliminary studies of nanoparticle formation, is sub-optimal for the synthesis of nanoparticles that aim to eventually be translated to effective drug products [142, 143].

Microfluidic technology has emerged as a robust platform for continuous synthesis of nanoparticles with controlled physiochemical properties [144-146]. These improvements are largely achieved through the reduction in mixing times that reduces the formation of precursor aggregates, a common issue in bench top synthesis. Several techniques can be used in microfluidic synthesis of nanoparticles that leverage the ability of microfluidics to precisely control flow patterns. In our lab, we employ convection based microfluidic mixing via microvortices to synthesize the multifunctional nanoparticles that will be evaluated on our MLS-BBB. This synthesis platform creates a controlled, rapid

mixing interface between two nanoparticle precursor solutions and enables continuous production (g/h) of nanoparticles with monodisperse physiochemical properties [145].

CHAPTER 3. DEVELOPMENT OF MLS-BBB

3.1 Introduction

The BBB is the specialized vasculature of the CNS responsible for the regulation of transport into the brain from systemic circulation. While the BBB is essential for proper neuronal function, it severely restricts the transport of molecules to the brain and poses a significant challenge to drug development and delivery [59]. Due to the species variation in BBB structure and function that exists between human and animal models, the development of a human cell based *in vitro* model of the BBB is critical for the cost-effective evaluation of novel drug candidates [100]. Despite a large number of increasingly complex *in vitro* BBB models being presented in the literature [105, 108, 112, 118], no model has been adapted for widespread use in preliminary drug studies in place of traditional, static, transwell culture systems. This can be attributed to a number of factors including a lack of sufficient evidence that demonstrates their increased predictive power over simpler models, increased cost of fabrication and operation, lack of ability to perform high throughput screening, and increased technical expertise required to establish these models [105].

Several key components contribute to the expression of physiologically relevant BBB endothelial cell specializations including exposure to shear stress [147], direct cell-cell interactions between NVU cell types [82], and a functional lumen structure [104]. Additionally, recent research indicates that proper ECM composition is necessary for non-reactive culture of astrocytes [84]. To date no existing *in vitro* BBB models simultaneously include flow and direct cell contact between astrocytes, pericytes, and endothelial cells in

a lumen geometry. Furthermore, all currently published microfluidic BBB models that include a hydrogel component use a collagen I gel [110, 112, 118], which has been demonstrated to induce reactive gliosis in astrocytes [84]. In this work, we address these challenges through the development of our novel microfluidic lumen system of the BBB (MLS-BBB). Our MLS-BBB is designed to directly co-culture human astrocytes (HA) and human brain vascular pericytes (HBVP) with a perfusable, cylindrical lumen of immortalized human brain endothelial cells (iHBMEC) contained within a 3D hydrogel system tuned to mimic the properties of brain ECM.

3.2 Materials and Methods

3.2.1 Hydrogel Optimization for Appropriate Astrocyte Culture

High concentration collagen I (Corning) and growth factor reduced, phenol red free, Matrigel (Corning) were studied individually, and in combination with brain relevant ECM proteins (Tenascin C, TC; hyaluronic acid HY) to determine the best 3D culture conditions for human astrocytes (P2-3, Sciencell). Matrigel was selected for use due to similarities between its composition (~30% collagen IV, ~60% laminin, ~8 entactin) and in vivo brain ECM. Collagen I was included for comparison to commonly used methodologies in existing *in vitro* BBB devices.

HAs were seeded in hydrogels at a concentration of 3E5 cells/mL and cultured for 1-7 days before being imaged or recovered for use in HT-qPCR analysis of reactive gliosis marker expression (**Figure 4**). Six 3D culture conditions were tested and compared to a 2D culture control. Composition of 3D ECM conditions tested were as follows: Collagen I (6mg/mL), Matrigel (6mg/mL), Collagen I (6mg/mL) + Hyaluronic Acid (3mg/mL) +

Matrigel (3mg/mL), Matrigel (6mg/mL) + Hyaluronic Acid 3mg/mL) + Tenascin C (5ug/mL), Matrigel (6 mg/mL) + Hyaluronic Acid (3mg/mL) and Matrigel (6mg/mL) + Tenascin C (5ug/mL). Cells were harvested after either one day or one week of culture for qPCR analysis of the expression of 13 genes associated with the presentation of a reactive gliosis state in astrocytes.

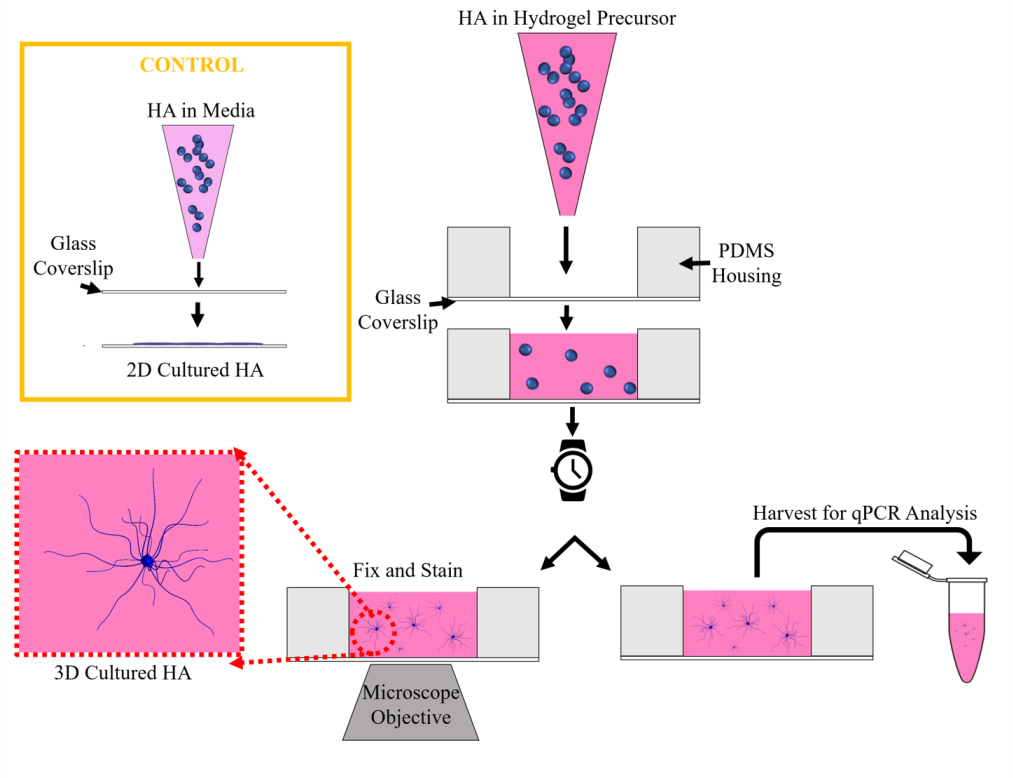

Figure 4. Schematic of workflow for gel tuning study. Human astrocytes were suspended in hydrogel precursor solutions and injected into PDMS culture wells bonded to glass coverslips.

3.2.2 qPCR Analysis

Markers of reactive gliosis were selected via review of relevant literature [72, 85-88, 148-152]. Sequences for each gene target were obtained from the NCBI nucleotide database and primers were developed for each target using Primer3Plus software and

BLAT tools. Primers were ordered from Eurofins Genomics and suspended in TE buffer (TekNova) at a concentration of 100μM. RNA was extracted from 3D cultures via Quiagen RNeasy micro kits. In samples obtained from 3D culture, 40μL of proteinase K was added to lysates and an additional incubation at 55ºC was added before removal of genomic DNA in order to remove residual matrix proteins from the sample as indicated by manufacturer. Hydrogels containing collagen I were further processed in a Qiashredder column to remove residual ECM proteins from the sample. A detailed discussion of RNA extraction methodologies and justification for differences in sample handling can be found in **Section 6.3**. Extracted RNA purity was determined from the 260/280 ratio for all samples. Samples were analyzed for degradation by obtaining a RNA integrity number (RIN) from bioanalyzer data. RIN scores of 6+ are considered of sufficient quality for use in HT-qPCR, and tested samples ranged in quality from 6.5-9.9. RNA concentration was measured via spectrophotometry (Take3, BioTek plate reader) and diluted to a homogenous concentration across all samples with RNase free water before conversion to cDNA for PCR. Conversion to cDNA was accomplished via high throughout reverse transcription kit (ThermoFischer) in a standard thermocycler via manufacturer's instructions. High throughput qPCR was carried out in the Georgia Tech Genomics Core via the Biomark Fluidigm System with Evagreen detection. Three biological replicates of each sample were included for analysis. Raw cycle threshold (Ct) values were normalized to the geometric mean of 3 housekeeping genes to obtain ΔCt values. ΔΔCt were obtained via normalization to 2D cultured astrocytes to facilitate comparison across 3D culture conditions and fold change values were obtained by taking $2^{-\Delta\Delta Ct}$.

3.2.3 Device Component Preparation and Device Assembly

3.2.3.1 PDMS Component Preparation

Polydimethylsiloxane (PDMS) was used for the fabrication of culture housings due to its optical properties [153] and permeability to gaseous oxygen exchange [154, 155]. All PDMS devices used were cast via traditional soft lithography on 3D printed molds (Objet Eden printer, Georgia Tech Invention Studio). PDMS base was combined with curing agent in a ten to one ratio before being thoroughly mixed and poured into molds. Molds were degassed for 20 minutes at room temperature to remove bubbles before being cured for at least 1 hour at 80ºC. After cooling to room temperature, PDMS slabs with housing, element, or reservoir features were cut out of molds and inlets and outlets were punched with a 1mm biopsy punch. Reservoirs were punched with 8mm biopsy punches to increase the volume available for flushing and to accommodate reservoir expanders for administering shear to devices.

3.2.3.2 Sacrificial Element Injection Mold Assembly

Cylindrical sacrificial element injection molds were made by reversibly bonding two semi-circular PDMS molds as depicted in **Figure 5A**. Two element molds were used to cast each batch of 150 μm elements. Inlets and outlets were punched in the alignment bulbs of one mold to allow for infusion of the gelatin solution after injection mold assembly. Inlets and outlets were punched with a ~30 degree angle offset in element molds to prevent the entrapment of bubbles in the alignment bulbs during injection molding. Both sides of the injection mold were cleaned three times with tape and one side of the mold was then plasma cleaned for 2 minutes before being aligned with its complimentary (un-

plasma cleaned) mold under a stereoscopic microscope. Assembled injection molds were clamped between aluminium slabs and heated to 80ºC for at least one hour before proceeding with the element casting process.

3.2.3.3 Sacrificial Element Casting

Elements were cast using previously validated methodologies depicted in **Figure 5A** [42]. Briefly, Pluronic F127 (PF127, 6% in PBS) was injected into each injection mold to prevent the attachment of gelatin elements to the PDMS. PF127 was allowed to adsorb to the PDMS for one hour and was aspirated out via vacuum suction immediately before gelatin injection. A solution of 10% gelatin (from porcine skin, in PBS) was vortexed and heated to 80ºC for ten minutes prior to injection into molds with a 1mL syringe and 22-gauge lure lock needle. In order to prevent gelation before injection was complete, the syringe and needle were also heated to 80ºC. In some cases, the gelatin solution was doped with GFP to allow for fluorescent imaging of sacrificial elements within devices. Sacrificial elements were placed in humid chambers and cured for at least 6 hours at 4ºC before use.

3.2.3.4 MLS-BBB Device Assembly

Double sided silicone tape (50µm thick, 3M) was laser cut (Universal Laser System VLS3.50) in designs matching housing and reservoir geometries and included in device assembly to reduce leaks occurring from incomplete plasma bonding caused by the surface roughness of PDMS parts cast from 3D printed molds. After fabrication of all individual components, device housings were assembled together as depicted in **Figure 5**.

Briefly, the bottom of the reservoirs and the top of the housings were cleaned three times each with scotch tape to remove dust before the application of silicone tape to the bottom of the reservoir. Housings and reservoirs were then plasma cleaned for 2 minutes on high and bonded together. Assembled housings were clamped between aluminium slabs and heated at 80ºC for at least 30 minutes before subsequent cleaning and sterilization (70% ethanol, UV sterilization) for use in cell culture.

Assembled housings were prepared for assembly into complete devices by cleaning the culture area of the housing with 70% ethanol, drying with a pressurized nitrogen gun, and cleaning three times with tape. Glass slides were cut to appropriate sizes with glass scorers and slides were subsequently cleaned with 70% ethanol and dried. Silicone tape for improved attachment of housings to glass was added after the glass was cleaned three times with tape. Prepared housings and glass slides were plasma cleaned for 2 minutes while a sacrificial element was carefully recovered from an injection mold with tweezers and prepared for placement. Sacrificial elements were carefully aligned within the culture chamber of the housing and were sealed in place in the device by careful alignment of the silicon tape coated glass slide to the housing. This design and assembly facilitates the complete encapsulation of the sacrificial element by the cell laden hydrogel while preserving access to eventual inlets and outlets for cell seeding and media perfusion.

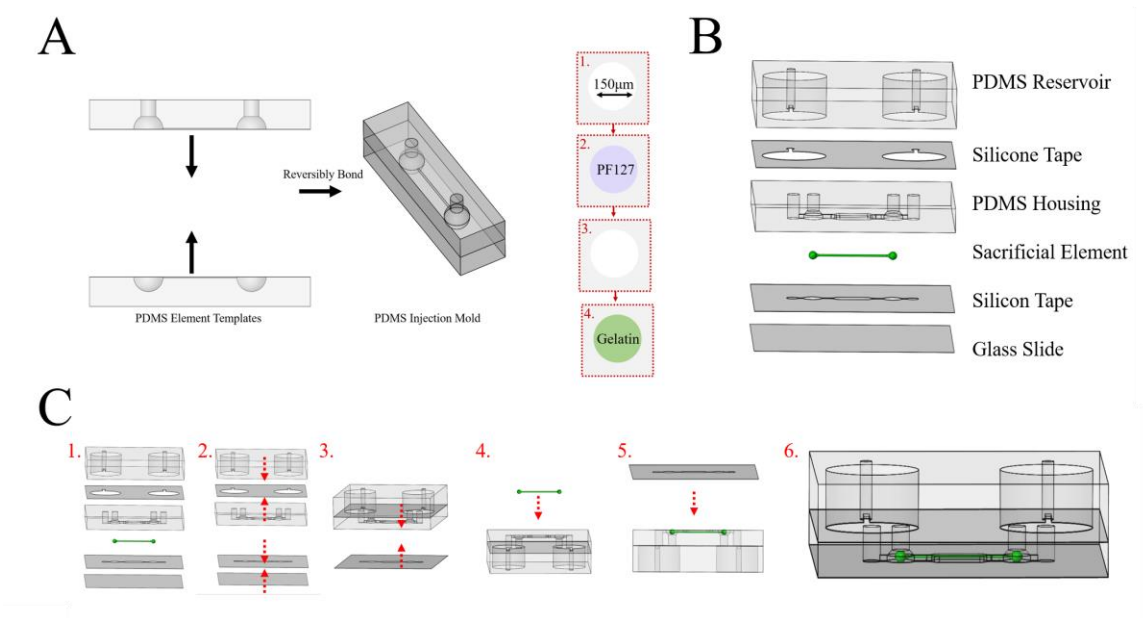

Figure 5. Sacrificial element formation and encapsulation in device. (A) Sacrificial element injection molds were fabricated by reversibly binding two PDMS slabs with semicircular features. (B) Explosion view of all device components (C) Schematic of the assembly process of device components.

3.2.4 Channel Formation and Cell Seeding

3.2.4.1 Channel Formation

After sealing elements in devices, PDL (1mg/mL, Advanced Biomatrix) was injected around the element to prevent delamination of the hydrogel from housing walls. Devices containing elements in PDL were incubated for at least one hour at room temperature, in a humid chamber. Devices were kept in clear petri dished during this incubation and placed under UV for additional sterilization. After sterilization, 1mm plugs were placed in the inside set of inlet/outlets to prevent the hydrogel from blocking them and preventing cell seeding and media perfusion. Reservoirs were filled with PBS prior to plug placement and hydrogel seeding to prevent bubbles from entering the culture chamber.

Cell laden or plain gel was then slowly injected around element via a 20uL injection. After gelation of hydrogel for 15min at room temperature, media was added to the reservoirs and the plugs were carefully removed from the inlet and outlet. Sacrificial elements were then melted by incubation at 37ºC for at least 15 minutes and exhaustively flushed via the periodic exchange of reservoir media. In some cases, sacrificial elements were doped with GFP during casting so that complete element clearance from the device could be confirmed before attempting cell seeding.

3.2.4.2 Cell Seeding

Human astrocytes (HA, Sciencell, P3) were included in the hydrogel at a concentration of 3E5 cells/device (~1.5cells/mL in hydrogel solution, 20µl/device). Human brain vascular pericytes (HBVP, Sciencell, P2) were added to the cleared channel in a single injection. Before injection, reservoirs were filled with media and inlet/outlet plugs were placed in the inlet and outlet used for hydrogel seeding to prevent HBVP cells from accumulating outside of the channel space. A 10µL injection of a 1.5E7 cell/mL solution was used for every chip. HBVP cells were allowed to adhere for 30 min before media exchange from reservoirs. HBVP presence in channels was confirmed via observation with phase contrast microscopy and cells were incubated for at least 12 hours before iHBMEC seeding. iHBMEC cells (P2-4) were injected into the channel space in 2 10µL injections of 3E7 cell/mL solutions. Chips were inverted after the first injection to encourage iHBMEC cell attachment to all channel walls. Inverted chips were incubated at 37ºC and 5% CO2 for 30 minutes before receiving the 2nd HBMEC injection. 30 minutes after the second iHBMEC injection, reservoirs were filled with media and devices were incubated overnight to allow for iHBMEC cell attachment and lumen establishment. Lumen

formation and constriction by endothelial cells was observable as soon as 5 hours after iHBMEC addition to channels. After at least 12 hours of iHBMEC static culture in the channels, devices were modified to facilitate exposure to physiologically relevant shear rates.

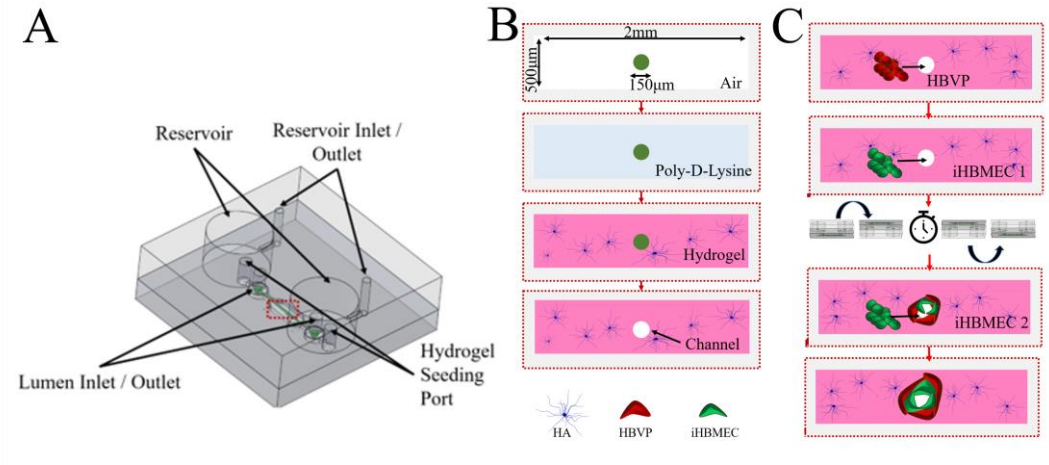

Figure 6. Channel formation and cell seeding in assembled device. (A) Schematic of assembled device with critical features labeled. (B) Sacrificial elements were suspended in empty housings with the alignment bulbs placed at the eventual inlet and outlets. PDL was injected and allowed to adsorb to the surface of the housing and element for one hour under UV sterilization before careful injection of the HA laden hydrogel precursor around the element. Devices were cured at room temperature for 15 minutes before being placed under incubation (37ºC, 5% CO_2) and flushed exhaustively with astrocyte media overnight to dissolve the sacrificial element and produce a channel. (C) HBVP and iHBMEC cells were added to culture via infusion into the channel space. HBVPs were seeded a single time and allowed to adhere for 12 hours before the addition of iHBMEC cells in two doses. After the first injection of iHBMECs, devices were flipped over and incubated for 30 minutes to allow iHBMEC cells to cover all sides of the channel space. Devices were then placed right side up and injected with iHBMEC cells a second time. Devices were incubated for at least 24 hours after cell seeding before administration of flow to allow time for lumen formation.

3.2.5 Administration of Shear via PF-GDF

After at least 12 hours of iHBMEC static culture in the channels, devices were modified to facilitate exposure to physiologically relevant shear rates. Autoclaved 1mL pipette tips (base diameter = 8mm = reservoir diameter) were inverted and carefully placed into the inlet reservoir to create a reservoir expander capable of accommodating the ΔV (547µL) necessary to generate a wall shear stress of ~ 4 dynes/cm^2. All reservoirs were then completely evacuated of media and programmable syringe pumps were used to fill the inlet reservoir with 547µL of media while the outlet reservoir was being help empty via vacuum aspiration. One minute later, infusion to the inlet reservoir was started at 8.93uL/min. The ΔV between the reservoirs was maintained over time via the continuous infusion of media and continuous vacuum aspiration of outlet reservoirs. Holes were drilled in the lids of the petri dish plates to accommodate the tubing for the inlets and outlets and the protruding reservoir expanders to minimize exposure of devices to circulating air in order to protect against contamination.

Devices were originally designed with the intention of submerging them in media and using programmable syringe pumps to withdraw media at a set flow rate as this method has proved successful for the generation of shear over endothelial monolayers in microfluidic transwell cultures [156]. However, due to the sensitivity of our hydrogel systems to mechanical fluctuations in pump activity, this method was not able to be used with our devices. As an alternative, we modified our design to include reservoirs atop the inlet and outlet of our device to enable the generation of flow from the pressure gradient generated by volume differences in the two reservoirs. This method of gravity driven flow is common in the field [58] and was sufficient for flushing, seeding, and feeding devices

but could not readily enable the generation of large enough volume gradients to drive flow at the rates needed to generate physiologically relevant shear rates. Additionally, this method requires the operator to repeatedly exchange media in the reservoirs to maintain the gradient necessary for the generation of flow. To eliminate these issues, we added separate inlets to our reservoirs that enabled media to be infused from the bottom, outer edge of the reservoirs. This enabled the reservoirs to serve as a bubble trap and provided insulation from disturbances generated from the syringe pump. To maintain a steady flow rate over time, vacuum aspiration lines were connected to the outlet reservoirs and vacuum aspiration was continually applied. This enabled the infusion pumps to be set to a flow rate that would maintain the volume difference between the two reservoirs necessary for the generation of a stable flow rate. In test cases where shear stress was necessary, reservoir expanders were added to the inlets of the device to accommodate larger volumes and thus facilitate higher flow rates thru the lumen **Figure 7**.

A

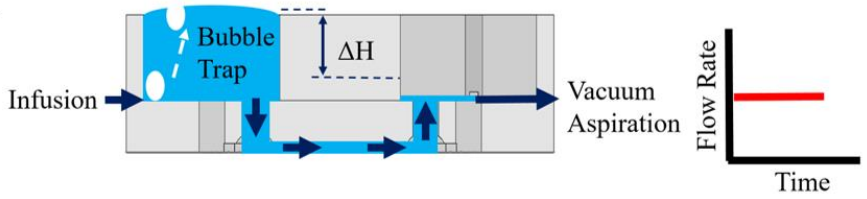

B

Legend		
τ	shear stress	dynes/cm^2
μ	viscosity	kg/ms
Q	flow rate	mL/s
π	pi	unitless
D_L	diameter of lumen	cm
ΔP	pressure drop	kg/ms^2
L	length of lumen	cm
R_L	radius of lumen	cm
ρ	density	kg/m^3
g	acceleration due to gravity	m/s^2
ΔH	fluid height difference between reservoirs	mm
ΔV	volume difference between reservoirs	mL
R_R	radius of reservoirs	cm

$$\tau = \frac{32\mu Q}{\pi D_L^{\,3}} \quad (1)$$

$$Q = \frac{\tau \pi D_L^{\,3}}{32\mu} \quad (2)$$

$$\Delta P = \frac{8\mu LQ}{\pi R_L^{\,4}} = \rho g(\Delta H) \quad (3)$$

$$\Delta H = \frac{8\mu LQ}{\rho g \pi R_L^{\,4}} \quad (4)$$

$$\Delta V = \Delta H \pi R_R^{\,2} \quad (5)$$

C

τ (dyne/cm^2)	ΔH (mm)	ΔV (μL)
1	3	137
2	5	273
3	8	410
4	11	547
5	14	684
6	16	820
7	19	957
8	22	1094
9	24	1230
10	27	1367

Max Volume of Reservoirs = 500uL

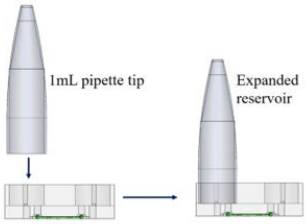

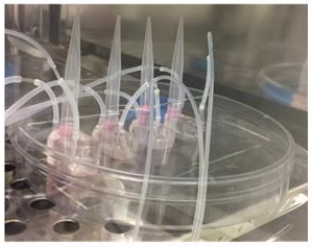

Figure 7. Administration of flow via PF-GDF. (A) Continual infusion and withdrawal from reservoir inlets and outlets enables the generation of a steady flow rate over time while also creating a bubble trap in the inlet reservoir. (B) Equations needed to relate wall shear stress to volume difference between reservoirs. Shear stress is directly related to flow rate and fluid viscosity and is inversely related to channel diameter (Eqns. 1-2). In this case, the pressure drop through the channel is equivalent to the pressure drop due to gravity between the two reservoirs, so the expressions for pressure drop from the Hagen Poiseuille and Bernoulli equations can be equated (Eqn. 3) and used to define a relationship between WSS and ΔH (Eqn. 4) which can in turn be used to define a relationship between ΔV and WSS (Eqn. 5). (C) Left: Table detailing the height/volume difference between reservoirs needed to drive flow at physiologically relevant rates. Middle: Schematic showing how reservoir expanders must be added when the volume difference needed exceeds the max fill volume of the reservoirs (500µL). Right: Image of MLS-BBB devices undergoing constant media infusion to generate a wall shear stress of 4 dynes/cm^2

3.2.6 Histology and Imaging

Traditional immunostaining techniques [71, 157] were used to examine expression of tight junctions (ZO-1) between neighboring endothelial cells. Distinct cell markers (CD31, αSMA, GFAP) were used to examine the spatial distribution and interaction of the NVU cell types. Confocal microscopy was used to acquire 3D reconstructions of cell models (Zeiss 700a). Images were processed with Volocity 3D Visualization software.

3.2.7 Statistics

Detailed discussion of data handling and statistical analysis can be found in **Section 6.5**. Briefly, data are presented are mean values ± standard error of the mean (S.E.M.) for N=3 replicates, unless otherwise noted. All statistical analysis was performed in GraphPad Prism software. For comparisons of the expression profiles of two groups, a Wilcoxon matched pairs signed rank test was used. For comparisons of the expression profiles of more than two groups, a Friedmans' test was used in conjunction with a Dunn's post-test to correct for multiple comparisons. When applicable, p values were adjusted for multiple comparisons. $p < 0.05$ was considered statistically significant.

3.3 Results and Discussion

3.3.1 Hydrogel Tuning Decreases the Expression of Reactive Gliosis Markers in Human Astrocytes

Reactive gliosis of astrocytes has been implicated in many disease states including AD, stroke, and neuro inflammation [85, 86]. Due to the interdependent relationship of the cell types of the NVU, it is likely that improper astrocyte culture conditions could create a

pathophysiological rather than a physiological model of the BBB, which would likely yield non-predictive results if used for preliminary drug studies. To address this potential pitfall, we tailored our hydrogel system to facilitate the appropriate culture of astrocytes via the inclusion of brain relevant extracellular matrix proteins. We tested various combinations of collagen I, Matrigel (Mat), hyaluronic acid (Hy), and tenascin C (TC) [158] to determine the most appropriate culture conditions via the evaluation of the expression of several markers [88] indicative of the presentation of a reactive gliosis state in astrocytes. Markers assessed include markers of astrocytic scar phenotype (NCAM, EGFR), intermediate filament proteins (BFGF, NES, GFAP, VIM), protective activation (SYNM, CLCF1, LIF), damaging activation (IL6, C1R, C1S) and reactive gliosis (LCN2, SERPINA3N, CD109). Expression levels were evaluated in astrocytes isolated from each culture condition to determine the best hydrogel system for physiological astrocyte culture. Additionally, we verified the presence and consistent expression of two markers commonly used for labeling of astrocytes (AQP4, ALDH1L1) as a control.

The fold change in marker expression relative to 2D was obtained for each hydrogel condition via normalization of raw qPCR data to the expression of 3 housekeeping genes and to 2D culture results. The resulting expression profiles were compared to determine which conditions provided the lowest relative expression of markers after one day and one week of culture. Our results support existing literature evidence that 3D culture results in a less reactive state than 2D culture [159]. While no single hydrogel condition performed best for every marker assessed, our results indicate that MatHy and MatTC each provide a significant reduction in marker expression when compared to collagen I gels after one week of culture. This result is consistent with literature evidence suggesting that TC can

contribute to the recovery of non-reactive state in the 2D culture of astrocytes [158], and makes logical sense as Matrigel is primarily composed of BBB relevant ECM proteins (~30% collagen IV, 60% laminin, and 8% entactin). Furthermore, comparison of expression profiles over time (one day vs. one week) indicates that both MatHy and MatTC hydrogels facilitate a significant reduction in marker expression over time, further indicating their ability to facilitate the recovery of a quiescent state. Based on these results, MatTC hydrogels were selected for use in our MLS-BBB device.

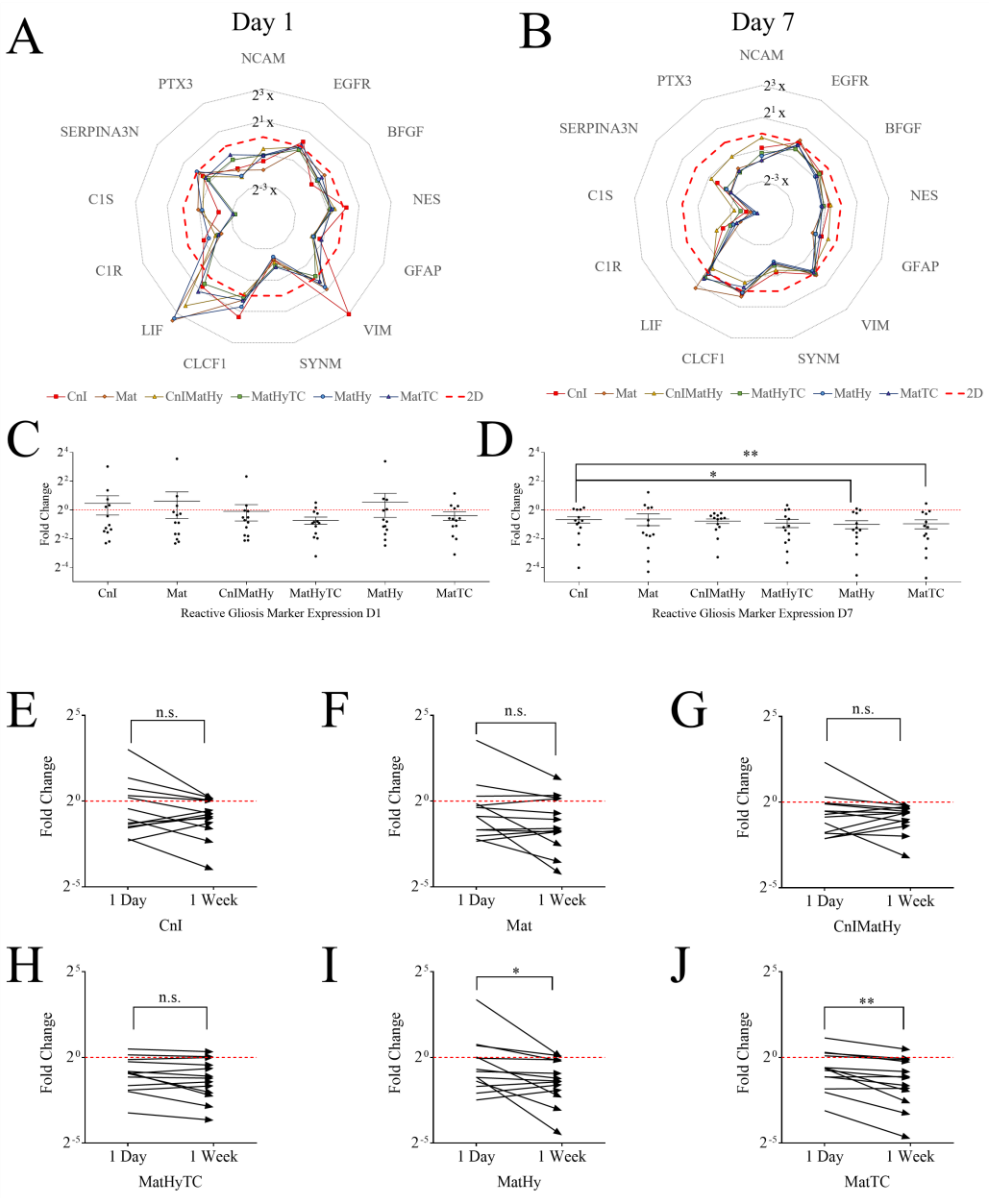

Figure 8. MatTC hydrogels exhibit lowest relative expression of reactive markers. Radar plots depicting the expression of markers for reactive gliosis relative to 2D culture after (A) 1 day and (B) one week of culture in various 3D hydrogel compositions. No significant differences in expression profiles were observed across the hydrogel compositions tested after one day of culture (C) Only MatHy and MatTC hydrogels have significantly different expression profiles than collagen I after one week of culture. (E-J) Before and after plots showing the change in expression profile over time for each hydrogel condition assessed. Only (I) MatHy and (J) MatTC demonstrate a significant reduction in marker expression over time. Data depicted as mean +/- SEM for an N=3 for all samples. *p<0.05, **p<0.01, n.s. – not significant.

Microscopic examination of astrocytes further validated the suitability of MatTC for appropriate 3D culture. Inspection reveals marked morphological differences from 2D culture including a reduction in cell body size and an increase in the number, length, and bifurcations of astrocyte projections (**Figure 9**)

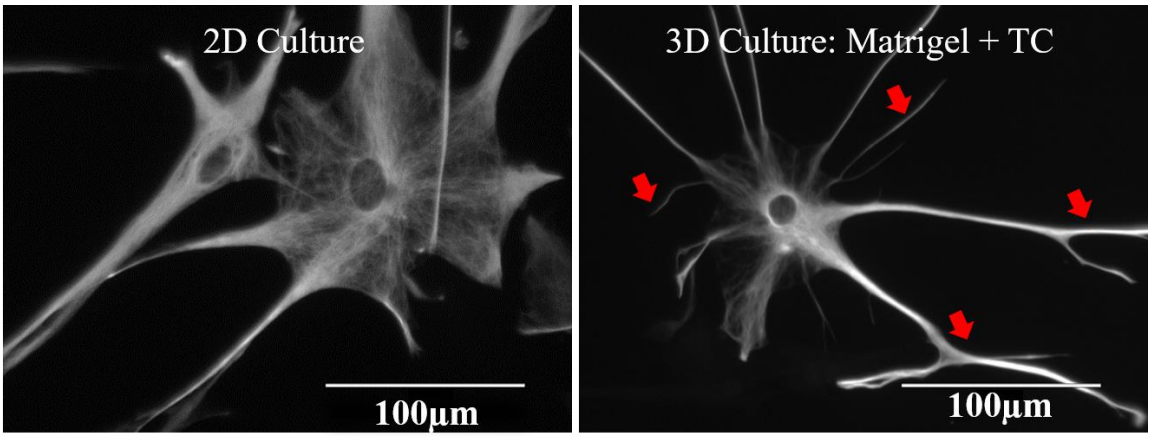

Figure 9. Observable morphological differences between 2D and 3D culture. HAs cultured in MatTC hydrogels exhibit more appropriate morphology indicated by the reduction in cell body size and an increase in the number, length and bifurcations of astrocytic projections (red arrows).

3.3.2 Sacrificial Element Methodology Enables the Formation of Perfusable iHBMEC Lumens

In this work, we adapted a sacrificial element method to craft perfusable channels within cell laden hydrogel systems as previously described [42]. Encapsulation of a preformed sacrificial gelatin element within our PDMS device housing enables the full encapsulation of the sacrificial element and the subsequent formation of a channel. However, direct infusion or withdrawal of media into these hydrogel channels often

resulted in the destruction of the formed channel due to the low mechanical strength of the hydrogel systems used and the propagation of mechanical disturbances from the syringe pump. Thus, reservoirs were added to enable the generation of flow via less disruptive gravity driven flow. In order to maintain a constant flow rate over time, generation of flow via gravity requires the constant (~12hour) refreshment of media in the reservoirs to prevent the cessation of flow due to reservoir equilibration. As this can become quite time consuming when the simultaneous culture of several MLS-BBBs is desired, we chose to maintain the volume difference between the inlet and outlet reservoirs via the constant infusion into the inlet reservoir from a programmable syringe pump and the constant aspiration of media from the outlet reservoir. Using this "pump-facilitated gravity driven flow" (PF-GDF) method, we were able to successfully culture as many as 70 MLS-BBB chips simultaneously. Through the addition of inverted pipette tips, we were also able to modify our devices to accommodate the volume difference necessary to drive flow at a rate that produces a wall shear stress similar to in vivo conditions (4 dynes/cm^2) [120].

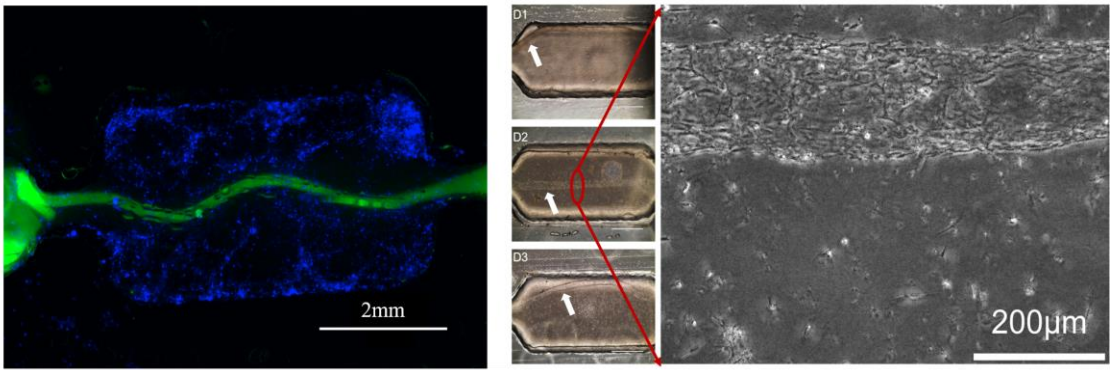

Figure 10. Sacrificial element methodology enables the formation of endothelial lumens within MLS-BBB device. (Left) GRP doped sacrificial element surrounded by Cell Tracker Deep Red labeled astrocytes (Right) Bright field images of three MLS-BBB devices with cutout to higher magnification phase contrast image. Lumen location in each device indicated by white arrows.

3.3.3 MLS-BBB Device Enables Culture of NVU Cell Types in Lumen Geometry

To assess the formation of BBB lumens within our MLS-BBB, our model was then stained for distinct cell markers to enable visualization of cell morphology and spatial arrangement of the relevant cell types of the NVU. Histological staining for ZO-1 verified the formation and connection of iHBMEC cells into a monolayer, GFAP staining revealed branched astrocytes and an interconnected system of astrocytic processes spanning the length of the lumen, and staining for αSMA enabled the visualization of pericyte localization and coverage of the endothelial lumen.

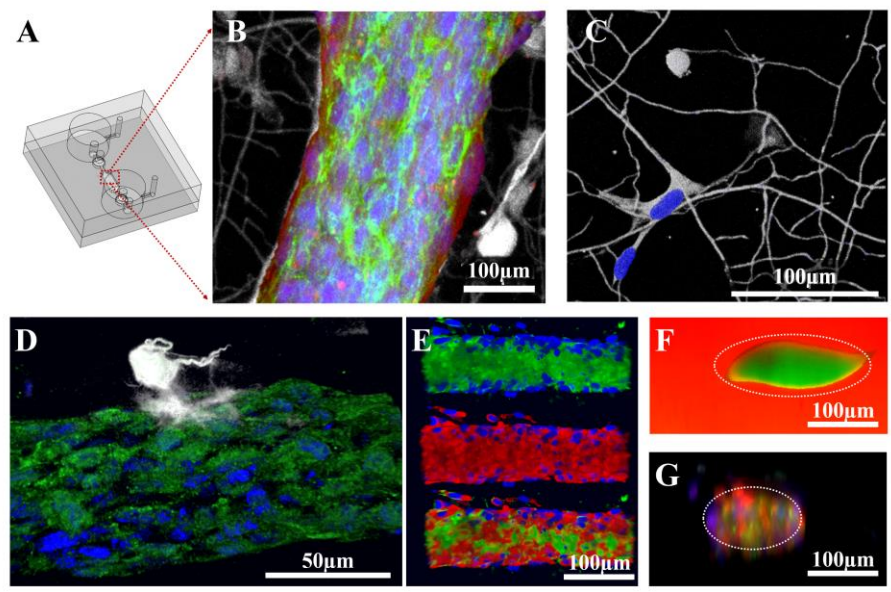

Figure 11. Lumen formation in MLS-BBB. (A) Schematic illustration of MLS-BBB device. Red dashed box indicates culture area (B) Extended focus image of iHBMEC (green, ZO-1) lumen lined by HBVP (red, αSMA) cells and wrapped with HA (white, GFAP) endfoot projections in MLS-BBB device. Cell nuclei visualized via DAPI staining (blue). (C) Astrocytes surrounding iHBMEC lumen form interconnected nets (D) ROI showing astrocyte contact with iHBMEC lumen. Image courtesy of S. Ahn. (E) 3D renderings of iHBMEC (green) HBVP (red) co-culture illustrating the localization and extent of HBVP coverage over iHBMEC lumen. (F) GFP doped sacrificial element suspended in TRITC doped Matrigel confirming rounded shape of injection molded elements used for channel formation (G) XZ projection of an MLS-BBB lumen confirming that this rounded channel shape is maintained in culture.

3.4 Opportunities for Improvement

While this work was successful in the creation of a MLS-BBB, there are several areas for potential improvement to the device design and workflow that warrant discussion. The sections that follow discuss areas for improvement identified by the issues encountered throughout experimentation with our MLS-BBB system along with suggested directions for improvement.

3.4.1 Limitations of 3D Printed Substrates for Soft Lithography

The current MLS-BBB device is limited by the dependency on 3D printing to generate cylindrical sacrificial element molds. While 3D printing technology is capable of printing reliable features at sizes down to the nanometer scale, the printers that can accomplish this are often not designed for printing of large surface areas. The Objet Eden System used could print features in the size necessary for our molds (~100-500µm) at a reasonable price point, but the minimum resolution of the printer (10µm) was high enough to cause variability on the surface of the mold. This significant and variable (from mold to mold), surface roughness was sufficiently high to produce leaks in devices unless PDMS pieces were used in conjunction with double sided silicone tape. The addition of silicon tape between housings and reservoirs and between housings and glass coverslips was sufficient to reduce device leaks; however, silicon tape could not be reliably used in the protocol for the formation of sacrificial elements due to difficulties with alignment. Thus, sacrificial element injection molds often leaked and the casting process was inefficient. On average, 50% if elements cast were usable for experimentation.

In addition, over the course of experimentation we observed that the Objet Eden 3D printed molds are not well suited for continuous use in the casting and curing of PDMS due to their tendency to warp after extended exposure to heat. On average, molds lasted for 25 castings before replacements became necessary. For future studies, we recommend either the use of a 3D printer capable of producing smoother surfaces in finished parts, post-treatment of 3D printed parts to smoothen surfaces, or the adaptation of a traditional photolithography based approach that utilizes silicon wafers for the creation of sacrificial element master molds.

3.4.2 Sterility

3.4.2.1 Mitigation of Contamination Hazards

The current workflow could be improved with modifications that would enable more steps to be carried out in a sterile field. Although device contamination was only observed in 1 out of 30+ batches of devices, the risk of contamination is quite high due to the number of process steps that must be completed outside of a sterile field (plasma cleaning, element placement in devices, etc.). Suggestions to reduce contamination hazard include: placing a stereoscopic microscope in a laminar flow hood for use during alignment and seeding steps, reduction in distance between plasma cleaner and laminar flow hood, and the acquisition of sterile containers of sufficient height to accommodate the full height of reservoir expanders.

3.4.2.2 Re-sterilization and Re-use of Device Components

Assembled housings, while intended for single use, were tested for their ability to be re-used successfully due to a looming PDMS shortage facing the Georgia Tech community in May of 2017. Removal of silicon tape with scotch tape, sterilization with 70% ethanol, and subsequent autoclaving proved efficient at preparing used housings for re-use as demonstrated by microscopic inspection of device features. Preliminary tests conducted with such devices yielded indistinguishable results from newly assembled housings, indicating that in some cases previously used, assembled housings could be re-used if properly sterilized.

3.4.3 Modification to High Throughput Design

This workflow is not currently conducive to scale up. The ability to produce massively paralleled and repeatedly identical devices is necessary if the are to be used for pharmaceutical development. Throughout the course of experimentation with these devices, a maximum of 70 devices were cultured simultaneously. While possible, this was extremely labor intensive, requiring the constant (18 hour/day) attention and care of the operator and an assistant. The necessity of individual element placement and injection into each chip greatly limits the speed with which devices can be made. A system in which replicate devices could be assembled and injected as a unit would be a significant improvement to the current workflow. Additionally, a system in which tubing could be easily connected to a number of devices in parallel would greatly expedite the setup of parallel experiments.

3.4.4 Material Limitations

3.4.4.1 Necessary Cell Lines

In order to ensure that cells form stable lumens, extremely high concentrations of brain endothelial cells must be injected into the channel. Primary HBMECs are expensive (~$700/vial) and are only guaranteed by most vendors for four population doublings (Note: this is distinctly less than 4 passages). Additionally, primary HBMEC cells are in short supply due to their sourcing, and were at times not available when needed. Due to limited sources of primary cells, cells from multiple vendors were ordered over the course of device design and troubleshooting, and we noted significant differences in cell quality and expansion potential from these different vendors. Based on our experience, we recommend Sciencell for the purchase of primary HBMECs, as they provided cells of the most robust and consistent quality. Due to this limitation, the majority of our experiments were carried out with immortalized HBMEC cells (iHBMEC, DV Biologics).

3.4.4.2 Media Requirements

This workflow also necessitates the use of a significant amount of media during the course of experimentation. For a shear stress of 4 dynes/cm^2, a flow rate of 8.93µL per minute (~13mL **per** day **per** device) is needed, which could quickly become unsustainable. To mitigate this waste, our MLS-BBB was only cultured in the presence of shear for 24 hours after the establishment of an HBMEC lumen in the device before being harvested for analysis. Subsequent iterations of our MLS-BBB would benefit from a design modification that allows for partial media recirculation or from a reduction in lumen diameter to decrease the flow rate needed per chip to generate physiologically relevant shear rates.

3.4.5 Post Processing of Samples

Our device assembly itself readily facilitates the recovery of lumens from the devices due to the presence of the silicone tape between the housing and the glass slide. Housings can be carefully peeled so that hydrogel constructs are left in place on the glass slide (failure rate of recovery <15%). These constructs can then be fixed and stained for microscopy using standard methods. However, we did note significant degradation of our hydrogel system (MatTC) throughout the course of fixation and staining. This challenge result in a loss of information that could be gathered if constructs could be imaged before degradation of the structure. This can be partially mitigated by fixing with 2% PFA in place of 4% PFA, but the multiple wash steps necessary for staining with good signal to noise ratio still remove a significant portion of the astrocyte containing hydrogel from the lumen structure before it can be imaged. This could be potentially mitigated via hydrogel stabilization with glutaraldehyde treatment prior to fixation. Alternatively, live cell staining techniques could be used in conjunction with antibodies for extracellularly located, cell type specific proteins.

3.5 Conclusion

Our MLS-BBB constitutes a significant contribution to the fields of OOAC development and tissue engineering in that we successfully produced the first *in vitro* BBB model system capable of simultaneous incorporation of a tubular endothelial lumen, non-reactive astrocytes, and pericytes in the presence of physiologically relevant flow rates. We validated the appropriate arrangement and interaction of the cells in our model via fluorescent microscopy of distinct cell markers and verified the presence of tight junctions

between endothelial cells via ZO-1 staining. We have also highlighted and discussed potential improvements for alteration in subsequent iterations of this device for consideration.

CHAPTER 4. HT-QPCR CHARACTERIZATION OF MLS-BBB

4.1 Introduction

One of the challenges facing wide spread implementation of OOAC model systems is the lack of evidence demonstrating their increased predictive power over simpler models. In the context of the BBB, predictivity depends on the appropriate expression of a number of BBB specific endothelial cell specializations such as increased expression of junctional proteins between neighboring endothelial cells (ZO-1), expression of drug resistant proteins and active drug efflux pumps (Pgp), and the appropriate expression of relevant surface receptors (GLUT-1) [100]. A cursory review of the literature yields hundreds of targets that are characteristically or differentially expressed in endothelial cells of the BBB [72, 148, 150-152]. Despite this, novel OOAC BBB models presented in the literature are largely characterized via histological verification of the expression of 1-5 relevant proteins in conjunction with TEER or permeability assays before proceeding to demonstrations of utility [108]. While these metrics do provide some insight as to the relevant specialization of the endothelial cells, they are by no means comprehensive. Additionally, such narrow analyses seem to be predicated on the assumption that the relative expression of a single endothelial cell specialization (such as ZO-1 or Pgp) could somehow be indicative of appropriate expression of all relevant specializations.

In order to determine whether our MLS-BBB provides a significant increase in the expression of BBB relevant endothelial cell specializations, we characterized our model via high throughput qPCR (HT-qPCR, Biomark Fluidigm System) analysis for the expression levels of 81 genes demonstrated in the literature to be differentially or

characteristically expressed in brain endothelial cells. By comparing the fold change in expression of each target relative to static culture of iHBMECs, we can begin to quantify the relative strengths of our model and identify areas of weakness for improvement in future iterations. We further expanded this study to evaluate whether our culture in our MLS-BBB facilitates the expression of more BBB relevant specializations than simpler models by comparing the expression profiles of endothelial cells extracted from our MLS-BBB and endothelial cells extracted from transwell and spheroid models. We further validated our MLS-BBB by assessing our model's ability to dynamically respond to stimulation by TNFα. Finally, we studied how ECM composition impacts BBB cell specialization by varying the composition of the hydrogel system used in our model.

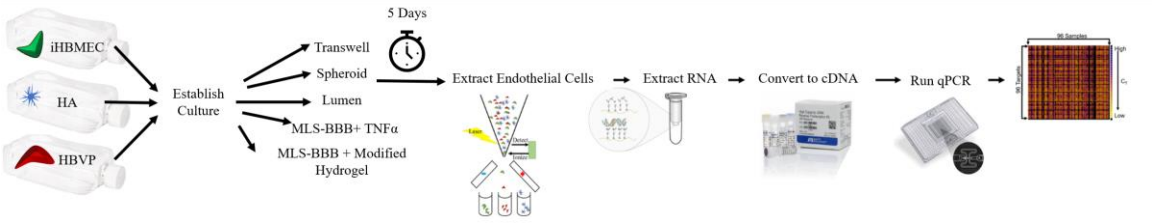

Figure 12. Schematic of experimental workflow for HT-qPCR experiments. iHBMEC, HBVP, and HA cells were grown to confluence in T300 flasks before trypsinization and seeding into various in vitro BBB models. After 5 days of culture, all model cultures were terminated and iHBMEC cells were recovered via FACS. RNA was isolated and converted to cDNA for use in HT-qPCR analysis for the expression of BBB relevant endothelial cell specialization.

4.2 Materials and Methods

4.2.1 Transwell Culture

Polyester transwell inserts (pore size 0.4um, Corning) were submerged in a 0.1% gelatin solution for at least one hour and rinsed with PBS before cell seeding. The inserts were inverted onto a petri dish and HBVPs were seeded on the bottom side of the inserts

while HAs were seeded in the wells. Cells were allowed to adhere for two hours before the HBVP laden transwell inserts were inverted into the HA wells. iHBMECs were then seeded onto the upper side of the transwell inserts. All cell types were seeded at a concentration of 1E5 cells/cm^2. Cell growth was monitored via fluorescent microscopy and monolayer formation and integrity was validated via TEER measurements.

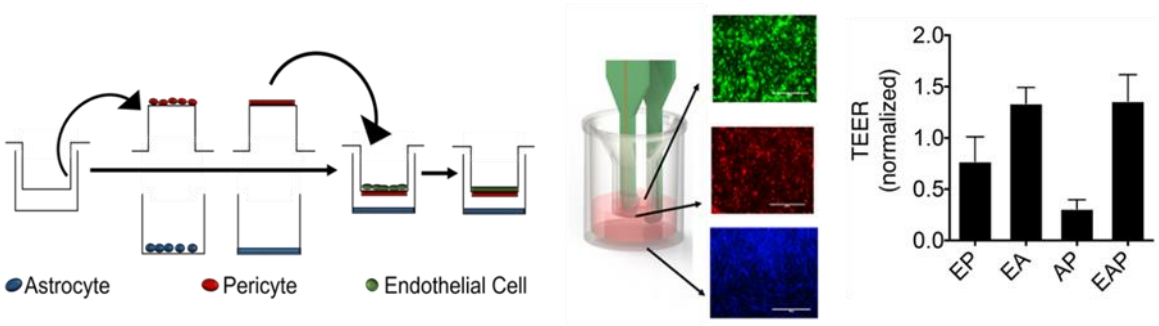

Figure 13. Schematic of tri-culture transwell (TWEAP) model establishment and model validation via TEER. TEER measurements of mono-, co-, and tri-culture conditions reflect previously reported data that barrier establishment and integrity is highly dependent on the presence of astrocyte cells.

4.2.2 Spheroid Culture

Round bottom, 96 well, ultra-low attachment culture plates were used to generate spheroids. Individual cell suspensions of iHBMEC, HA, and HBVP cells were prepared at a concentration of 5E4 cells/mL in cell specific media and seeded in a ratio of 2:1:1, iHBMEC:HA:HBVP. Cell suspensions were distributed into ultra-low attachment plates (200µL/well) via a multichannel pipette to reduce variation.

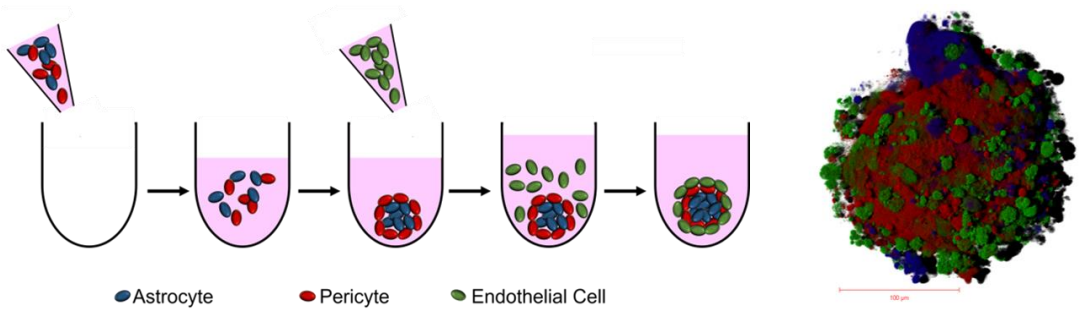

Figure 14. Schematic of tri-culture spheroid (SPEAP) seeding protocol and 3D rendering confocal image of a SPEAP. Image: HBMEC (green), HBVP (red), NHA (blue) cells confirms the formation and appropriate arrangement of relevant cell types. Scale bar 100μm.

4.2.3 MLS-BBB Culture

MLS-BBB Culture was conducted as outlined in **Section 3.2.4** for mono- co- and tri- culture experiments. In cases where administration of TNFα was necessary, MLS-BBB models were cultured with TNFα supplemented media (40ng/mL) during the 24 hours following administration of shear and preceding harvesting. Additional hydrogel compositions were included for analysis including plain collagen, plain Matrigel (no tenascin C), and a CnIMatHy combination hydrogel. Hydrogel compositions were kept consistent with those used in **Section 3.2.1**.

4.2.4 Fluorescent Activated Cell Sorting

In order to collect pure iHBMEC samples from co-culture experiments for qPCR analysis, iHBMEC cells were stained with a conjugated antibody for a distinct endothelial cell marker (CD31) after termination of culture. Where applicable, cell constructs were dissociated from tri-culture models with 5% trypsin solution (2D culture) or 1:1 mixture of trypsin and Corning Dispace (3D culture). Cell suspensions were centrifuged and re-

suspended in FACS buffer to remove any residual ECM proteins before being filtered thru a 40uM cell strainer and used for FACS to isolate endothelial cells from astrocytes and pericytes. FACS protocols were built via standard methods, and controls for dyed and undyed cells were included in each sorting session to reduce capture of non-iHBMEC cells. Cells were sorted directly into lysis buffer stabilized with RNase inhibitors to prevent the degradation of genetic material prior to analysis. Careful attention was payed to ensure that the volume of the sorted cell suspension being added to the lysis buffer was not enough to dilute its potency (indicated as critical by kit manufacturer. A 3:1 or greater ratio was maintained between volumes).

4.2.5 qPCR Analysis

Targets for BBB relevant endothelial specializations were selected via review of relevant literature [72, 148-152]. Sequences for each target were obtained from the NCBI nucleotide database and primers were developed for each target using Primer3Plus software and BLAT tools. Primers were ordered from Eurofins Genomics and suspended in TE buffer (TekNova) at a concentration of 100uM. RNA was extracted from FACS sorted endothelial cell populations via Quiagen RNeasy micro kits. In samples obtained from 3D culture, 40µL of proteinase K was added to lysates and an additional incubation at 55ºC was added before removal of genomic DNA (as indicated by manufacturer). RNA concentration was measured (Take3, BioTek plate reader) and diluted to a homogenous concentration across all samples. RNA purity was determined from the 260/280 ratio for all samples. 11 randomly selected samples were analyzed for degradation by obtaining a RNA integrity number (RIN) from bioanalyzer data. RIN scores of 6+ are considered of sufficient quality for use in HT-qPCR, and randomly tested samples ranged in quality from

7.0-9.9. RNA was converted to cDNA via a high throughout reverse transcription kit (ThermoFischer) and a standard thermocycler via manufacturer's instructions. High throughput qPCR was carried out via the Biomark Fluidigm System with Evagreen detection by the Georgia Tech Genomics Core. Three biological replicates of each sample were included for analysis. Expression levels of each target were normalized to the geometric mean of 2 housekeeping genes with consistent expression (OAZ1, HRPT1) to convert raw cycle threshold (Ct) values to ΔCt values. ΔΔCt were obtained via normalization to the 2D cultured iHBMEC static mono-culture condition to facilitate comparison across BBB models Fold change values were obtained by taking $2^{-\Delta\Delta Ct}$.

4.2.6 Statistics

Detailed discussion of data handling and statistical analysis can be found in **Section 6.5**. Briefly, data are presented as mean values ± standard error of the mean (S.E.M.) for N=3 replicates, unless otherwise noted. All statistical analysis was performed in GraphPad Prism software. For comparisons of the expression profiles of two groups, a Wilcoxon matched pairs signed rank test was used. For comparisons of the expression profiles of more than two groups, a Friedmans' test was used in conjunction with a Dunn's post-test to correct for multiple comparisons. When applicable, p values were adjusted for multiple comparisons. $p < 0.05$ was considered the cutoff for statistical significance.

4.3 Results and Discussion

HT-qPCR was performed in the Georgia Tech Genomics Core. Results were reviewed and failed samples and assays were removed prior to data processing and analysis. Details regarding the removal of failed samples and assays can be found in

Section 6.4.2. After removal of fails, 63 targets and 12 sample groups (N=2-3) remained for analysis.

4.3.1 MLS-BBB Culture Increases Expression of Specializations Relative to 2D Culture

Our results confirm our hypothesis that an increase in physiological relevance of in vitro model design results in an increase in the expression of BBB relevant endothelial cell specializations as indicated by the significant upregulation of 26 specializations relative to 2D static mono-culture of iHBMECs. Subgroup analysis indicates that culture in MLS-BBB devices significantly increases the expression of major drug resistant proteins, junctional proteins, and transporters.

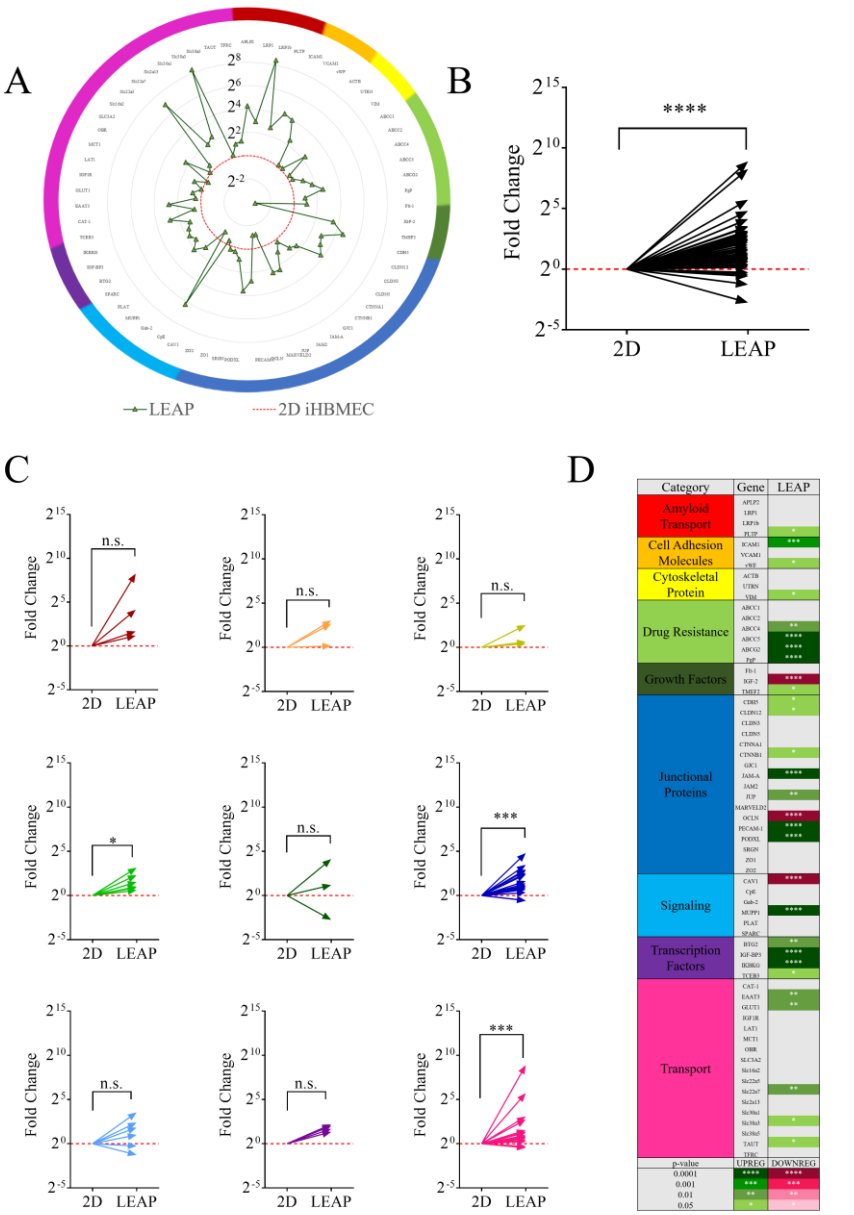

Figure 15. Expression profile for tri-culture MLS-BBB device (LEAP) is significantly better than 2D control. (A) Radar plot depicting the fold change in expression of each target (N=2) relative to 2D static mono-culture of iHBMECs (N=3) indicates that MLS-BBB culture results in the upregulation of most gene targets. Values above one indicate higher expression in MLS-BBB relative to controls, and values below one indicate lower expression. (B) Wilcoxon matched pairs signed rank analysis indicates that 2D and LEAP expression profiles are significantly different. (C) Subgroup analysis reveals significant changes in the expression of drug resistant proteins, junctional proteins, and transport proteins in MLS-BBB models. (D) Summary of individual target expression in MLS-BBB devices. Targets that are significantly up (green) or down (red) regulated are annotated with asterisks to denote magnitude of p-value. n.s. – not significant.

4.3.2 Direct Cell Contact Increases Physiological Relevance of In Vitro Models

One of the primary goals of this study was to evaluate the expression of endothelial cells specializations in different culture conditions to enable us to quantify the relative strengths and weaknesses of our MLS-BBB. In order to do this, each culture condition was separately assessed for its performance relative to 2D static mono-culture of iHBMECs to obtain an expression profile across all targets. Expression profiles were then compared using statistical methods to determine whether they were significantly different between sample groups. Our results indicate that all three tri-culture models (TWEAP, SPEAP, LEAP) exhibit significantly more expression of the specialization targets compared to 2D controls (**Figure 16 D-F**). Furthermore, comparison of TWEAP, SPEAP, and LEAP expression profiles indicates that both LEAP and SPEAP have significantly higher target expression than TWEAP, but that there is no statistically significant difference between the performance of SPEAP and LEAP models (**Figure 16 B**). This finding supports our hypothesis that direct cell contact will result in an increase in the expression of relevant specializations.

Additional investigation via subgroup analysis revealed that the expression profiles for the junctional protein category of targets were significantly different between TWEAP and SPEAP groups but not between LEAP and SPEAP groups or LEAP and TWEAP groups. This result was not expected as it is well established that exposure to flow leads to the significant upregulation of junctional associated proteins in endothelial cells [120]. However, when the difference in the models and their seeding protocols are considered, it is likely that the result is due to either a lack of confluence in the MLS-BBB model,

administration of flow for too short a period before harvesting, or too little shear stress (i.e. flow rate not sufficiently high).

Such similar results between LEAP and SPEAP models seem to indicate that direct cell contact is more critical to upregulation of key specializations than other critical parameters such as the presence of relevant ECM proteins, physiologically relevant cell geometries, and exposure to flow. Follow up experimentation over longer culture periods and with variable shear stress conditions could potentially clarify these results further.

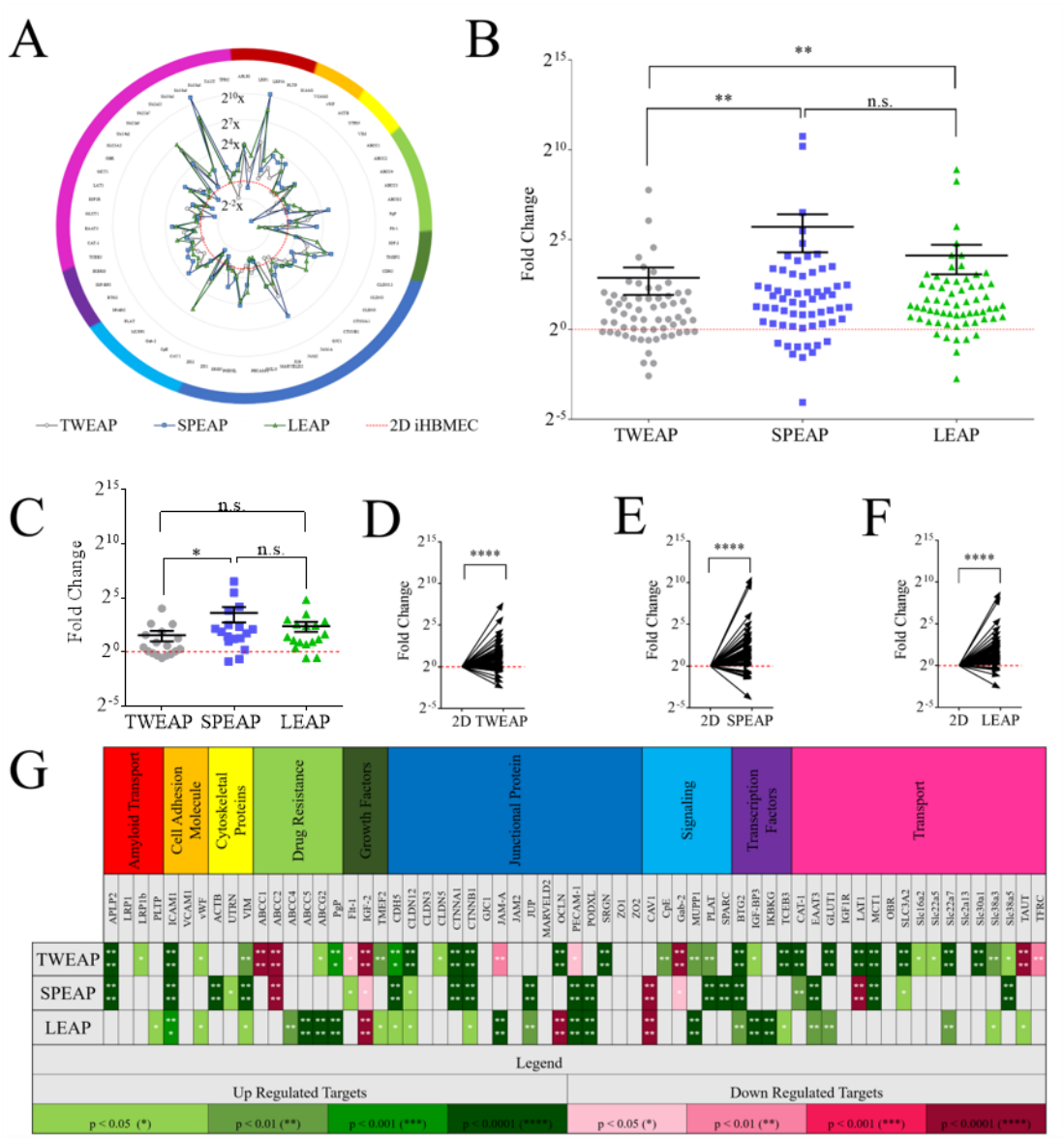

Figure 16. Comparison of TWEAP SPEAP and LEAP models. (A) Radar plot depicting the spread of expression profiles for tri-culture transwell (TWEAP, N=3), spheroid (SPEAP, N=3) and LEAP (N=2) models. (B) SPEAP and LEAP models both provide significant increases in the expression of relative specializations compared to TWEAP models when examined across all targets (C) Comparison of the expression profiles of junctional associated proteins indicates that SPEAP significantly outperformed TWEAP culture in that category, but was not significantly better than LEAP culture in that category. (D-E) Individual comparison of each model to the 2D control case indicates that all three tri-culture models provide significant increases in the expression of markers relative to 2D controls. (F) Summary of targets determined to be significantly up or down regulated in models relative to 2D static culture controls.

4.3.3 MLS-BBB Model Response to Inflammatory Signals

In order to begin to assess the functional utility of our MLS-BBB, we administered 40ng/mL of tumor necrosis factor alpha (TNFα) in media to tri-culture MLS-BBB models. After 24 hours of exposure to TNFα supplemented media, endothelial cells were harvested from all cultures and evaluated for expression changes for targets. TNFα is an inflammatory signaling molecule involved in recruiting leukocytes and other immune cells to sites of injury. In the context of the BBB, inflammatory cytokines such as TNFα have been demonstrated to be involved in the activation of endothelial cells, the presentation of an inflammatory phenotype, and extravasation of immune cells [160]. Upon exposure to TNFα, transcription factors are activated that induce an increase in the expression of relevant cell adhesion molecules (VCAM1, ICAM1) [161] on the surface of endothelial cells. TNFα has also been shown to induce the degradation of junctional proteins (VE-Cadherin, ZO-1, ZO-2) [162, 163].

Addition of TNFα to tri-culture MLS-BBB culture results in a significant change in the expression profile across all targets (**Figure 17 A-B**). Our results further indicate that adhesion molecules ICAM1 and VCAM1 are significantly upregulated after exposure to TNFα. (**Figure 17 C**). Subgroup analysis of the expression profiles of each specialization category did not yield significant results; however, the junctional protein, signaling, and cytoskeletal protein groups had noticeably lower p-values than the remaining groups ($p\sim0.15$ vs. $p\sim0.5$-0.999). This could potentially indicate that the expression profiles of these categories are trending towards being significantly different and that repetition of the experiment with longer TNFα exposure times could potentially yield more significant results.

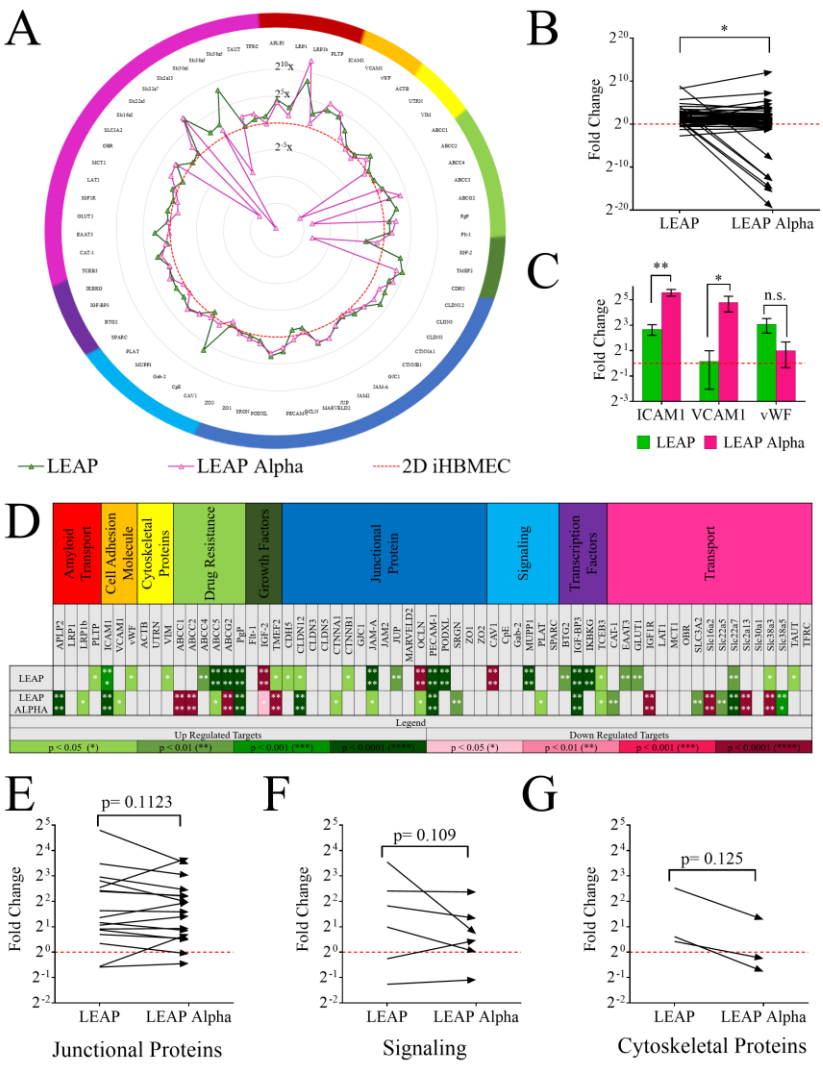

Figure 17. MLS-BBB device response to the administration of TNFα. (A) Radar plot comparing the expression profiles of tri-culture MLS-BBB (LEAP, N=2) and tri-culture MLS-BBB devices exposed to TNFα administration (LEAP Alpha, N=2) (B) Direct comparison of LEAP and LEAP Alpha expression profiles indicates that there is significantly different expression of specialization targets following exposure to inflammatory cues (C) ICAM1 and VCAM1 are significantly upregulated in LEAP Alpha models (D) Summary of targets determined to be significantly up or down regulated in models relative to 2D static culture controls. (E-F) While not significant, analysis of the change in expression of targets within each specialization category indicates that the expression profiles of markers in the junctional protein, signaling, and cytoskeletal protein categories may be trending towards a significant decrease between the LEAP and LEAP Alpha groups.

4.3.4 Hydrogel Composition Impacts Specialization Expression

To further assess the utility of our model and the validity of our hydrogel tuning study, we altered the composition of our hydrogel in a subset of MLS-BBB devices and examined the resulting effect on the specialization target expression profiles. We hypothesised that sub optimal hydrogel culture would result in a decrease in the expression of relevant endothelial cell specializations due to presence of reactive astrocytes in culture. Tri-culture MLS-BBB models made with CnI, Mat, MatTC and CnIMatHy hydrogels were included on the HT-qPCR panel for analysis (N=3 per group) with the goal of quantifying the effects of optimal (MatTC), and suboptimal (Mat, CnI, CnIMatHy) ECM composition on the expression profiles of the endothelial cells. In addition, tri-culture CnI and MatTC MLS-BBB models were included in the TNFα study with the goal of determining whether appropriate ECM composition could provide a protective effect or enable the more appropriate response of endothelial cells to stimulation. Unfortunately, a large number of samples failed on our qPCR panel, resulting in a decrease in or elimination of biological replicates available for analysis. Of the groups tested, only the MatTC (N=2) and CnIMatHy (N=2) sample groups were successfully amplified on the qPCR panel, limiting data available for discussion to comparison between the performance of those two models.

Both the MatTC and CnIMatHy MLS-BBB culture conditions resulted in very significant shifts in the expression profiles of iHBMEC cells relative to 2D controls (**Figure 18, C-D**), but when directly compared across all targets, the expression profiles of the two ECM compositions are not significantly different (**Figure 18, B**). Furthermore, while the CnIMatHy hydrogel condition exhibited a larger number of significantly upregulated specialization targets in comparison to 2D static mono-culture, additional

analysis of model performance by subcategory (amyloid transport, junctional proteins, etc.) did not reveal any significant differences in performance by category between the two groups.

At first glance, these results seem to suggest the ECM composition is not a as critical of a parameter as previously thought, but when considered in context, this result not surprising at all given that CnIMatHy hydrogels were originally selected for inclusion in this study based off of literature evidence indicating their suitability for the non-reactive culture of astrocytes despite the inclusion of CnI [84].

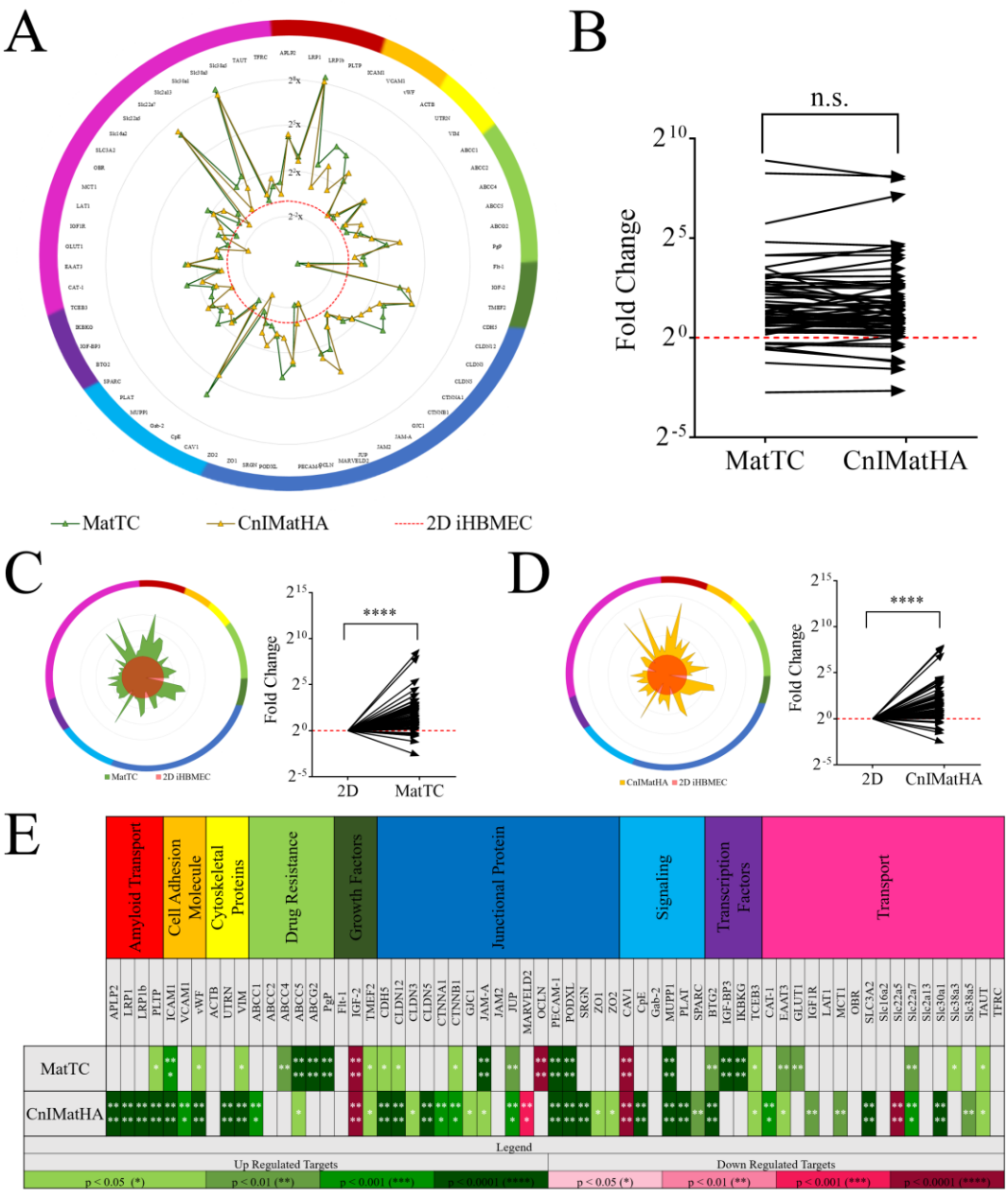

Figure 18. MatTC and CnIMatHy hydrogels are both suitable candidates for in vitro BBB model development. (A) Radar plot comparing the expression of each specialization target in MatTC MLS-BBB (N=2), CnIMatHy MLS-BBB (N=2), and 2D static monoculture of iHBMEC cells (N=3). (B) The expression profiles of the two ECM compositions are not significantly different and (C-D) both cases results in a significant increase in marker expression relative to 2D culture (E) Summary of targets that are up or down regulated in iHBMEC cells isolated from either MatTC or CnIMatHy relative to 2D controls.

4.4 Conclusion

In this work, we characterized our MLS-BBB relative to two simple *in vitro* models of the BBB to assess whether our device provided a marked improvement in the expression of BBB relevant endothelial cell specializations. Our results further support literature evidence that direct contact between cellular constituents is critical for proper expression of specializations. Additionally, we demonstrated the functional utility of our device through analyses of model response to TNFα administration. Finally, we evaluated the degree to which ECM composition impacts the expression of relevant specializations by comparing the expression profiles obtained from MLS-BBB devices made with MatTC and CnIMatHy hydrogels. While MLS-BBB devices cultured in CnIMatHy exhibited a larger number of significantly upregulated targets relative to 2D controls, ranked comparison and sub group analysis did not reveal and significant differences in the performance of the models for any category tested (transport, drug resistance, etc.) indicating that both MatTC and CnIMatHy are suitable ECM compositions for use *in vitro* BBB culture.

CHAPTER 5. CONCLUSIONS AND FUTURE DIRECTIONS

5.1 Summary

The work presented in this thesis constitutes a significant contribution to the fields of tissue engineering and OOAC development by producing the first *in vitro* model of the BBB to simultaneously incorporate both astrocyte and pericyte cells with a perfusable lumen of brain endothelial cells. Furthermore, the comprehensive characterization of our models relative to commonly used *in vitro* BBB models enables us to weight the relative strengths afforded by our model (increased relevance) with its weaknesses (increased complexity, cost, etc.). This data provides insight that will enable the intelligent design of subsequent iterations of this and other devices and ultimately aid researchers in better balancing simplicity and physiological relevance when selecting an *in vitro* model of the BBB for preliminary drug studies.

5.1.1 Development of MLS-BBB

To develop our MLS-BBB, we first determined the most suitable 3D culture conditions for the most appropriate culture of astrocytes by tuning the composition of two commonly used hydrogel systems (Matrigel and Collagen I) to minimize the upregulation of genes that are indicative of a reactive gliosis state. We then used our tuned hydrogel (MatTC) in conjunction with a previously described sacrificial element method to craft cylindrical channels through the astrocyte embedded hydrogels. Channels were then serially seeded with pericyte and endothelial cells to form our MLS-BBB. After lumen establishment, flow was administered to MLS-BBB devices via pump-facilitated gravity

driven flow (PF-GDF) to maintain a constant wall shear stress of 4 dynes/cm^2, a value consistent with estimates of *in vivo* conditions. Our MLS-BBB facilitates the incorporation, relevant arrangement, and direct interaction of all three cell types as was visually confirmed via histological staining for distinct cell proteins (ZO-1, αSMA, GFAP). Histological and morphological observation confirms the contact of astrocyte endfoot projections with endothelial cells, the presence of tight junctions between endothelial cells, and the lining of endothelial lumens by pericyte cells.

5.1.2 Characterization of MLS-BBB

In order to evaluate the relevance of our model, we utilized high throughput qPCR techniques to simultaneously measure the relative expression of 81 endothelial cell specializations demonstrated to be differentially or characteristically expressed at the BBB. To enable meaningful interpretation of our data, we also analyzed endothelial cells from transwell and spheroid models, two simple, high throughput models that are currently used for preliminary drug studies. Our results indicate that our model provides a significant improvement over transwell culture models, and that direct cell contact *in vitro* is critically important for the expression of BBB relevant specializations. Further experimentation with our MLS-BBB revealed that model can respond appropriately to inflammatory stimulation (TNFα) via the upregulations of cellular adhesion molecules (ICAM1, VCAM1) and that small perturbations to the hydrogel composition can be made without negatively impacting MLS-BBB culture.

5.2 Future Directions

5.2.1 Ongoing Research

One of the ultimate goals of OOAC model development is eventual adaptation for preclinical assessment of novel drug compounds [12]. Despite an abundance of OOAC BBB models available in the literature, to date, very few have been employed in the context of a preclinical study for the development of a new drug candidate. To this end, we propose the use of our MLS-BBB in parallel with transwell culture and *ex vivo* assays for the evaluation of a novel, multifunctional nanomedicine for the treatment of SSH driven MB. Through such experimentation, we aim to demonstrate the utility of our MLS-BBB model for preclinical studies and compare the functional utility of our MLS-BBB to that of transwell culture and ex vivo approaches, while also assessing whether functionalization with ApoA1 will increase penetrance of LPNP NPs through the BBB. We believe that such rigorous, parallelized, evaluation of OOAC models in the context of preclinical studies is critical for the continual improvement of OOAC devices.

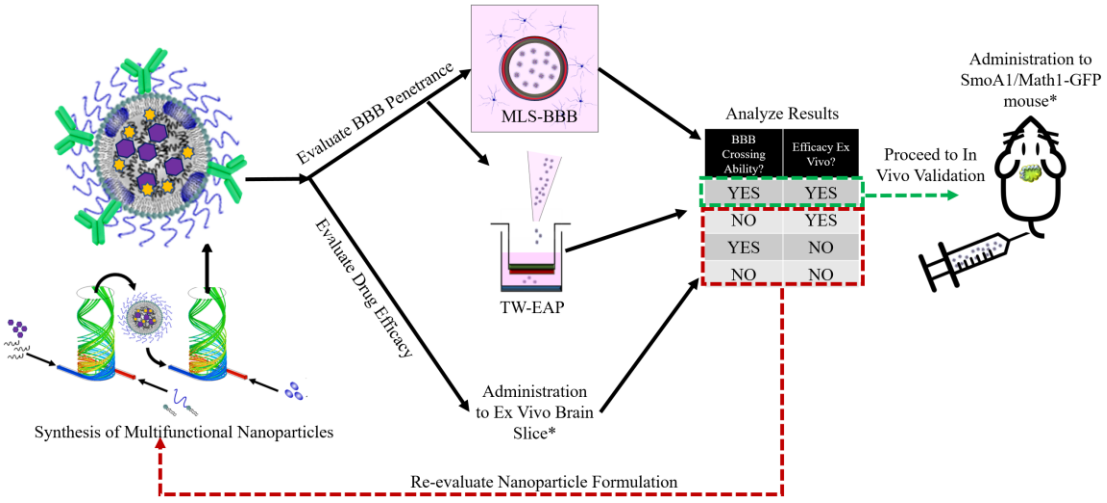

Figure 19. Experimental workflow for the evaluation of multifunctional nanomedicines with MLS-BBB. Libraries of custom, drug loaded, protein functionalized lipid polymer nanoparticles will be microfluidically synthesized for use in *in vitro* evaluation of their ability to cross the BBB and induce tumor cell death. Our MLS-BBB will be used in parallel with TWEAP permeability assays to assess the degree to which particles can penetrate the BBB. *Ex vivo* slices of PDX mouse tumors will be used to evaluate the therapeutic effect and tumor targeting abilities of drug loaded nanoparticle administration. Results from *in vitro* and *ex vivo* study approaches will be used to determine if *in vivo* validation is warranted or if re-design of nanoparticles is necessary.

5.2.2 Short Term Directions

By virtue of its demonstrated increased physiological relevance relative to standard models (static monoculture, tri-culture transwell), our MLS-BBB could be used “as is” to study a wide range of topics including BBB formation and embryogenesis. Additionally, our MLS-BBB could be altered to study pathophysiological BBBs such as those found in AD, PD, and MB. As discussed in previous sections, our MLS-BBB could be further improved by facilitating the inclusion of more NVU cell types (microglia and neurons) and through modification to a higher throughput platform. When combined with insight gained from our ongoing work, such modifications could enable the widespread implementation

of our MLS-BBB in the fields of tissue engineering, drug discovery, and drug development. Furthermore, as one of the eventual goal of OOAC research is the realization of a "human-on-a-chip" platform for use in drug discovery and evaluation, a potential future direction of our model is connection and integration with other OOAC model systems. Gut-on-a-chip model systems are prime candidate for integration with BBB-on-a-chip due the demonstrated link between gut health and Parkinson's disease (PD) [164, 165] and the demonstrated ability of the gut to impact BBB function through hormone secretion and microbe composition [166], but the potential applications are numerous and varied due to the ability of OOAC culture to enable detailed mechanistic observation of cellular phenomena.

5.3 Conclusion

In this work, we present a novel *in vitro* model of the BBB (MLS-BBB) that simultaneously incorporates three neurovascular unit cell types (endothelial, astrocyte, pericyte) in a 3D hydrogel system tuned to mimic the properties of brain extracellular matrix. Our model enables the formation of perfusable endothelial cell lumens that are lined with pericytes and wrapped with astrocyte endfoot projections. Through the comprehensive characterization of our MLS-BBB we have demonstrated that *in vitro* models that facilitate the direct interaction of cellular constituents increase the expression of BBB relevant endothelial cell specializations. Furthermore, we have demonstrated that our MLS-BBB responds appropriately to inflammatory stimulation with TNFα, indicating its potential suitability for the preliminary evaluation of drug effects. Taken together, our work constitutes a significant contribution to the fields of tissue engineering and organ-on-a-chip development.

CHAPTER 6. SUPPLEMENTARY MATERIAL

6.1 Fluorescent Activated Cell Sorting (FACS)

6.1.1 FACS is Necessary for Reliable qPCR Data Interpretation

The gene targets selected for quantification in our MLS-BBB characterization study are all endothelial cell specializations. These targets are varied in nature and function, and in some cases, are also expressed in astrocyte and pericyte cells at levels sufficiently high to distort or falsely inflate qPCR result interpretation. Similarly, there is the potential for data distortion if HBVP or HA genetic material is present in an RNA sample thought to be pure iHBMEC cDNA. Such contamination could lead to falsely deflated expression values. Thus, the reliable purification of iHBMEC cells from co-culture conditions was critical to this work.

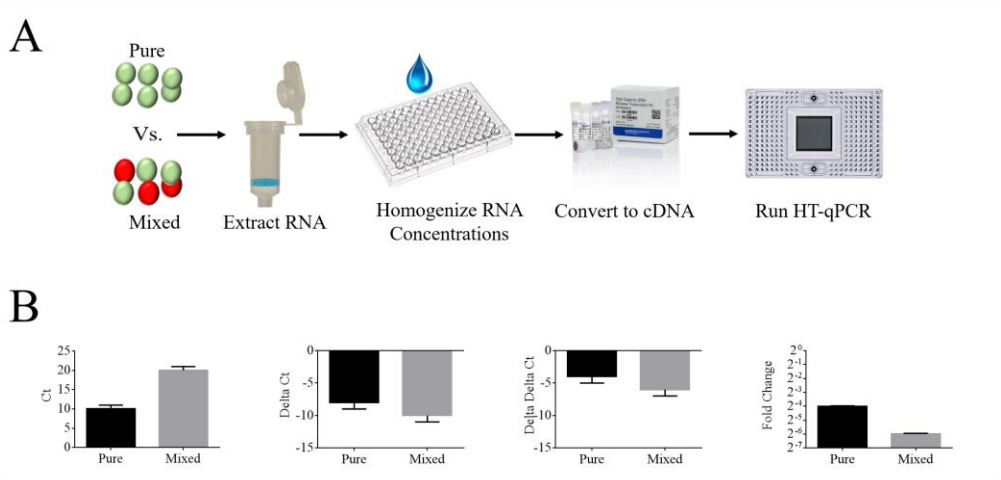

Figure 20. Schematic illustration of the effect of poor sorting on qPCR results. (A) Schematic of RNA processing workflow and (B) an example of the difference in qPCR data results obtained from pure and mixed cell samples given raw Ct values of 14, 10, 20, and 18 for the control sample, pure experimental sample, mixed experimental sample, and

housekeeping gene, respectively. The presence of non-relevant cells will falsely deflate obtained fold change results relative to the control. More explanation of qPCR data processing and the calculation of fold change values from raw Ct values can be found in **Section 6.4.1**.

6.1.2 FACS Protocol

MLS-BBB devices we disassembled via careful peeling of the PDMS housing from the glass slide to expose the hydrogel. The hydrogel containing the formed lumen was then carefully retrieved and placed in a 2mL Eppendorf tube for dissolution with a 1:1 mixture of trypsin (0.1%) and Dispace (Corning). Tubes were placed under incubation and slight rocking for 30 minutes. Samples were further disaggregated via passage thru a 40μm cell strainer, and dissolution of the lumen constructs to a single cell suspension was verified via microscopic inspection of tubes before proceeding with staining. Single cell suspensions were stained for sorting via flow cytometry in a FACS buffer composed of PBS (1X, Gibco) supplemented to contain 2% BSA, 1mM EDTA and 0.1% sodium azide. Endothelial cells were selectively stained with an Alexa Fluor® 647 conjugated anti-human CD31 Antibody (BioLegend) according to manufacturer instructions and were sorted on a BD FACS ARIA Fusion flow cytometer system (Georgia Tech Core Facilities). Positivity was selected by comparing to unstained sample to account for background auto fluorescence. Prior to sorting experimental samples, test sorts were conducted in which captured cells were sorted into media, re-plated, and expanded to confirm that a pure endothelial cell population was being captured. When sorting for data collection, cells with the fluorescent marker were captured and sorted directly into RLT buffer to preserve RNA integrity and minimize loss of cells during centrifugation and transport from tube to tube.

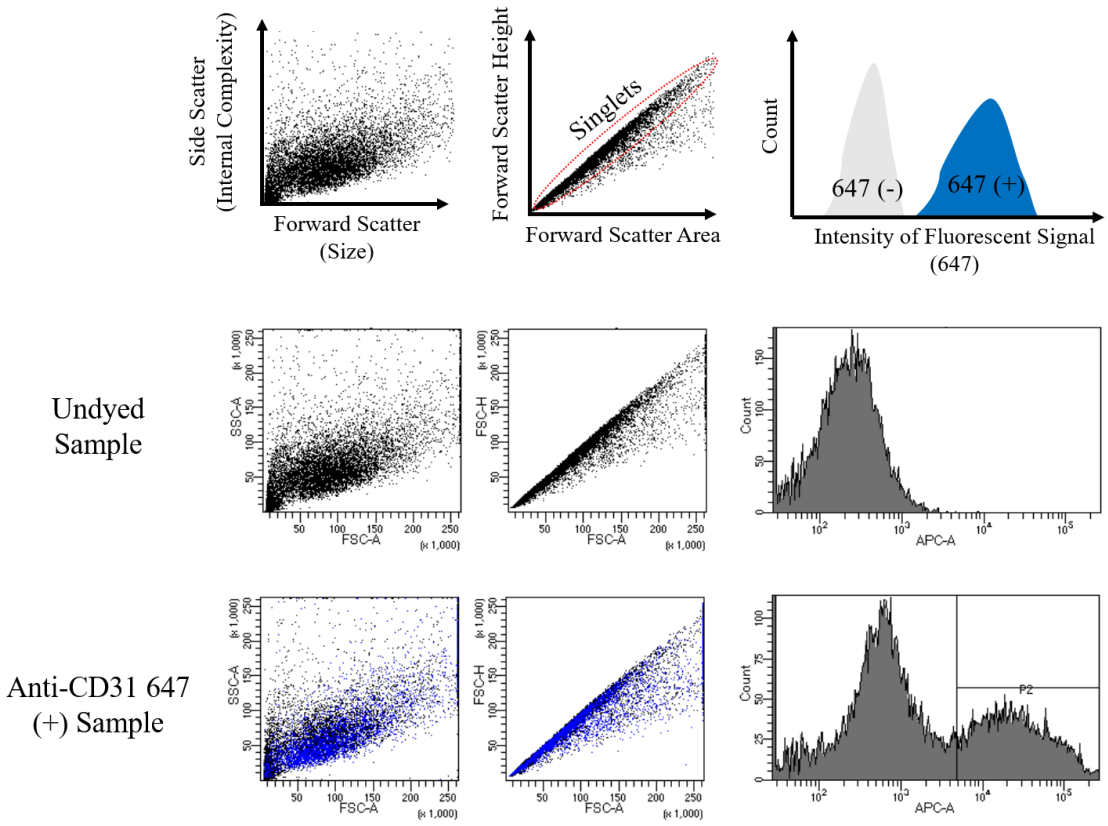

Figure 21. Example of FACS set up. (A) Schematic examples of scatter and intensity plots observed during sorting with singlet population indicated. (B) When no cells are tagged, only a single peak is observable. (C) Addition of the anti-CD31-647 antibody produces a peak in the appropriate range.

6.2 Isolation of RNA from 3D Cultured Cells

In this work, we utilized the RNeasy Plus Micro kit (Qiagen) for all RNA extraction due to the limited number of cells available for recovery from our culture systems. High quality RNA is essential to successful qPCR (see MIQE guidelines [167], also **Section 6.4**); thus, the purity, yield, and stability of sample RNA was assessed via established methods before proceeding to qPCR. The purity and yield of samples were obtained via spectrophotometric analysis (BioTek Plate Reader, Take3 Attachment) and sample stability was assessed via a chip based capillary electrophoresis system (Agilent

Bioanalyzer, Georgia Tech Genomics Core). Thresholds for each parameter are as follows: RNA yield must be at least 2ng/μL, RNA purity as determined by the 260/280 ratio should be >1.6 (pure RNA~2), and RNA integrity number (RIN) should be 6+ if samples are to be reliably used in qPCR analysis.

Unexpectedly, upon analysis of our samples, we noted that RNA extracted from 3D culture in hydrogels had significantly lower RIN scores than those obtained from 2D culture even when kit instructions were followed exactly (**Figure 22 B**). We were quite surprised with this result, given that our experimental parameters fell well within the working range of the kit. Qiagen technical support indicated that the degradation was most likely due to the incomplete removal of ECM components from samples during the kit workflow and recommended the addition of a proteinase K incubation step (40μL/sample, 15 minutes, 55ºC) when extracting RNA from 3D cultured samples. Addition of the proteinase K incubation was successful for most of the 3D culture conditions tested, with the RIN scores as high as 9.8 on some samples. Interestingly, addition of proteinase K alone was not sufficient in cases where the ECM was composed predominantly of collagen I. Upon further consultation with Qiagen technical support, it was determined that an additional processing column (Qiashredder) is necessary when relatively high concentrations of fibrous proteins like collagen I are present in a sample. Addition of the additional Qiashredder processing step (in conjunction with the proteinase K incubation) facilitated the recovery of pure, stable RNA from samples cultured in collagen I.

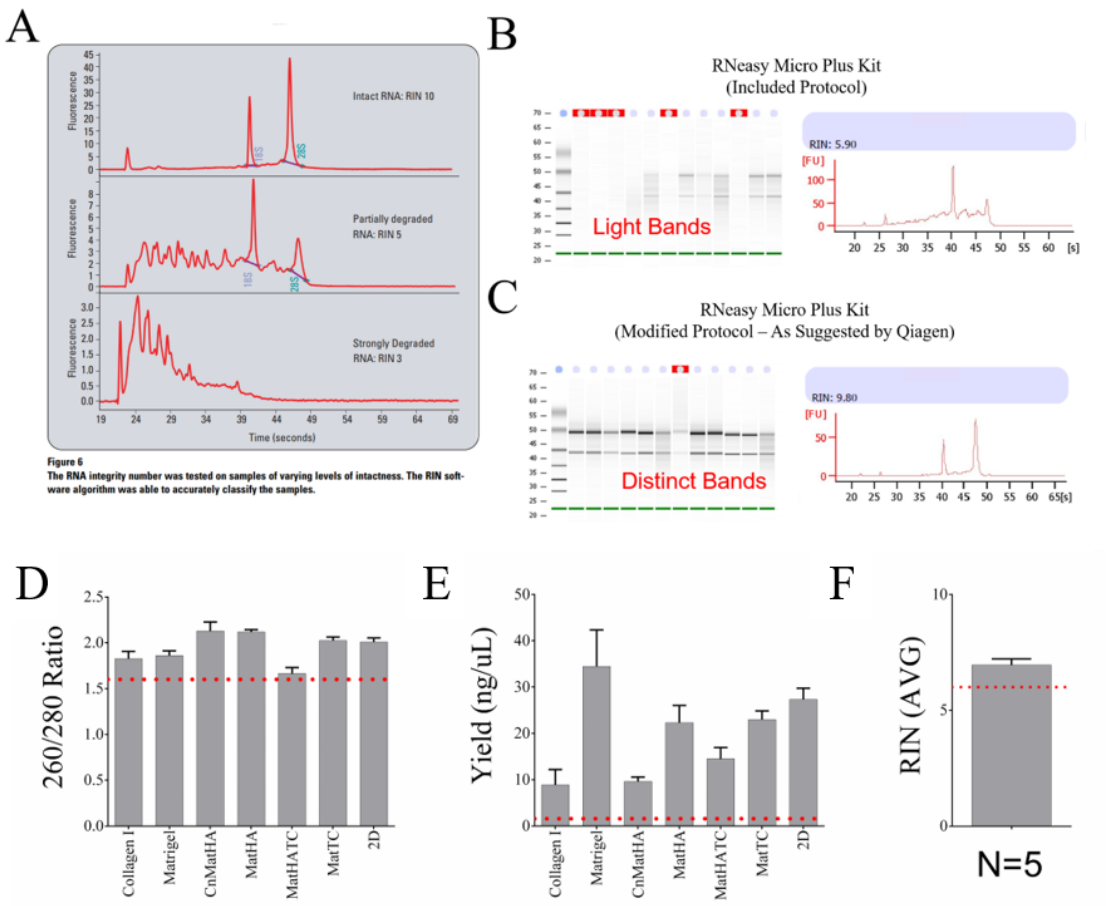

Figure 22. Optimization of RNA isolation protocol. (A) Example of electrophoretic traces of intact, partially degraded, and strongly degraded RNA samples from Agilent Biosystems (https://www.agilent.com/cs/library/applications/5989-1165EN.pdf)(B) Exactly following RNeasy Plus Micro kit instructions resulted in low quality RNA product due to incomplete removal of residual ECM components during purification (C) Addition of a proteinase K incubation to the RNA isolation workflow for samples obtained from 3D ECM enabled recovery of high quality RNA. (D-F) Summary of RNA purity, yield and quality of samples assessed for markers of reactive gliosis. All samples tested had acceptable (D) purity, N=6 per sample (E) yield, N=6 per sample and (F) stability values, N=5. Red dotted lines indicate minimum threshold for each parameter. (F) For RIN scores, 5 samples were randomly selected from the 42 total samples to assess purity. RIN scores of these samples were all above the threshold for use in qPCR.

6.3 Development of qPCR Primers

6.3.1 Primer Design

Gene targets were selected from literature review and the gene name for each target was obtained from the GeneCards database (genecards.org). Complete CDS sequences for each gene target were obtained from the NCBI (ncbi.nlm.nih.gov) nucleotide database and were copied into the Primer3Plus software (bioinformatics.nl/cgi-bin/primer3plus/primer3plus.cgi) to generate primers. Suggested primer pairs were then analyzed in an online BLAT tool to determine their suitability for use (http://genome.ucsc.edu/). Primers selected had 20 base pairs, a melting temperature of 60ºC, produced a product size between 150-200 base pairs, and returned a single match in BLAT analysis. Chromosomal location of the target was confirmed for each target using NCBI and other genomic resources.

6.3.2 Primer Details

Designed primers were ordered dry from Eurofins Genomics and resuspended to a homogenous concentration of 100µM in TE buffer before use. Dry primer plates were warmed to room temperature before resuspension with buffer and were incubated at 4ºC with gentle shaking overnight to ensure complete dissolution of primers. Once resuspended, primers were aliquoted into multiple plates for use to prevent the necessity of multiple free thaw cycles. Forward and reverse sequences for each primer pair used as well as primer details (gene name, NCBI reference sequence used for primer development, category for use) can be found in **Table 4.**

Table 4. Summary of primer pairs used in HT-qPCR analysis

Gene (Homo Sapien)	NCBI Reference Sequence	Category	Forward Primer	Reverse Primer
LRP1	NM_002332.2	Amyloid Transport	ggtactacctgcgcaagctc	cacattgctcccgttaaggt
APLP2/YWK-II	NM_001642.2	Amlyoid Transport	ttccaagccatggttaaagc	ctttgttctcagcacggaca
LRP1b	NM_018557.2	Amlyoid Transport	cggcatttacagtccctgat	tccactgctagccctctgat
CCL2	NM_002982.3	Amlyoid Transport	ccccagtcacctgctgttat	tggaatcctgaacccacttc
GJB6	NM_001110219.2	Astrocyte Marker	tttctgcgtctgtgatttgc	gcttgggaaacctgtgattg
AQP4	NM_001317384.1	Astrocyte Marker	agatcagcatcgccaagtct	aaccaggagaccatgaccag
ALDH1L1	NM_001270364.1	Astrocyte Marker	cacccctcatcatctttgct	tcatcttccgcacctcttct
vWF	NM_000552.3	Cell Adhesion Molecule	cacatcgtgaccttgatgg	gtgcttcacctcgatggatt
SELE	NM_000450.2	Cell Adhesion Molecule	ggacacagcaaatcccagtt	cacattggagccttttggat
VCAM1	NM_001078.3	Cell Adhesion Molecule	tgttgagatctcccctggac	gaattggtcccctcactcct
ICAM1	NM_000201.2	Cell Adhesion Molecule	cagaggttgaaccccacagt	cctctggcttcgtcagaatc
PROM1	NM_006017.2	Cell Membrane Protein	ttgtggcaaatcaccaggta	tcagatctgtgaacgccttg
PLP-1	NM_000533.4	Cell Membrane Protein	ctggctgagggcttctacac	cctagccattttcccaaaca
ACTB	NM_001101.2	Cytoskeletal Protein	agaaaatctggcaccacacc	agaggcgtacagggatagca
VIM	NM_003380.3	Cytoskeletal Protein	ccctcacctgtgaagtggat	ctcaatgtcaagggccatct
UTRN	NM_007124.2	Cytoskeletal Protein	gagctgaatgttgtgctgga	ttctcaggcaggacctctgt
ABCB1/MDR1 (Pgp)	AF016535.1	Drug Resistance	tgattgcatttggaggacaa	ccagaaggccagagcataag
ABCC1	NM_004996.3	Drug Resistance	aggtggacctgtttcgtgac	accctgtgatccaccagaag
ABCC2	NM_000392.4	Drug Resistance	agagctggcccttgtactca	agggacaggaaccaggagtt
ABCC3	NM_001144070.1	Drug Resistance	ttttctttgtcacccccttg	aaaggatcttggagcggaat
ABCC4/MRP4	NM_005845.4	Drug Resistance	ggcttgtgctctgaaaaagg	ctgagaggatcgtccaggag
ABCC5	NM_005688.2	Drug Resistance	agctgggtacttccagagca	tctgtcaacagccactgagg
ABCG2/BCRP	NM_004827.2	Drug Resistance	ttatccgtggtgtgtctgga	gatgattgttcgtccctgct
ELTD1/ADGRL4	NM_022159.3	Endothelial Cell Marker	ttcaaagcaccaggacaaca	catccatgcaaaagcagcta
ESAM	NM_138961.2	Endothelial Cell Marker	tcatccgtgggtctttaagc	aaccagggtacccacaacag
ICAM2	NM_001099786.1	Endothelial Cell Marker	caaacatctcccatgacacg	ctgcactcaatggtgaagga
APOLD1	NM_001130415.1	Endothelial Cell Marker	tccgatctctcgctgatctt	aattgtacagggcgatggag
Flt-1	NM_002019.4	Growth Factor	tttggatgagcagtgtgagc	cggcacgtaggtgatttctt
PTN / HARP	BC005916.1	Growth Factor	gaaaatttgcagctgccttc	ctgggtcttcatggtttgct
IGF-2	NM_000612.5	Growth Factor	cgttgaggagtgctgtttcc	ggactgcttccaggtgtcat
IGF-BP3	M31159.1	Growth Factor	cctgccgtagagaaatggaa	aggctgcccatacttatcca
FGF-19	AF110400.1	Growth Factor	tcggaggaagactgtgcttt	ggcaggaaatgagagagtgg
Tomoregulin/TMEFF2	AB004064.1	Growth Factors	ccagtttggtgcagaatgtg	ttgacatcgacccaaagaca
OAZ1	AY865622.1	Housekeeping Gene	gagccgaccatgtcttcatt	cccgaagactctctctcgaa
PMM1	NM_002676.2	Housekeeping Gene	tagagtgcagatcggtgtgg	caggtggttctggatggtct
HPRT1	NM_000194.2	Housekeeping Gene	gaccagtcaacaggggacat	cttgcgaccttgaccatctt
RPL30	N/A [168]	Housekeeping Gene	acagcatgcggaaaatactac	aaaggaaaattttgcaggttt
PSMB6	NM_002798.2	Housekeeping Gene	cctattcacgaccgcatttt	cccggtatcggtaacacatc
CLDN12	NM_001185072.2	Junctional Protein	ctccccatctatctgggtca	tgggtggatgggagtacaat

CLDN3	NM_001306.3	Junctional Protein	caacaccattatccgggact	cttggtggccgtgtacttct
CLDN5	NM_001130861.1	Junctional Protein	gttttacgacccgtctgtgc	gtacttcacggggaagctga
ZO1/TJP1	NM_003257.4	Junctional Protein	tgaggcagctcacataatgc	gggagttggggttcataggt
ZO2/TJP2	NM_004817.3	Junctional Protein	gggatattgcaggcacagtt	cgctgtctcccttcttgaac
ZO3/TJP3	NM_001267560.1	Junctional Protein	atcgagcgcctcaactatgt	agaggtggctgctgtgtttt
CTNNB1	NM_001098209.1	Junctional Protein	gaaacggctttcagttgagc	ctggccatatccaccagagt
SRGN	NM_002727.1	Junctional Protein	cgctgcaatccagacagtaa	ccgaagcctgatccagagta
VE-cadherin	X79981.1	Junctional Protein	cagcccaaagtgtgtgagaa	cggtcaaactgcccatactt
PECAM-1	M28526.1	Junctional Protein	atgatgcccagtttgaggtc	acgtcttcagtggggttgtc
F11R/JAM-A	BC001533.2	Junctional Protein	agctatggggaggtcaaggt	cccatctttgaaccaggtgt
GJC1	NM_005497.3	Junctional Protein	cacccgttttatgtgtgcag	gagtctcgaatggtcccaaa
OCLN	NM_002538.3	Junctional Protein	tggcaaagtgaatgacaagc	gcaggtgctctttttgaagg
CTNNA1	NM_001903.3	Junctional Protein	aagtagaagcagccgtggaa	cgtcctgcttctgacatcaa
JAM2	NM_021219.3	Junctional Protein	agaagtgatgcggggaaata	ccacagttccactcagagca
JUP	NM_002230.2	Junctional Protein	aaggtgctatccgtgtgtcc	gacgttgacgtcatccacac
MARVELD2	NM_001038603.2	Junctional Protein	aaagaggctgacgcagtgtt	gctccaccacacccagtatt
PODXL	XM_004727.1	Junctional Protein	gagcagtcaaagccaccttc	tggtcccctagcttcatgtc
ITM2aB17:H27	NM_004867.4	Junctional Protein	ccgtggagagatgtgctttt	tgctgcagggtcactatcag
RGS5	AF030108.1	Pericyte Marker	cgtgattccctggacaaact	tttgccttctcagccatctt
PGDFR beta	M21616.1	Pericyte Marker	cactgcctgtcccctatgat	acagtctgcactgcgttcac
NG2 (CSPG4)	AY359468.1	pericyte marker	gctgtggctgtgtcttttga	ctgtgtgacctggaagagca
NCAM	NM_000615.6	Reactive Astrocyte Marker	gtgtggttacaggcgaggat	gatgacatctcggcctttgt
EGFR	NM_005228.3	Reactive Astrocyte Marker	ccaaccaagctctcttgagg	gctttcggagatgttgcttc
bFGF	NM_002006.4	Reactive Astrocyte Marker	ccgttacctggctatgaagg	actgcccagttcgtttcagt
NES	NM_006617.1	Reactive Astrocyte Marker	agaaacagggcctacagagc	gcttggggtcctgaaagctg
GFAP	XM_008388.1	Reactive Astrocyte Marker	ggaagattgagtcgctggag	atactgcgtgcggatctctt
VIM	NM_003380.3	Reactive Astrocyte Marker	ccctcacctgtgaagtggat	ctcaatgtcaagggccatct
SYNM	NM_145728.2	Reactive Astrocyte Marker	ggctcgggatattcttcctc	tgtatctccggcttttggtc
CLCF1	NM_013246.2	Reactive Astrocyte Marker	gctacctggagcaccaactc	tggctgtaggcctcgtagtt
LIF	NM_002309.4	Reactive Astrocyte Marker	tgccaatgccctctttattc	ggggttgaggatcttctggt
IL6	M54894.1	Reactive Astrocyte Marker	tacccccaggagaagattcc	ttttctgccagtgcctcttt
C1r	NM_001733.4	Reactive Astrocyte Marker	tgacttccgttacaccacca	cattcttccaaatgccctgt
C1s	NM_201442.2	Reactive Astrocyte Marker	aagagcgttttacggggttt	tgaatacatccccactgcaa
Lcn2	NM_005564.4	Reactive Astrocyte Marker	acgctgggcaacattaagag	cgaagtcagctccttggttc
Serpina3n	NM_001085.4	Reactive Astrocyte Marker	ggcccctgataagaatgtca	agctcatcgctggactgatt
Ptx3	NM_002852.3	Reactive Astrocyte Marker	tgcgattctgttttgtgctc	tgaagagcttgtcccattcc
Cd109	AF410459.1	Reactive Astrocyte Marker	ttgaattcccaatcctggag	ttgttgccactaaccaccaa
A2M	NM_000014.3	Signaling and Regulatory Protein	gagctttgtccaccttgagc	gcttcacaagcagtccatga
CAV1	NM_001753.4	Signaling and Regulatory Protein	gagctgagcgagaagcaagt	caaatgccgtcaaaactgtg
Osteonectin/SPARC	XM_003989.1	Signaling and Regulatory Protein	atgagggcctggatcttctt	ctcttcggtttcctctgcac
CpE	NM_001873.2	Signaling and Regulatory Protein	tgaaccggaactttccagac	taattggccacaaggtctcc

PLAT	NM_000930.4	Signaling and Regulatory Protein	acatgctgtgtgctggagac	gtcgcatgttgtcacgaatc
Gab-2	AB018413.1	Signaling and Regulatory Protein	aaagccaacaccacttgacc	gtgatgctctgggtggagat
MUPP1	AF093419.1	Signaling and Regulatory Protein	tcctgcagaaagccaaagat	caatcgtttccatgtgttgc
BTG2/PC3	NM_006763.1	Transcription Factor	aagatggaccccatcatcag	tcgtacaagacgcagatgga
IKBKG	NM_001099857.2	Transcription Factor	agagtctcctctggggaagc	gcttggaaatgcagaagctc
TCEB3	NM_003198.2	Transcription Factor	catgttcaatcccctccatc	gttcacccaggtgtcgttct
TFRC	AF187320.1	Transport	gctgccagctttactggaga	ttgtcaatgtcccaaacgtc
PLTP	NM_006227.3	Transport	ttctgtggacgagcttgttg	gaaggccacatacaccatcc
ATP1A2	NM_000702.1	Transport	cgcaaataccaagtggacct	aagcagaggatagccccaat
xCT/4F2hc/ SLC3A2	NM_001012662.2	Transport	tcctgccttagcttccaaga	cgggctctaactcattcagc
Slc16a2	NM_006517.4	Transport	gcctgcgctacttcacctac	cttgatcttatcccccagca
Slc22a5	NM_001308122.1	Transport	ggattgttgtgccttccact	aaagcccaaaatagcccact
Slc22a7	NM_006672.3	Transport	gagtcctgagcagcaccttc	tacctgtgggcctctttcac
Slc22a8/OAT3	NM_004254.3	Transport	caccgtcatcttgaatgtgg	accaaccagcgtatggactc
Slc2a13	NM_052885.3	Transport	cagactcagaaggcccgtag	tgggggataactcagcattc
Slc30a1/ZNT1	NM_021194.2	Transport	tgctggaagcagaatcattg	gttctgcaggcaagttcaca
Slc38a3/SNAT4	NM_006841.5	Transport	ttcgggatgtcagtgttcaa	gtagcccagctgctcatagg
Slc38a5/SNAT5	NM_033518.3	Transport	ccacaatgaaacagcaatgg	cgtatagatgggcagcacct
Slco1a2/Oatp1a2	NM_134431.3	Transport	tttggcgctttaatggattc	aaggctggaacaaagcttga
Slco1c1/BSAT	NM_001145946.1	Transport	tggttgtcaaacctccaaca	agctgtggcttaatgcacct
SlcO2B1	NM_007256.4	Transport	ggcatccagttcatgttcct	ggtttcggagcaggtcatta
EAAT1/SLC1A3	NM_001289940.1	Transport	catgcacagagaaggcaaaa	gtcacggtgtacatggcaag
EAAT2/SLC1A2	NM_001195728.2	Transport	cgccatctttatagcccaaa	agcaggctgatgtcctctgt
EAAT3/SLC1A1	NM_004170.5	Transport	cctggtgtcacccagaaagt	ggaggcttcacttcttcacg
GLUT1/SLC2A1	NM_006516.2	Transport	cctgcagtttggctacaaca	taacgaaaaggcccacagag
TAUT (SLC6A6)	NM_003043.5	Transport	agggttatcgtcgggaaatc	agaatgcaacccacaaaagg
MCT1	AL162079.1	Transport	tccagctctgaccatgattg	gcccccaagaattagaaagc
LAT1 (SLC7A5)	NM_003486.5	Transport	gaaggcaccaaactggatgt	gaagtaggccaggttggtca
CAT-1	AF078107.1	Transport	atggccttcctctttgacct	ggtgcttgccaattcatttt
CNT2 (SLC28A2)	NM_004212.3	Transport	gccttgtgcaatgggtagtt	agagtgtcatgtccccaagg
IGF1R	NM_000875.4	Transport	aaccccaagactgaggtgtg	tgacatctctccgcttcctt
OBR (LEPR)	NM_002303.5	Transport	aggacgaaagccagagacaa	aaatgcctgggcctctatct

6.4 HT-qPCR Data Handling

6.4.1 General Introduction to qPCR

The real time quantitative polymerase chain reaction (qPCR) is a technique used to quantify a specific portion of DNA using target specific nucleotide sequences called primers. qPCR reactions are widely used for the quantification gene expression due to their specificity and sensitivity and they are often cited as the most sensitive and reliable method for the detection and quantification of nucleic acids. qPCR quantification is based on the detection of fluorescent reporter molecule in real time. In each qPCR reaction, amplification is carried out via temperature cycling through a protocol designed to sequentially denature double stranded DNA, anneal target specific primers, and elongate the target strand. Fluorescent molecules (Eva Green) are inserted into each newly formed double stranded DNA product, enabling detection of target amplification over time. The cycle at which the amplification of a target becomes detectable is noted by the machine as the cycle threshold (Ct) value for that sample and can be used in the relative quantification of the expression of targets across different samples [169, 170].

Due to the increasing frequency of use and variability in protocols used for qPCR analysis, a set of guidelines detailing the minimum information for publication of quantitative real-time qPCR Experiments (MIQE) was published in 2009 [167]. The MIQE guidelines, as well as information provided by the Georgia Tech Genomics Core was used in the development of all experimental procedures and protocols to ensure reliability of produced data.

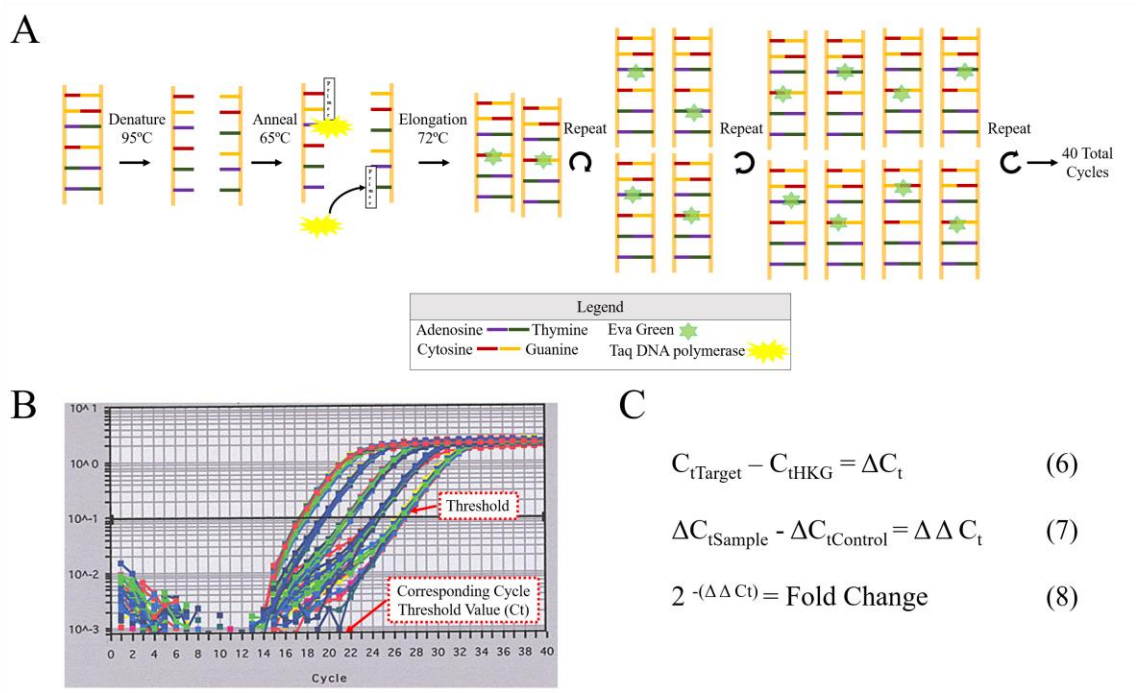

Figure 23. Fundamentals of qPCR. (A) Schematic of amplification and detection process used in qPCR. Double stranded DNA is denatured to enable the attachment of target specific primers. Enzymes then catalyze the recruitment of complementary base pairs to the segment identified by the primer pair. Amplification of target strands is detected via the incorporation of a double strand specific fluorescent probe (Eva Green). Each time the cycle of the machine repeats, the reaction begins again, resulting in a two-fold increase in the abundance of the selected target sequence per amplification cycle. (B) Example of amplification curves obtained during qPCR. For a given target, there will be a specific cycle number at which the fluorescent intensity of the EvaGreen dye reaches a threshold value. This cycle number is denoted as the cycle threshold value (Ct) and is used to quantify the relative expression of targets across samples. (C) The Ct value of each sample is normalized with housekeeping genes to account for variability in starting material concentration (Eqn. 6), before being normalized to a control for relative quantification (Eqn. 7) and calculation of the fold change in expression for each target.

6.4.2 qPCR Data Processing

Before processing data to obtain fold change values, we first examined the HT-qPCR assay results to identify and remove failed samples and targets. It is critical that assay fails be identified and removed prior to data processing or results can be significantly skewed from the inclusions of default "fail" Ct values (999).

Samples were classified as failed assays if the sample failed to amplify any of the 4 endothelial cell specific markers included on the panel (Samples: 24, 31-33, 41, 44-46, 48, 50-52, 56,57, 59, 60, 64, 67-75, 80, 85-87, 94) or if the sample failed to express more than 50% of targets tested (Note: Distinct cell markers were excluded from this calculation. Samples: 25, 27, 80, 89). Samples 76-96 were included for a lab mate (S. Ahn) and are not relevant to this study, so they were also removed prior to data analysis. Failed samples were deleted from the results table before removal of targets.

Targets were considered failures if they failed to amplify in more than one of the TWE/static culture iHBMEC replicates needed for data normalization to 2D culture (Targets: SELE, Slc22a8/OAT3, Slco1a2/Oatp1a2), if they failed to amplify in the assay positive control samples (Targets: GJB6), if they failed to amplify in the commercially available human cDNA positive control sample (Targets: AQP4, ALDH1L1, ABCC3, ATP1A2, EAAT2, CNT2), or if the total number of failed assays for that target was more than one standard deviation above the average number of failed assays per target (Targets: EAAT1/SLC1A3, SlcO2B1, Slco1c1/BSAT, ITM2aB17:H27, ZO3, FGF-19, HARP, PLP-1, PROM1, SELE).

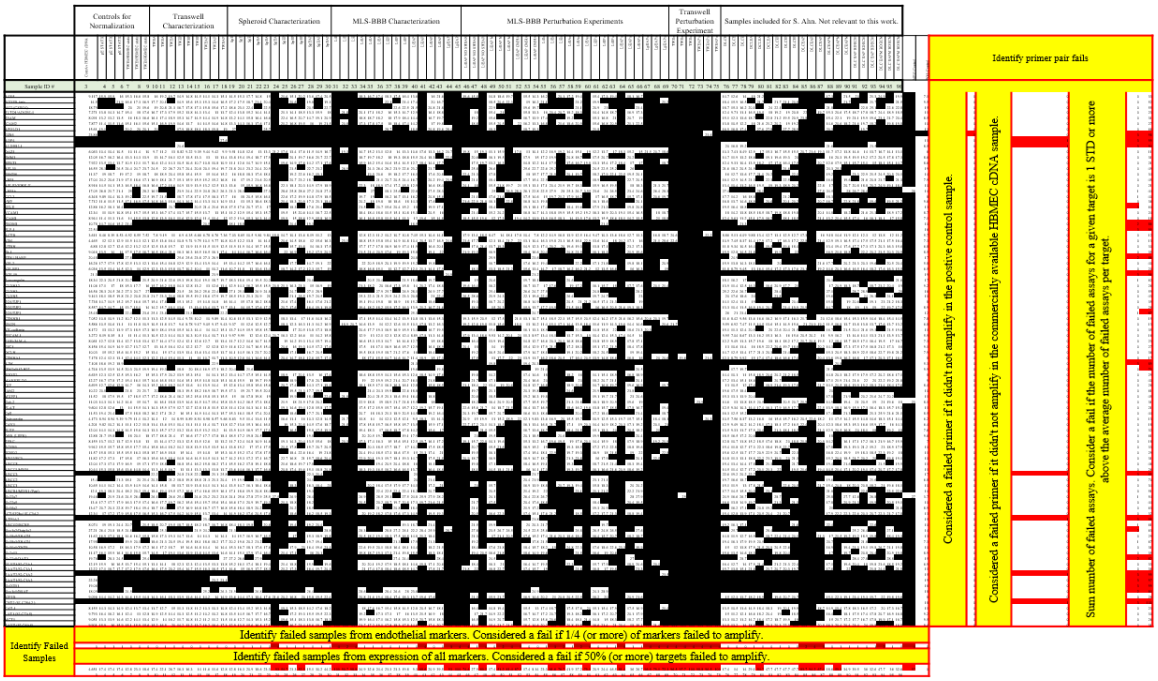

Figure 24. Identification of failed assays from HT-qPCR array. Failed samples and failed targets were identified (red cells) and removed prior to data processing and analysis to prevent distortion of results. Failed assays are designated a placeholder Ct value of 999 (blacked out cells) that will skew ΔCt, ΔΔCt, and fold change values if they are not removed.

After the removal of all assay fails, fold change values were obtained from the equations listed in **Figure 24.** Briefly, housekeeping genes were selected from a review relevant literature, and careful attention was paid to be sure that they were suitable for study [168]. As an extra precaution, extra housekeeping genes were included on the panel to ensure that more than one would be available for normalization of data. Ct values were normalized to the geometric mean of at least two housekeeping genes (BBB studies: OAZ1, HRPT1; HA study: OAZ1, HRPT1, PMM1) to account for variation in the amount of genetic material present in each sample to obtain ΔCt values. ΔCt values were then converted to ΔΔCt values via subtraction of the ΔCt of the control sample (either 2D HA or static, mono-culture iHBMECs) from the ΔCt of each sample for each target. Fold

change values were then calculated by taking $2^{-\Delta\Delta Ct}$. All data processing was performed in Excel before being exported for importation into statistical analysis software.

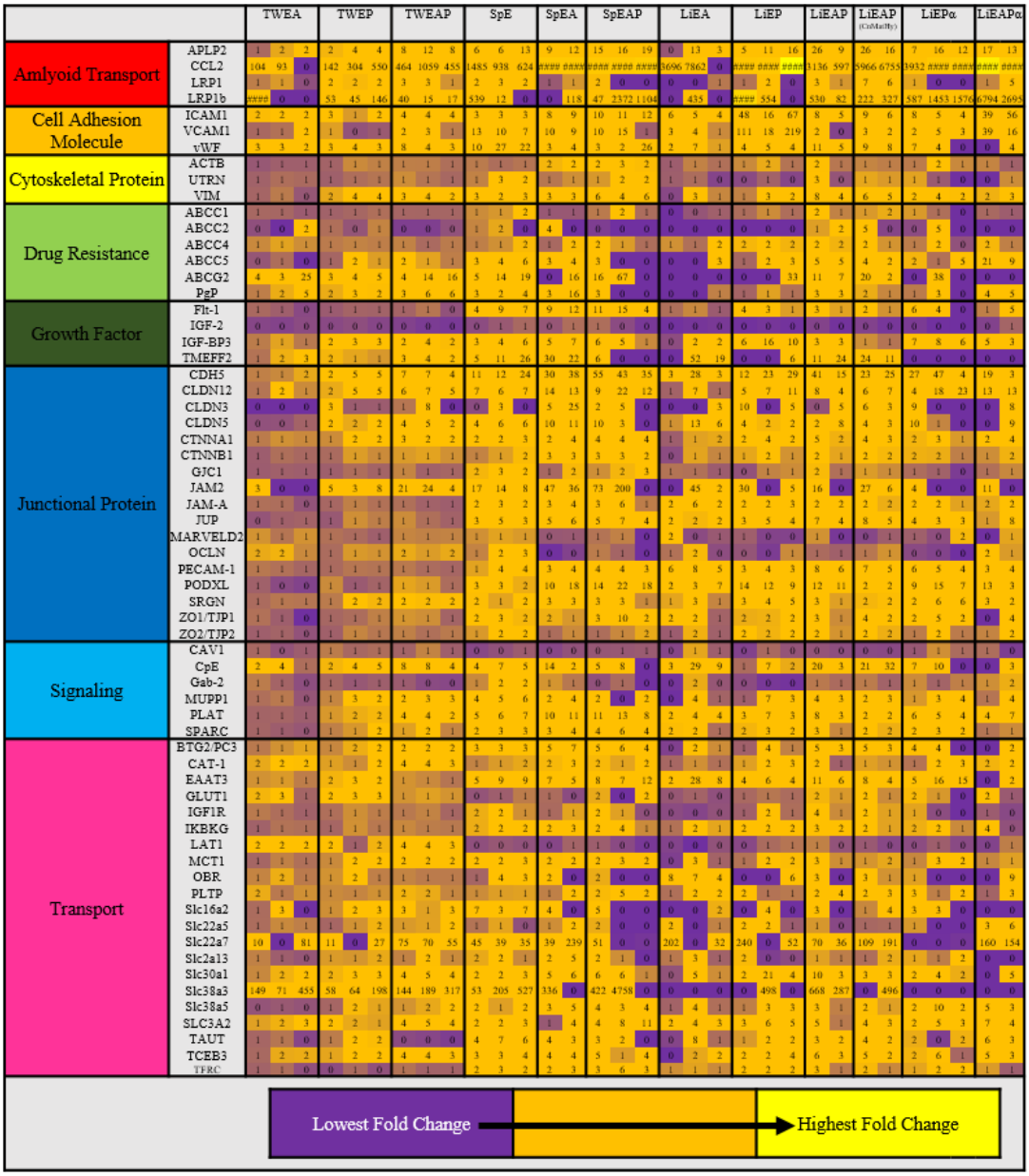

Figure 25. Heat map of fold change values sorted by specialization category (rows) and sample (columns). Fold change values are color coded with conditional formatting in excel with the highest fold change relative to 2D static culture indicated by yellow, and the lowest fold change relative to 2D static culture indicated by purple.

6.4.3 Statistical Analysis of Fold Change Data

Statistical analysis methods are predicated on assumptions that must hold true for the analysis to be robust and accurately reflect the data in question. Although qPCR is widely used, statistical analysis performed on results varies widely from study to study. The primary reason for the lack of a gold standard practice for determining the statistical significance of relative expression (fold change) data is the ambiguity regarding the underlying probability distribution of relative expression data [171]. When small sample numbers are used (N<20) and the underlying probability distribution is unknown, it is recommended that re-sampling methods be used to assess percentiles and the related statistical significance of the data [172].

After careful review of the relevant literature, we chose to use the BootstRatio online tool to determine which targets from our data sets were significantly up or down regulated relative to the control group [167, 169-176]. The BootstRatio tool is based on bootstrapping resampling and permutation methods that enable the assessment of the significance of gene expression ratios without any assumptions regarding the underlying probability distributions of the data set [172]. The BootstRatio online tool has two functionalities. It can be used to determine which targets are significantly up or down regulated in given a single sample (already normalized to a control) or it can determine which targets are significantly up or down regulated between two samples.

In our analysis, we used the BootstRatio tool to identify targets that had significantly higher or lower expression between two samples. All other analysis was performed via GraphPad Prism software. Wilcoxon matched pairs singed rank tests were used to

determine if two expression profiles (i.e. all target expression in a given sample, or expression for a subset of targets within a category) were significantly different between two samples. A Friedmans' test with a Dunn's post-test to account for multiple comparisons was used to compare the expression profiles of three or more groups. All reported p-values are two-tailed and significance was assigned as follows: not significant, n.s.; *$p < 0.05$; **$p < 0.01$; ***$p < 0.001$; ****$p < 0.0001$.

6.5 Proof of Concept Studies

6.5.1 Media Optimization for Co-Culture Experiments

Different cell lines have different suggested media compositions for optimal *in vitro* culture. We conducted a proof of concept study to verify that combination of the relevant cell specific medias would not negatively impact cell morphology in co-culture models containing more than one cell type. From this study, we determined that using 1:1 ratios of all relevant cell specific media caused the least observable difference in cell morphologies across the various cell types used.

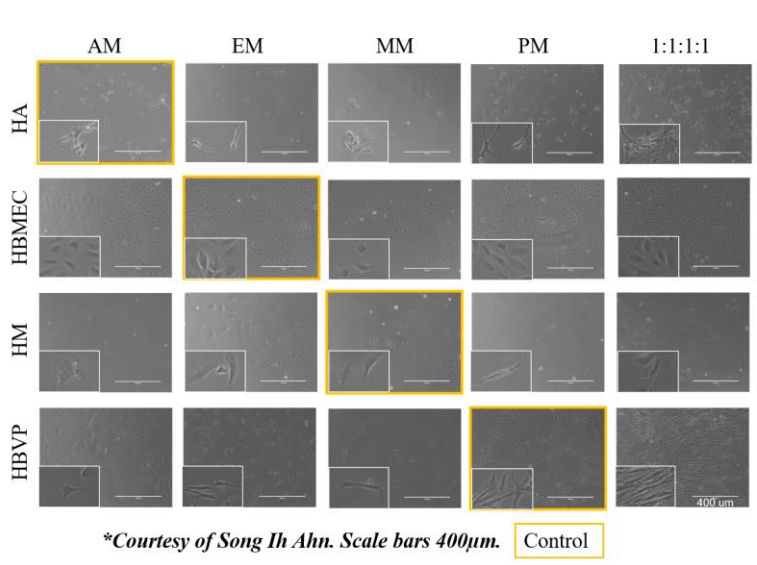

Figure 26. Results of media optimization experiment. Morphological changes to cells are easily observed when cells are cultured in the wrong cell type specific media, but culture in combination media is able to mitigate these changes.

6.5.2 Formation of Round Sacrificial Elements

The sacrificial element protocol utilized in this work had previously only been used to craft square elements using silicon wafer master molds for soft lithography of element molds. Using this method, the authors were able to craft channel geometries with features as small as 5μm x 5μm (h x w) [42]. We were successful in adapting this method to produce both square and round sacrificial elements ranging in diameter from 50-500μm. However, throughout the course of our studies, we noted that square elements cast with better resolution and preservation of original injection mold shape due to the difference in the substrate properties between silicon wafer molds and 3D printed molds. Additionally, round elements require the perfect alignment of injection mod slabs or the channel shape can become distorted (**Figure 26:** Bottom row, middle panel). Literature evidence indicate that shear stress plays a larger role influencing endothelial cells than lumen geometry [177],

and preliminary experimentation with both square and round sacrificial elements yielded indistinguishable results in lumen formation, indicating that square elements could be used for future studies to eliminate fabrication issues associated with round sacrificial elements.

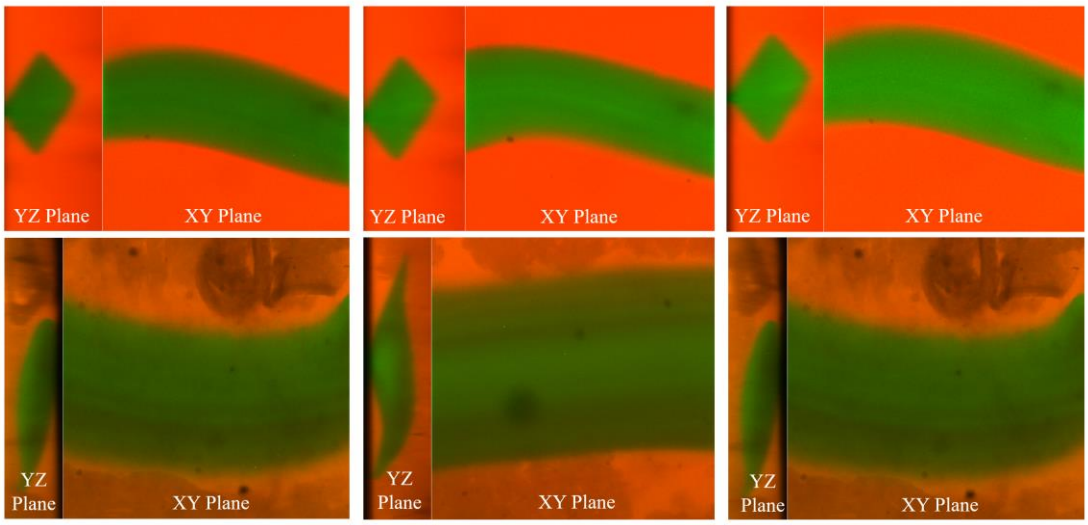

Figure 27. XY-plane and YZ-plane views of square and round sacrificial elements. Elements were doped GFP and encapsulated in RFP doped Matrigel for imaging. Noticeable variability exists in the YZ projections of round elements due to issues with injection mold alignment during fabrication (bottom row). Square element injection molds do not require alignment, and the resulting shape is more consistent (top row).

6.5.3 Dose Determination for TNFα Administration to MLS-BBB

In order to conduct qPCR on recovered cells, it is essential that the administration concentration of TNFα is sufficiently high to induce inflammation, but not so high as to kill all the cells. Similar studies are available in the literature, and sources that examined similar cells types used concentrations ranging from 50pg/mL - 50 ng/mL [160, 178]. Prior to experimentation, we administered various concentration of TNFα to static cultured iHBMEC cells to determine the most appropriate dosing concentration for our study. iHBMEC cells were seeded into 0.1% gelatin coated wells (96 well plate, 200µL/well, 1E5

cells/mL) and allowed to expand for three days prior to experimentation. TNFα was prepared in cell specific media at concentrations of 0, 1, 10, 20, and 40 ng/mL. Cells were incubated with TNFα media for 24 hours before conducting a Live/Dead assay to visualize cell death. Our results confirmed those found in literature that a dosing concentration of 40ng/mL would be sufficient to elicit cell death, but not so harsh as to kill all the cells.

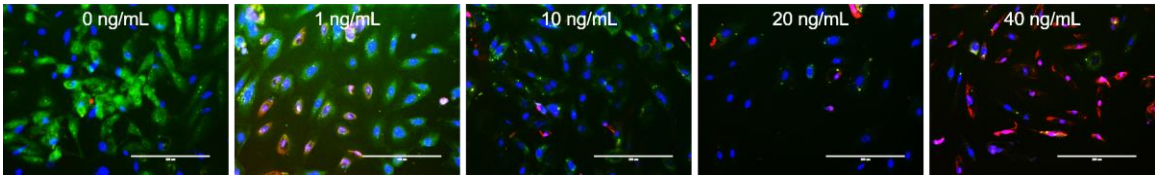

Figure 28. Live/Dead staining of 2D cultured iHBMEC cells. Live/Dead assay results of TNFα administration to static mono-culture iHBMEC cells indicate that a dosing concentration of 40ng/mL should be sufficient to initiate response from models.

6.5.4 Permeability Studies with MLS-BBB

While the primary goal of this work was the construction and high throughput characterization of a novel in vitro BBB model, the downstream application as a preclinical screening tool necessitates compatibility with standard permeability protocol workflows if the model is to be useful. Thus, we conducted a proof of concept study to demonstrate that our model will facilitate the conduction of fluorescence based permeability assays. Protocols for such assays are readily available and have been carried out in similar lumen models with good success [110].

Monoculture iHBMEC lumens were grown in MLS-BBB devices for 5 days before use in permeability assays. Culture media was supplemented with 5μg/mL fluorescently tagged dextran (either 4kDa or 150 kDa) and a shear rate of 1dyne/cm^2 was initiated via the establishment of a 137 μL volume difference between the reservoirs. Fluorescent

images were obtained every 5 seconds for 15 minutes via the time lapse capture function on an EVOS FL Auto microscope. Mean fluorescent intensity values in the channel, surrounding region, and background were obtained via Image J for N=3 devices and n=10 measurements in each case. Apparent permeability values were calculated using equation 9 and compared to previously published results from previous studies. Our results indicate that our mono-culture iHBMEC lumen has apparent permeabilities of 3.17E-6 cm/s (+/- 2.85E-8) and 3.125E-5 cm/s (+/- 1.0223E-6) for 150kDa and 4kDa dextrans, respectively. Comparison to previously published results (**Figure 28 D)** indicates that our MLS-BBB device performs comparably to other models available in the literature [108, 110].

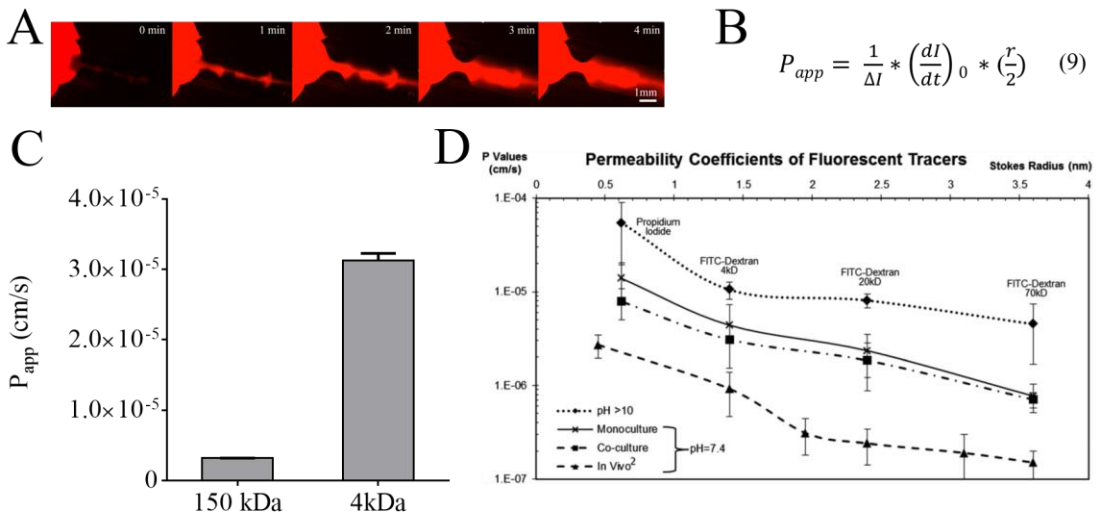

Figure 29. Proof of concept permeability study. (A) Representative images of 150kDa TRITC-Dextran permeability in MLS-BBB device. (B) Equation for the calculation of apparent permeability where ΔI is the increase in total fluorescence intensity upon adding labeled dextran, $(dI/dt)_0$ is the initial rate of increase in intensity as dextran diffuses out of the tube into the surrounding gel, and r is the radius of the tube (C) Results of preliminary permeability studies conducted with 4kDa and 150kDa tagged dextran. Data depicted are mean +/- SEM apparent permeability values (N=3) (D) Excerpt from Booth and Kim study [108] indicates that observed permeability values fall within range of expected results.

6.5.5 Recovery of All Three 3 NVU Cell Types via FACS

As discussed, the function of the BBB is largely dependent on the function and health of the supporting cell types of the NVU. Thus, the next logical assessment of our (or other) devices would be detailed examination of the health and physiological relevance of the support cell types present in culture in addition to the endothelial cells. Preliminary protocol development for the purification and recovery of all cells types from co-culture was attempted using cell specific probes for each cell type that were successfully used for imaging protocols as they were cross listed for use in FACS by the manufacturers (HBMEC, Anti-CD31; HBVP, αSMA; HA, Anti-GFAP). Manufacturer instructions for dilution and sample preparation were followed exactly and compensation controls were used during initialization of FACS sorting protocol development to prevent crossover between channels with potentially overlapping spectra.

Preliminary results of staining are shown in **Figure 29.** Of the probes tested, only the CD31 probe performed well. The GFAP probe appears unable to bind, and the αSMA peak separation was poor. Consultation of the Human Protein Atlas (http://www.proteinatlas.org) indicates that this is most likely due to the partial or complete internal localization αSMA and GFAP. While these probes could be used with good success when sorting was carried out on fixed and permeabilized samples, fixation can significantly degrade RNA, rendering it useless for qPCR analysis [179]. Unfortunately, a set of three externally located, distinct cell marker antibodies that were also conjugated to spectrally distinct fluorophores was unavailable during the course of experimentation. For future experimentation we recommend the use of multiple antibodies per cell type so that the distinct combinations of a certain set of fluorophores could be used to gate for live

sorting, rather than a single fluorophore or the modification of the RNA extraction and purification protocols to facilitate processing of fixed samples [180].

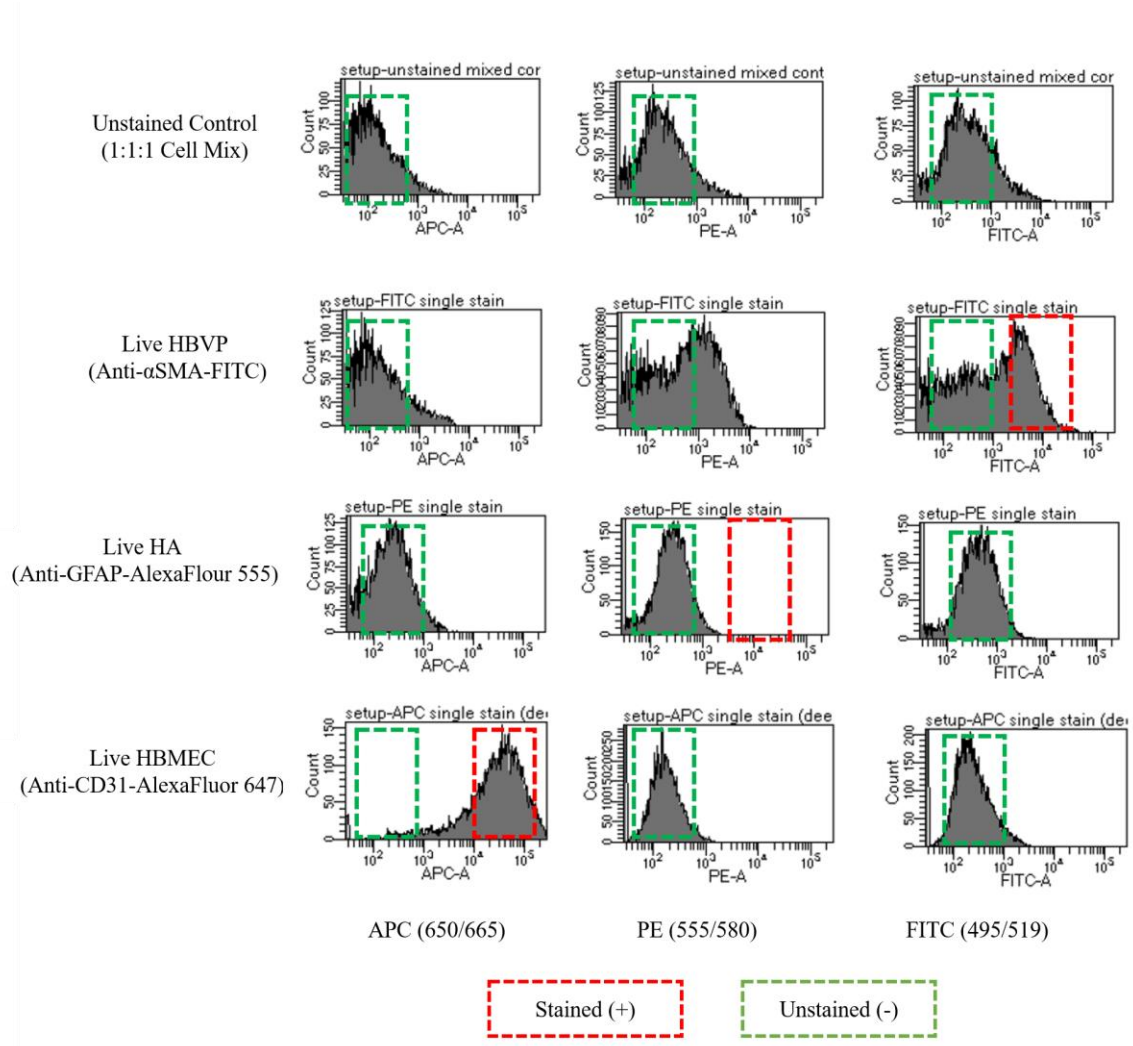

Figure 30. Live staining requires distinctly tagged extracellularly located proteins as antibody targets. Histograms from a test sort of all three cell types are presented with stained (red) and unstained peaks (green) indicated. HBMEC staining was successful, as indicated by a peak shift into the stained region of the histogram after staining. HBVP staining yielded split peaks potentially due to partial endocytosis of the antibody by the HBVPs before FACS. HA staining was completely ineffective due to the internal localization of GFAP.

REFERENCES

1. Thomas D, Burns J, Audette J, Carrol A, Dow-Hygelund C, Hay M: **Clinical development success rates 2006-2015**. *San Diego: Biomedtracker/Washington, DC: BIO/Bend: Amplion* 2016.

2. Gallet CA, Doucouliagos H: **The impact of healthcare spending on health outcomes: A meta-regression analysis**. *Social Science & Medicine* 2017, **179**:9-17.

3. Workman P, Draetta GF, Schellens JHM, Bernards R: **How Much Longer Will We Put Up With $100,000 Cancer Drugs?** *Cell* 2017, **168**(4):579-583.

4. Becker KP, Baehring JM: **Current Standard Treatment Options for Malignant Glioma**. In: *Malignant Brain Tumors.* edn.: Springer; 2017: 123-131.

5. Naik P, Cucullo L: **In vitro blood-brain barrier models: current and perspective technologies**. *J Pharm Sci* 2012, **101**(4):1337-1354.

6. Arrowsmith J, Miller P: **Trial Watch: Phase II and Phase III attrition rates 2011-2012**. *Nat Rev Drug Discov* 2013, **12**(8):569-569.

7. Junaid A, Mashaghi A, Hankemeier T, Vulto P: **An end-user perspective on Organ-on-a-Chip: Assays and usability aspects**. *Current Opinion in Biomedical Engineering* 2017, **1**:15-22.

8. van der Meer AD, van den Berg A: **Organs-on-chips: breaking the in vitro impasse**. *Integrative Biology* 2012, **4**(5):461-470.

9. Neuzi P, Giselbrecht S, Länge K, Huang TJ, Manz A: **Revisiting lab-on-a-chip technology for drug discovery**. *Nature reviews Drug discovery* 2012, **11**(8):620.

10. Bhatia SN, Ingber DE: **Microfluidic organs-on-chips**. *Nat Biotech* 2014, **32**(8):760-772.

11. Huh D, Matthews BD, Mammoto A, Montoya-Zavala M, Hsin HY, Ingber DE: **Reconstituting organ-level lung functions on a chip**. *Science* 2010, **328**(5986):1662-1668.

12. Esch EW, Bahinski A, Huh D: **Organs-on-chips at the frontiers of drug discovery**. *Nat Rev Drug Discov* 2015, **14**(4):248-260.

13. Huh D, Torisawa Y-s, Hamilton GA, Kim HJ, Ingber DE: **Microengineered physiological biomimicry: organs-on-chips**. *Lab on a chip* 2012, **12**(12):2156-2164.

14. Fabre KM, Livingston C, Tagle DA: **Organs-on-chips (microphysiological systems): tools to expedite efficacy and toxicity testing in human tissue**. *Experimental Biology and Medicine* 2014:1535370214538916.

15. Association As: **2017 Alzheimer's disease facts and figures**. *Alzheimer's & Dementia* 2017, **13**(4):325-373.

16. Sung JH, Esch MB, Prot J-M, Long CJ, Smith A, Hickman JJ, Shuler ML: **Microfabricated mammalian organ systems and their integration into models of whole animals and humans**. *Lab on a Chip* 2013, **13**(7):1201-1212.

17. Huh D, Leslie DC, Matthews BD, Fraser JP, Jurek S, Hamilton GA, Thorneloe KS, McAlexander MA, Ingber DE: **A human disease model of drug toxicity–induced pulmonary edema in a lung-on-a-chip microdevice**. *Science translational medicine* 2012, **4**(159):159ra147-159ra147.

18. Lee K-H, Lee J, Lee S-H: **3D liver models on a microplatform: well-defined culture, engineering of liver tissue and liver-on-a-chip**. *Lab on a Chip* 2015, **15**(19):3822-3837.

19. Prot J-M, Bunescu A, Elena-Herrmann B, Aninat C, Snouber LC, Griscom L, Razan F, Bois FY, Legallais C, Brochot C: **Predictive toxicology using systemic biology and liver microfluidic "on chip" approaches: application to acetaminophen injury**. *Toxicology and applied pharmacology* 2012, **259**(3):270-280.

20. Grosberg A, Alford PW, McCain ML, Parker KK: **Ensembles of engineered cardiac tissues for physiological and pharmacological study: heart on a chip**. *Lab on a chip* 2011, **11**(24):4165-4173.

21. Agarwal A, Goss JA, Cho A, McCain ML, Parker KK: **Microfluidic heart on a chip for higher throughput pharmacological studies**. *Lab on a Chip* 2013, **13**(18):3599-3608.

22. Kim HJ, Li H, Collins JJ, Ingber DE: **Contributions of microbiome and mechanical deformation to intestinal bacterial overgrowth and inflammation in a human gut-on-a-chip**. *Proceedings of the National Academy of Sciences* 2016, **113**(1):E7-E15.

23. Kim HJ, Ingber DE: **Gut-on-a-Chip microenvironment induces human intestinal cells to undergo villus differentiation**. *Integrative Biology* 2013, **5**(9):1130-1140.

24. Kim HJ, Huh D, Hamilton G, Ingber DE: **Human gut-on-a-chip inhabited by microbial flora that experiences intestinal peristalsis-like motions and flow**. *Lab on a Chip* 2012, **12**(12):2165-2174.

25. Mu X, Zheng W, Xiao L, Zhang W, Jiang X: **Engineering a 3D vascular network in hydrogel for mimicking a nephron**. *Lab Chip* 2013, **13**(8):1612-1618.

26. Ha L, Jang K-J, Suh K-Y: **Kidney on a Chip**. In: *Microfluidics for Medical Applications.* edn.; 2014: 19-39.

27. Wilmer MJ, Ng CP, Lanz HL, Vulto P, Suter-Dick L, Masereeuw R: **Kidney-on-a-chip technology for drug-induced nephrotoxicity screening**. *Trends in biotechnology* 2016, **34**(2):156-170.

28. Ferrell N, Desai RR, Fleischman AJ, Roy S, Humes HD, Fissell WH: **A microfluidic bioreactor with integrated transepithelial electrical resistance (TEER) measurement electrodes for evaluation of renal epithelial cells**. *Biotechnol Bioeng* 2010, **107**(4):707-716.

29. Kim S, LesherPerez SC, Yamanishi C, Labuz JM, Leung B, Takayama S: **Pharmacokinetic profile that reduces nephrotoxicity of gentamicin in a perfused kidney-on-a-chip**. *Biofabrication* 2016, **8**(1):015021.

30. Torisawa Y-s, Spina CS, Mammoto T, Mammoto A, Weaver JC, Tat T, Collins JJ, Ingber DE: **Bone marrow–on–a–chip replicates hematopoietic niche physiology in vitro**. *Nature methods* 2014, **11**(6):663-669.

31. Wagner I, Materne E-M, Brincker S, Süßbier U, Frädrich C, Busek M, Sonntag F, Sakharov DA, Trushkin EV, Tonevitsky AG: **A dynamic multi-organ-chip for long-term cultivation and substance testing proven by 3D human liver and skin tissue co-culture**. *Lab on a Chip* 2013, **13**(18):3538-3547.

32. Black AF, Berthod F, L'Heureux N, Germain L, Auger FA: **In vitro reconstruction of a human capillary-like network in a tissue-engineered skin equivalent**. *FASEB J* 1998, **12**(13):1331-1340.

33. Ataç B, Wagner I, Horland R, Lauster R, Marx U, Tonevitsky AG, Azar RP, Lindner G: **Skin and hair on-a-chip: in vitro skin models versus ex vivo tissue maintenance with dynamic perfusion**. *Lab on a chip* 2013, **13**(18):3555-3561.

34. Pamies D, Hartung T, Hogberg HT: **Biological and medical applications of a brain-on-a-chip**. *Experimental biology and medicine* 2014, **239**(9):1096-1107.

35. Park J, Lee BK, Jeong GS, Hyun JK, Lee CJ, Lee S-H: **Three-dimensional brain-on-a-chip with an interstitial level of flow and its application as an in vitro model of Alzheimer's disease**. *Lab on a Chip* 2015, **15**(1):141-150.

36. Low LA, Tagle DA: **Organs-on-chips: Progress, challenges, and future directions**. *Experimental Biology and Medicine* 2017:1535370217700523.

37. Reardon S: **'Organs-on-chips' go mainstream: drug companies put in vitro systems through their paces**. *Nature* 2015, **523**(7560):266-267.

38. Hasan A, Paul A, Vrana NE, Zhao X, Memic A, Hwang Y-S, Dokmeci MR, Khademhosseini A: **Microfluidic techniques for development of 3D vascularized tissue**. *Biomaterials* 2014, **35**(26):7308-7325.

39. Lovett M, Lee K, Edwards A, Kaplan DL: **Vascularization strategies for tissue engineering**. *Tissue engineering Part B, Reviews* 2009, **15**(3):353-370.

40. Kim S, Lee H, Chung M, Jeon NL: **Engineering of functional, perfusable 3D microvascular networks on a chip**. *Lab Chip* 2013, **13**(8):1489-1500.

41. Huang GY, Zhou LH, Zhang QC, Chen YM, Sun W, Xu F, Lu TJ: **Microfluidic hydrogels for tissue engineering**. *Biofabrication* 2011, **3**(1):012001.

42. Golden AP, Tien J: **Fabrication of microfluidic hydrogels using molded gelatin as a sacrificial element**. *Lab Chip* 2007, **7**(6):720-725.

43. Miller JS, Stevens KR, Yang MT, Baker BM, Nguyen D-HT, Cohen DM, Toro E, Chen AA, Galie PA, Yu X *et al*: **Rapid casting of patterned vascular networks for perfusable engineered 3D tissues**. *Nature materials* 2012, **11**(9):768-774.

44. Bischel LL, Lee S-H, Beebe DJ: **A practical method for patterning lumens through ECM hydrogels via viscous finger patterning**. *Journal of laboratory automation* 2012, **17**(2):96-103.

45. Zheng Y, Chen J, Craven M, Choi NW, Totorica S, Diaz-Santana A, Kermani P, Hempstead B, Fischbach-Teschl C, López JA: **In vitro microvessels for the study of angiogenesis and thrombosis**. *Proceedings of the National Academy of Sciences* 2012, **109**(24):9342-9347.

46. Li X, Mearns SM, Martins-Green M, Liu Y: **Procedure for the development of multi-depth circular cross-sectional endothelialized microchannels-on-a-chip**. *Journal of visualized experiments : JoVE* 2013(80):e50771.

47. Hasan A, Paul A, Memic A, Khademhosseini A: **A multilayered microfluidic blood vessel-like structure**. *Biomedical microdevices* 2015, **17**(5):88-88.

48. Wilson ME, Kota N, Kim Y, Wang Y, Stolz DB, LeDuc PR, Ozdoganlar OB: **Fabrication of circular microfluidic channels by combining mechanical micromilling and soft lithography**. *Lab Chip* 2011, **11**(8):1550-1555.

49. Kolesky DB, Homan KA, Skylar-Scott MA, Lewis JA: **Three-dimensional bioprinting of thick vascularized tissues**. *Proceedings of the National Academy of Sciences* 2016, **113**(12):3179-3184.

50. Chang R, Nam J, Sun W: **Direct cell writing of 3D microorgan for in vitro pharmacokinetic model**. *Tissue Engineering Part C: Methods* 2008, **14**(2):157-166.

51. Lee W, Lee V, Polio S, Keegan P, Lee JH, Fischer K, Park JK, Yoo SS: **On-demand three-dimensional freeform fabrication of multi-layered hydrogel scaffold with fluidic channels**. *Biotechnology and bioengineering* 2010, **105**(6):1178-1186.

52. Culver JC, Hoffmann JC, Poché RA, Slater JH, West JL, Dickinson ME: **Three-Dimensional Biomimetic Patterning in Hydrogels to Guide Cellular Organization**. *Advanced materials* 2012, **24**(17):2344-2348.

53. Heintz KA, Bregenzer ME, Mantle JL, Lee KH, West JL, Slater JH: **Fabrication of 3D biomimetic microfluidic networks in hydrogels**. *Advanced healthcare materials* 2016, **5**(17):2153-2160.

54. Heintz KA, Mayerich D, Slater JH: **Image-guided, Laser-based Fabrication of Vascular-derived Microfluidic Networks**. *Journal of visualized experiments: JoVE* 2017(119).

55. Patan S: **Vasculogenesis and angiogenesis**. *Cancer treatment and research* 2004, **117**:3-32.

56. Chung S, Sudo R, Mack PJ, Wan C-R, Vickerman V, Kamm RD: **Cell migration into scaffolds under co-culture conditions in a microfluidic platform**. *Lab on a Chip* 2009, **9**(2):269-275.

57. Pill K, Hofmann S, Redl H, Holnthoner W: **Vascularization mediated by mesenchymal stem cells from bone marrow and adipose tissue: a comparison**. *Cell Regeneration* 2015, **4**:8.

58. Byun CK, Abi-Samra K, Cho Y-K, Takayama S: **Pumps for microfluidic cell culture**. *ELECTROPHORESIS* 2014, **35**(2-3):245-257.

59. Abbott NJ, Patabendige AA, Dolman DE, Yusof SR, Begley DJ: **Structure and function of the blood-brain barrier**. *Neurobiol Dis* 2010, **37**(1):13-25.

60. Abbott NJ, Ronnback L, Hansson E: **Astrocyte-endothelial interactions at the blood-brain barrier**. *Nat Rev Neurosci* 2006, **7**(1):41-53.

61. Pardridge WM: **Blood–brain barrier delivery**. *Drug Discovery Today* 2007, **12**(1–2):54-61.

62. Pardridge WM: **Blood-brain barrier genomics**. *Stroke; a journal of cerebral circulation* 2007, **38**(2 Suppl):686-690.

63. Shusta EV: **Blood-Brain Barrier Genomics, Proteomics, and New Transporter Discovery**. *NeuroRx* 2005, **2**(1):151-161.

64. Zlokovic BV: **The Blood-Brain Barrier in Health and Chronic Neurodegenerative Disorders**. *Neuron* 2008, **57**(2):178-201.

65. Zlokovic BV: **Neurovascular mechanisms of Alzheimer's neurodegeneration**. *Trends in Neurosciences* 2005, **28**(4):202-208.

66. Pottiez G, Flahaut C, Cecchelli R, Karamanos Y: **Understanding the blood–brain barrier using gene and protein expression profiling technologies**. *Brain Research Reviews* 2009, **62**(1):83-98.

67. Bauer H-C, Krizbai IA, Bauer H, Traweger A: **"You Shall Not Pass"—tight junctions of the blood brain barrier**. *Frontiers in neuroscience* 2014, **8**:392.

68. Kniesel U, Wolburg H: **Tight junctions of the blood–brain barrier**. *Cellular and molecular neurobiology* 2000, **20**(1):57-76.

69. Wolburg H, Lippoldt A: **Tight junctions of the blood–brain barrier: development, composition and regulation**. *Vascular pharmacology* 2002, **38**(6):323-337.

70. Abbott NJ: **Blood-brain barrier structure and function and the challenges for CNS drug delivery**. *J Inherit Metab Dis* 2013, **36**(3):437-449.

71. Nag S: **The Blood-Brain and Other Neural Barriers**. *Review and protocols* 2011.

72. Pardridge WM: **The Blood-Brain Barrier: Bottleneck in Brain Drug Development**. *NeuroRx* 2005, **2**(1):3-14.

73. Hawkins BT, Davis TP: **The blood-brain barrier/neurovascular unit in health and disease**. *Pharmacological reviews* 2005, **57**(2):173-185.

74. Lok J, Gupta P, Guo S, Kim WJ, Whalen MJ, van Leyen K, Lo EH: **Cell–cell signaling in the neurovascular unit**. *Neurochemical research* 2007, **32**(12):2032-2045.

75. Zlokovic BV: **Neurodegeneration and the neurovascular unit**. *Nature medicine* 2010, **16**(12):1370-1371.

76. Obermeier B, Daneman R, Ransohoff RM: **Development, maintenance and disruption of the blood-brain barrier**. *Nat Med* 2013, **19**(12):1584-1596.

77. Ballabh P, Braun A, Nedergaard M: **The blood–brain barrier: an overview: Structure, regulation, and clinical implications**. *Neurobiology of Disease* 2004, **16**(1):1-13.

78. Wolburg H, Noell S, Mack A, Wolburg-Buchholz K, Fallier-Becker P: **Brain endothelial cells and the glio-vascular complex**. *Cell Tissue Res* 2009, **335**(1):75-96.

79. Bonneh-Barkay D, Wiley CA: **Brain Extracellular Matrix in Neurodegeneration**. *Brain pathology (Zurich, Switzerland)* 2009, **19**(4):573-585.

80. Al Ahmad A, Gassmann M, Ogunshola O: **Maintaining blood–brain barrier integrity: pericytes perform better than astrocytes during prolonged oxygen deprivation**. *Journal of cellular physiology* 2009, **218**(3):612-622.

81. Bergers G, Song S: **The role of pericytes in blood-vessel formation and maintenance**. *Neuro-Oncology* 2005, **7**(4):452-464.

82. Urich E, Patsch C, Aigner S, Graf M, Iacone R, Freskgard PO: **Multicellular Self-Assembled Spheroidal Model of the Blood Brain Barrier**. *Scientific reports* 2013, **3**.

83. Novak U, Kaye AH: **Extracellular matrix and the brain: components and function**. *Journal of Clinical Neuroscience* 2000, **7**(4):280-290.

84. Placone AL, McGuiggan PM, Bergles DE, Guerrero-Cazares H, Quiñones-Hinojosa A, Searson PC: **Human astrocytes develop physiological morphology and remain quiescent in a novel 3D matrix**. *Biomaterials* 2015, **42**:134-143.

85. Pekny M, Nilsson M: **Astrocyte activation and reactive gliosis**. *Glia* 2005, **50**(4):427-434.

86. Cabezas R, Ávila M, Gonzalez J, El-Bachá RS, Báez E, García-Segura LM, Jurado Coronel JC, Capani F, Cardona-Gomez GP, Barreto GE: **Astrocytic modulation of blood brain barrier: perspectives on Parkinson's disease**. *Frontiers in Cellular Neuroscience* 2014, **8**:211.

87. Pekny M, Wilhelmsson U, Pekna M: **The dual role of astrocyte activation and reactive gliosis**. *Neuroscience Letters* 2014, **565**:30-38.

88. Zamanian JL, Xu L, Foo LC, Nouri N, Zhou L, Giffard RG, Barres BA: **Genomic Analysis of Reactive Astrogliosis**. *The Journal of neuroscience : the official journal of the Society for Neuroscience* 2012, **32**(18):6391-6410.

89. Groothuis DR: **The blood-brain and blood-tumor barriers: a review of strategies for increasing drug delivery**. *Neuro Oncol* 2000, **2**(1):45-59.

90. Vykhodtseva N, McDannold N, Hynynen K: **Progress and problems in the application of focused ultrasound for blood–brain barrier disruption**. *Ultrasonics* 2008, **48**(4):279-296.

91. Rapoport SI: **Osmotic opening of the blood–brain barrier: principles, mechanism, and therapeutic applications**. *Cellular and molecular neurobiology* 2000, **20**(2):217-230.

92. Pardeshi CV, Belgamwar VS: **Direct nose to brain drug delivery via integrated nerve pathways bypassing the blood–brain barrier: an excellent platform for brain targeting**. *Expert opinion on drug delivery* 2013, **10**(7):957-972.

93. Mistry A, Stolnik S, Illum L: **Nanoparticles for direct nose-to-brain delivery of drugs**. *International Journal of Pharmaceutics* 2009, **379**(1):146-157.

94. Hada N, Netzer WJ, Belhassan F, Wennogle LP, Gizurarson S: **Nose-to-brain transport of imatinib mesylate: A pharmacokinetic evaluation**. *European Journal of Pharmaceutical Sciences* 2017, **102**:46-54.

95. Illum L: **Nasal drug delivery—possibilities, problems and solutions**. *Journal of Controlled Release* 2003, **87**(1):187-198.

96. Nazar H: **The potential for delivery of drugs via the nasal route is not to be sniffed at**. *Depression* 2017, **15**:23.

97. Veiseh O, Sun C, Fang C, Bhattarai N, Gunn J, Kievit F, Du K, Pullar B, Lee D, Ellenbogen RG *et al*: **Specific targeting of brain tumors with an optical/magnetic resonance imaging nanoprobe across the blood-brain barrier**. *Cancer Res* 2009, **69**(15):6200-6207.

98. Tiwari SB, Amiji MM: **A review of nanocarrier-based CNS delivery systems**. *Current Drug Delivery* 2006, **3**(2):219-232.

99. Schroeder A, Heller DA, Winslow MM, Dahlman JE, Pratt GW, Langer R, Jacks T, Anderson DG: **Treating metastatic cancer with nanotechnology**. *Nature Reviews Cancer* 2012, **12**(1):39-50.

100. Abbott NJ: **Prediction of blood–brain barrier permeation in drug discovery from in vivo, in vitro and in silico models**. *Drug Discovery Today: Technologies* 2004, **1**(4):407-416.

101. Clark DE: **In silico prediction of blood–brain barrier permeation**. *Drug Discovery Today* 2003, **8**(20):927-933.

102. Shityakov S, Roewer N, Broscheit J-A, Förster C: **In silico models for nanotoxicity evaluation and prediction at the blood-brain barrier level: A mini-review**. *Computational Toxicology* 2017, **2**:20-27.

103. Di L, Kerns EH, Fan K, McConnell OJ, Carter GT: **High throughput artificial membrane permeability assay for blood–brain barrier**. *European Journal of Medicinal Chemistry* 2003, **38**(3):223-232.

104. Bischel LL, Sung KE, Jimenez-Torres JA, Mader B, Keely PJ, Beebe DJ: **The importance of being a lumen**. *Faseb j* 2014, **28**(11):4583-4590.

105. Vandenhaute E, Sevin E, Hallier-Vanuxeem D, Dehouck MP, Cecchelli R: **Case study: adapting in vitro blood-brain barrier models for use in early-stage drug discovery**. *Drug Discov Today* 2012, **17**(7-8):285-290.

106. Wilhelm I, Krizbai IA: **In Vitro Models of the Blood-Brain Barrier for the Study of Drug Delivery to the Brain**. *Molecular pharmaceutics* 2014.

107. Culot M, Lundquist S, Vanuxeem D, Nion S, Landry C, Delplace Y, Dehouck MP, Berezowski V, Fenart L, Cecchelli R: **An in vitro blood-brain barrier model for high throughput (HTS) toxicological screening**. *Toxicol In Vitro* 2008, **22**(3):799-811.

108. Booth R, Kim H: **Characterization of a microfluidic in vitro model of the blood-brain barrier (muBBB)**. *Lab Chip* 2012, **12**(10):1784-1792.

109. Eigenmann DE, Xue G, Kim KS, Moses AV, Hamburger M, Oufir M: **Comparative study of four immortalized human brain capillary endothelial cell lines, hCMEC/D3, hBMEC, TY10, and BB19, and optimization of culture conditions, for an in vitro blood-brain barrier model for drug permeability studies**. *Fluids and barriers of the CNS* 2013, **10**(1):33.

110. Herland A, van der Meer AD, FitzGerald EA, Park T-E, Sleeboom JJF, Ingber DE: **Distinct Contributions of Astrocytes and Pericytes to Neuroinflammation Identified in a 3D Human Blood-Brain Barrier on a Chip**. *PLoS ONE* 2016, **11**(3):e0150360.

111. Cucullo L, Marchi N, Hossain M, Janigro D: **A dynamic in vitro BBB model for the study of immune cell trafficking into the central nervous system**. *Journal of cerebral blood flow and metabolism : official journal of the International Society of Cerebral Blood Flow and Metabolism* 2011, **31**(2):767-777.

112. Alcendor DJ, Block FE, 3rd, Cliffel DE, Daniels JS, Ellacott KL, Goodwin CR, Hofmeister LH, Li D, Markov DA, May JC *et al*: **Neurovascular unit on a chip: implications for translational applications**. *Stem Cell Res Ther* 2013, **4 Suppl 1**:S18.

113. Nakagawa S, Deli MA, Kawaguchi H, Shimizudani T, Shimono T, Kittel Á, Tanaka K, Niwa M: **A new blood–brain barrier model using primary rat brain endothelial cells, pericytes and astrocytes**. *Neurochemistry International* 2009, **54**(3–4):253-263.

114. Cucullo L, McAllister MS, Kight K, Krizanac-Bengez L, Marroni M, Mayberg MR, Stanness KA, Janigro D: **A new dynamic in vitro model for the multidimensional study of astrocyte-endothelial cell interactions at the blood-brain barrier**. *Brain Res* 2002, **951**(2):243-254.

115. Cucullo L, Hossain M, Tierney W, Janigro D: **A new dynamic in vitro modular capillaries-venules modular system: cerebrovascular physiology in a box**. *BMC Neurosci* 2013, **14**:18.

116. Deosarkar SP, Prabhakarpandian B, Wang B, Sheffield JB, Krynska B, Kiani MF: **A Novel Dynamic Neonatal Blood-Brain Barrier on a Chip**. *PLOS ONE* 2015, **10**(11):e0142725.

117. Wang JD, Khafagy el S, Khanafer K, Takayama S, ElSayed ME: **Organization of Endothelial Cells, Pericytes, and Astrocytes into a 3D Microfluidic in Vitro Model of the Blood-Brain Barrier**. *Molecular pharmaceutics* 2016, **13**(3):895-906.

118. Brown JA, Pensabene V, Markov DA, Allwardt V, Neely MD, Shi M, Britt CM, Hoilett OS, Yang Q, Brewer BM *et al*: **Recreating blood-brain barrier physiology and structure on chip: A novel neurovascular microfluidic bioreactor**. *Biomicrofluidics* 2015, **9**(5):054124.

119. Grant GA, Abbott NJ, Janigro D: **Understanding the Physiology of the Blood-Brain Barrier: In Vitro Models**. *Physiology* 1998, **13**(6):287-293.

120. Cucullo L, Hossain M, Puvenna V, Marchi N, Janigro D: **The role of shear stress in Blood-Brain Barrier endothelial physiology**. *BMC Neuroscience* 2011, **12**:40-40.

121. Griffith LG, Swartz MA: **Capturing complex 3D tissue physiology in vitro**. *Nat Rev Mol Cell Biol* 2006, **7**(3):211-224.

122. Li L, Zhou Q, Voss TC, Quick KL, LaBarbera DV: **High-throughput imaging: Focusing in on drug discovery in 3D**. *Methods* 2016, **96**:97-102.

123. Li G, Simon MJ, Cancel L, Shi ZD, Ji X, Tarbell JM, Morrison B, Fu BM: **Permeability of in vitro blood-brain barrier models**. In: *Proceedings of the 2010 IEEE 36th Annual Northeast Bioengineering Conference (NEBEC): 26-28 March 2010 2010*; 2010: 1-2.

124. Santaguida S, Janigro D, Hossain M, Oby E, Rapp E, Cucullo L: **Side by side comparison between dynamic versus static models of blood-brain barrier in vitro: a permeability study**. *Brain Res* 2006, **1109**(1):1-13.

125. Urich E, Lazic SE, Molnos J, Wells I, Freskgård P-O: **Transcriptional Profiling of Human Brain Endothelial Cells Reveals Key Properties Crucial for Predictive In Vitro Blood-Brain Barrier Models**. *PLoS ONE* 2012, **7**(5):e38149.

126. Griep LM, Wolbers F, de Wagenaar B, ter Braak PM, Weksler BB, Romero IA, Couraud PO, Vermes I, van der Meer AD, van den Berg A: **BBB on chip: microfluidic platform to mechanically and biochemically modulate blood-brain barrier function**. *Biomed Microdevices* 2013, **15**(1):145-150.

127. Yeon JH, Na D, Choi K, Ryu SW, Choi C, Park JK: **Reliable permeability assay system in a microfluidic device mimicking cerebral vasculatures**. *Biomed Microdevices* 2012, **14**(6):1141-1148.

128. Prabhakarpandian B, Shen MC, Nichols JB, Mills IR, Sidoryk-Wegrzynowicz M, Aschner M, Pant K: **SyM-BBB: a microfluidic Blood Brain Barrier model**. *Lab Chip* 2013, **13**(6):1093-1101.

129. Adriani G, Ma D, Pavesi A, Kamm RD, Goh EL: **A 3D neurovascular microfluidic model consisting of neurons, astrocytes and cerebral endothelial cells as a blood–brain barrier**. *Lab on a Chip* 2017.

130. Zhan C, Lu W: **The blood-brain/tumor barriers: challenges and chances for malignant gliomas targeted drug delivery**. *Curr Pharm Biotechnol* 2012, **13**(12):2380-2387.

131. Guerit S, Liebner S: **Blood-Brain Barrier Breakdown Determines Differential Therapeutic Outcome in Genetically Diverse Forms of Medulloblastoma**. *Cancer cell* 2016, **29**(4):427-429.

132. von Roemeling C, Jiang W, Chan CK, Weissman IL, Kim BYS: **Breaking Down the Barriers to Precision Cancer Nanomedicine**. *Trends in Biotechnology* 2017, **35**(2):159-171.

133. Caster JM, Patel AN, Zhang T, Wang A: **Investigational nanomedicines in 2016: a review of nanotherapeutics currently undergoing clinical trials**. *Wiley Interdisciplinary Reviews: Nanomedicine and Nanobiotechnology* 2017, **9**(1):e1416-n/a.

134. Bose RJC, Ravikumar R, Karuppagounder V, Bennet D, Rangasamy S, Thandavarayan RA: **Lipid–polymer hybrid nanoparticle-mediated therapeutics delivery: advances and challenges**. *Drug Discovery Today*.

135. Wang AZ, Langer R, Farokhzad OC: **Nanoparticle Delivery of Cancer Drugs**. *Annual Review of Medicine* 2012, **63**(1):185-198.

136. Saha M: **Nanomedicine: promising tiny machine for the healthcare in future-a review**. *Oman Med J* 2009, **24**(4):242-247.

137. Rosenson RS, Brewer HB, Jr., Ansell B, Barter P, Chapman MJ, Heinecke JW, Kontush A, Tall AR, Webb NR: **Translation of high-density lipoprotein function into clinical practice: current prospects and future challenges**. *Circulation* 2013, **128**(11):1256-1267.

138. Lundqvist M, Stigler J, Elia G, Lynch I, Cedervall T, Dawson KA: **Nanoparticle size and surface properties determine the protein corona with possible implications for biological impacts**. *Proceedings of the National Academy of Sciences* 2008, **105**(38):14265-14270.

139. Pinto MP, Arce M, Yameen B, Vilos C: **Targeted brain delivery nanoparticles for malignant gliomas**. *Nanomedicine* 2017, **12**(1):59-72.

140. Lockman P, Mumper R, Khan M, Allen D: **Nanoparticle technology for drug delivery across the blood-brain barrier**. *Drug development and industrial pharmacy* 2002, **28**(1):1-13.

141. Sanchez-Gaytan BL, Fay F, Lobatto ME, Tang J, Ouimet M, Kim Y, van der Staay SEM, van Rijs SM, Priem B, Zhang L *et al*: **HDL-Mimetic PLGA Nanoparticle To Target Atherosclerosis Plaque Macrophages**. *Bioconjugate Chemistry* 2015, **26**(3):443-451.

142. Tenzer S, Docter D, Rosfa S, Wlodarski A, Kuharev Jr, Rekik A, Knauer SK, Bantz C, Nawroth T, Bier C: **Nanoparticle size is a critical physicochemical determinant of the human blood plasma corona: a comprehensive quantitative proteomic analysis**. *ACS nano* 2011, **5**(9):7155-7167.

143. Murday JS, Siegel RW, Stein J, Wright JF: **Translational nanomedicine: status assessment and opportunities**. *Nanomedicine: Nanotechnology, Biology and Medicine* 2009, **5**(3):251-273.

144. Lu M, Ozcelik A, Grigsby CL, Zhao Y, Guo F, Leong KW, Huang TJ: **Microfluidic hydrodynamic focusing for synthesis of nanomaterials**. *Nano Today*.

145. Wang J, Song Y: **Microfluidic Synthesis of Nanohybrids**. *Small* 2017.

146. Kim Y, Fay F, Cormode DP, Sanchez-Gaytan BL, Tang J, Hennessy EJ, Ma M, Moore K, Farokhzad OC, Fisher EA *et al*: **Single step reconstitution of multifunctional high-density lipoprotein-derived nanomaterials using microfluidics**. *ACS nano* 2013, **7**(11):9975-9983.

147. Krizanac-Bengez L, Kapural M, Parkinson F, Cucullo L, Hossain M, Mayberg MR, Janigro D: **Effects of transient loss of shear stress on blood-brain barrier endothelium: role of nitric oxide and IL-6**. *Brain Res* 2003, **977**(2):239-246.

148. Li JY, Boado RJ, Pardridge WM: **Blood–brain barrier genomics**. *Journal of Cerebral Blood Flow & Metabolism* 2001, **21**(1):61-68.

149. Pardridge WM: **CNS drug design based on principles of blood-brain barrier transport**. *Journal of neurochemistry* 1998, **70**(5):1781-1792.

150. Pardridge WM: **Molecular biology of the blood-brain barrier**. *Molecular biotechnology* 2005, **30**(1):57-69.

151. Li JY, Boado RJ, Pardridge WM: **Rat Blood—Brain Barrier Genomics. II**. *Journal of Cerebral Blood Flow & Metabolism* 2002, **22**(11):1319-1326.

152. Shusta EV, Boado RJ, Mathern GW, Pardridge WM: **Vascular genomics of the human brain**. *Journal of cerebral blood flow and metabolism : official journal of the International Society of Cerebral Blood Flow and Metabolism* 2002, **22**(3):245-252.

153. Schneider F, Draheim J, Kamberger R, Wallrabe U: **Process and material properties of polydimethylsiloxane (PDMS) for Optical MEMS**. *Sensors and Actuators A: Physical* 2009, **151**(2):95-99.

154. Friend J, Yeo L: **Fabrication of microfluidic devices using polydimethylsiloxane**. *Biomicrofluidics* 2010, **4**(2).

155. Leclerc E, Sakai Y, Fujii T: **Cell culture in 3-dimensional microfluidic structure of PDMS (polydimethylsiloxane)**. *Biomedical microdevices* 2003, **5**(2):109-114.

156. Kim Y, Lobatto ME, Kawahara T, Lee Chung B, Mieszawska AJ, Sanchez-Gaytan BL, Fay F, Senders ML, Calcagno C, Becraft J *et al*: **Probing nanoparticle translocation across the permeable endothelium in experimental atherosclerosis**. *Proceedings of the National Academy of Sciences* 2014, **111**(3):1078-1083.

157. Nag S: **The Blood-brain Barrier: Biology and Research Protocols**. Totowa, NJ: Humana Press; 2003.

158. Holley JE, Gveric D, Whatmore JL, Gutowski NJ: **Tenascin C induces a quiescent phenotype in cultured adult human astrocytes**. *Glia* 2005, **52**(1):53-58.

159. East E, Golding JP, Phillips JB: **A versatile 3D culture model facilitates monitoring of astrocytes undergoing reactive gliosis**. *Journal of Tissue Engineering and Regenerative Medicine* 2009, **3**(8):634-646.

160. O'Carroll SJ, Kho DT, Wiltshire R, Nelson V, Rotimi O, Johnson R, Angel CE, Graham ES: **Pro-inflammatory TNFα and IL-1β differentially regulate the inflammatory phenotype of brain microvascular endothelial cells**. *Journal of Neuroinflammation* 2015, **12**(1):131.

161. Mattila P, Majuri ML, Mattila PS, Renkonen R: **TNF alpha-induced expression of endothelial adhesion molecules, ICAM-1 and VCAM-1, is linked to protein kinase C activation**. *Scandinavian journal of immunology* 1992, **36**(2):159-165.

162. Haines RJ, Beard RS, Wu MH: **Protein tyrosine kinase 6 mediates TNFalpha-induced endothelial barrier dysfunction**. *Biochem Biophys Res Commun* 2015, **456**.

163. Afonso PV, Ozden S, Prevost MC, Schmitt C, Seilhean D, Weksler B: **Human blood-brain barrier disruption by retroviral-infected lymphocytes: role of myosin light chain kinase in endothelial tight-junction disorganization**. *J Immunol* 2007, **179**.

164. Scheperjans F, Aho V, Pereira PA, Koskinen K, Paulin L, Pekkonen E, Haapaniemi E, Kaakkola S, Eerola-Rautio J, Pohja M: **Gut microbiota are related to Parkinson's disease and clinical phenotype**. *Movement Disorders* 2015, **30**(3):350-358.

165. Natale G, Pasquali L, Ruggieri S, Paparelli A, Fornai F: **Parkinson's disease and the gut: a well known clinical association in need of an effective cure and explanation**. *Neurogastroenterology & Motility* 2008, **20**(7):741-749.

166. Braniste V, Al-Asmakh M, Kowal C, Anuar F, Abbaspour A, Tóth M, Korecka A, Bakocevic N, Ng LG, Kundu P: **The gut microbiota influences blood-brain barrier permeability in mice**. *Science translational medicine* 2014, **6**(263):263ra158-263ra158.

167. Bustin SA, Benes V, Garson JA, Hellemans J, Huggett J, Kubista M, Mueller R, Nolan T, Pfaffl MW, Shipley GL *et al*: **The MIQE Guidelines: Minimum Information for Publication of Quantitative Real-Time PCR Experiments**. *Clinical Chemistry* 2009, **55**(4):611-622.

168. de Jonge HJM, Fehrmann RSN, de Bont ESJM, Hofstra RMW, Gerbens F, Kamps WA, de Vries EGE, van der Zee AGJ, te Meerman GJ, ter Elst A: **Evidence Based Selection of Housekeeping Genes**. *PLoS ONE* 2007, **2**(9):e898.

169. Gallup JM, Ackermann MR: **The 'PREXCEL-Q Method' for qPCR**. *International Journal of Biomedical Science : IJBS* 2008, **4**(4):273-293.

170. Taylor S, Wakem M, Dijkman G, Alsarraj M, Nguyen M: **A practical approach to RT-qPCR—Publishing data that conform to the MIQE guidelines**. *Methods* 2010, **50**(4):S1-S5.

171. Pabinger S, Rödiger S, Kriegner A, Vierlinger K, Weinhäusel A: **A survey of tools for the analysis of quantitative PCR (qPCR) data**. *Biomolecular Detection and Quantification* 2014, **1**(1):23-33.

172. Clèries R, Galvez J, Espino M, Ribes J, Nunes V, de Heredia ML: **BootstRatio: a web-based statistical analysis of fold-change in qPCR and RT-qPCR data using resampling methods**. *Computers in biology and medicine* 2012, **42**(4):438-445.

173. Citri A, Pang ZP, Sudhof TC, Wernig M, Malenka RC: **Comprehensive qPCR profiling of gene expression in single neuronal cells**. *Nat Protocols* 2012, **7**(1):118-127.

174. Morey JS, Ryan JC, Van Dolah FM: **Microarray validation: factors influencing correlation between oligonucleotide microarrays and real-time PCR**. *Biol Proced Online* 2006, **8**:175-193.

175. Schmittgen TD, Lee EJ, Jiang J, Sarkar A, Yang L, Elton TS, Chen C: **Real-time PCR quantification of precursor and mature microRNA**. *Methods* 2008, **44**(1):31-38.

176. Goni R, García P, Foissac S: **The qPCR data statistical analysis**. *Integromics White Paper* 2009:1-9.

177. Esch MB, Post DJ, Shuler ML, Stokol T: **Characterization of In Vitro Endothelial Linings Grown Within Microfluidic Channels**. *Tissue Engineering Part A* 2011, **17**(23-24):2965-2971.

178. Kralingen C, Kho DT, Costa J, Angel CE, Graham ES: **Exposure to inflammatory cytokines IL-1β and TNFα induces compromise and death of astrocytes. Implications for chronic neuroinflammation**. *PLoS One* 2013, **8**.

179. Evers DL, Fowler CB, Cunningham BR, Mason JT, O'Leary TJ: **The Effect of Formaldehyde Fixation on RNA: Optimization of Formaldehyde Adduct Removal**. *The Journal of Molecular Diagnostics : JMD* 2011, **13**(3):282-288.

180. Russell JN, Clements JE, Gama L: **Quantitation of Gene Expression in Formaldehyde-Fixed and Fluorescence-Activated Sorted Cells**. *PLOS ONE* 2013, **8**(9):e73849.